UNIVERSITÀ DEGLI STUDI DI NAPOLI FEDERICO II
SCUOLA DI MEDICINA E CHIRURGIA

DEPARTMENT OF PHARMACY

PhD in Pharmaceutical Science- XXXIII cycle

DESIGN & SYNTHESIS OF PEPTIDOMIMETICS AS TOOLBOX TO PROBE EMERGING ANTIMICROBIAL AND ANTICANCER STRATEGIES

PhD Coordinator:
Chiar.ma Prof.ssa
MARIA VALERIA D'AURIA

Tutor:
Chiar.mo Prof.
PAOLO GRIECO

Candidate:
ROSA BELLAVITA

LIST OF PUBLICATIONS

Bellavita R, Falanga A, Buommino E, Merlino F, Casciaro B, Cappiello F, Mangoni ML, Novellino E, Catania MR, Paolillo R, Grieco P, Galdiero S. Novel temporin L antimicrobial peptides: promoting self-assembling by lipidic tags to tackle superbugs. *Journal of Enzyme Inhibition Medicinal Chemistry*. 2020, 35, 1751–1764.

Bellavita R, Vollaro A, Catania MR, Merlino F, De Martino L, Nocera FP, Della Greca M, Lembo F, Grieco P, Buommino E. Novel antimicrobial peptide from Temporin L in the treatment of *Staphylococcus pseudintermedius* and *Malassezia pachydermatis* in polymicrobial inter-Kingdom infection. *Antibiotics (Basel)*. 2020, 9:530.

Bellavita R, Raucci F, Merlino F, Piccolo ML, Ferraro MG, Irace C, Santamaria R, Iqbal AJ, Novellino E, Grieco P, Mascolo N, Maione F. Temporin L-derived peptide as a regulator of the acute inflammatory response in zymosan-induced peritonitis. *Biomedicine and Pharmacotherapy*. 2019, 123:109788.

Buommino E, Carotenuto A, Antignano I, **Bellavita R**, Casciaro B, Loffredo MR, Merlino F, Novellino E, Mangoni ML, Nocera FP, Brancaccio D, Punzi P, Roversi D, Ingenito R, Bianchi E, Grieco P. The Outcomes of Decorated Prolines in the Discovery of Antimicrobial Peptides from Temporin-L. *Chem Med Chem*. 2019, 14, 1283–1290.

Merlino F, Billard E, Yousif AM, Di Maro S, Brancaccio D, Abate L, Carotenuto A, **Bellavita R**, D'Emmanuele di Villa Bianca R, Santicioli P, Marinelli L, Novellino E, Hebert T, Lubell WD, Chatenet D, Grieco P. Functional selectivity revealed by *N*-methylation scanning of human Urotensin II and related peptides. *Journal of Medicinal Chemistry*. 2019, 62, 1455–1467.

Yousif AM, Ingangi V, Merlino F, Brancaccio D, Monopoly M, **Bellavita R**, Novellino E, Carriero MV, Carotenuto A, Grieco P. Urokinase receptor derived peptides as potent inhibitors of the Formyl Peptide Receptor type 1-triggered cell migration. *European of Journal Medicinal Chemistry*. 2018, 143, 348–360.

PATENT PENDING

Inventors: Mascolo Nicola, Maione Francesco, Carotenuto Alfonso, Novellino Ettore, Merlino Francesco, **Bellavita Rosa**, Buommino Elisabetta, Grieco Paolo.
Title: "Temporin L Analogues with anti-inflammatory and antimicrobial activity".
Application: P021300IT-01/lm. **Date:** 19/06/2019.

Table Of Contents

LIST OF ABBREVIATIONS

AMPs	Antimicrobial peptides
ANTS	8-Aminonaphtalene-1,3,6-trisulfonic acid, disodium salt
Ac_2O	Acetic anhydride
Alloc	Allyloxycarbonyl group
CD	Circular dichroism
CAC	Critical Aggregation Concentration
CL	Cardiolipin
CuAAC	Copper-catalyzed azide-alkyne cycloadditions
DCM	Dichloromethane
DMF	Dimethylformamide
DIC	*N-N'*-Diisopropylcarbodiimide
DPC	Dodecylphospocholine
DCE	1,2-Dichloroethane
DIEA	Diisopropylethyl amine
DPX	*p*-Xylene-bis-pyridinium bromide
DOPG	1,2-Dioleoyl-sn glycero-3-phospho-(1′-rac-glycerol) sodium salt
DOPE	1,2-Dioleoyl-sn-glycero-3-phosphoethanolamine
DBCO	Dibenzocyclooctyne
Dex	Dexamethasone
Fam	Carboxyfluorescein
FITC	Fluorescein isothiocyanate
FP	Fluorescence polarization
FIC	Fractional inhibitory concentration
GP	Generalized Polarization

HOA	1-Hydroxy-7-azabenzotriazole
HATU	2-(7-Aza-1H-benzotriazole-1-yl)-1,1,3,3-tetramethyluronium hexafluorophosphate
HBTU	2-(1H-Benzotriazole-1-yl)-1,1,3,3-tetramethyluronium hexafluorophosphate
HOBt	1-Hydroxybenzotriazole
HPLC	High-Performance Liquid Chromatography
HRMS	High resolution mass spectrometry
IC50	Median inhibition concentration
LC	Liquid Chromatography
Laurdan	6-Dodecanoyl-*N*,*N*-dimethyl-2-naphthylamine
LUVs	Large unilamellar vesicles
MS	Mass spectrometry
MTBE	Tert-butyl methyl ether
MTT	3-(4,5-dimethylthiazol-2-yl)-2,5-Diphenyltetrazolium bromide
MMC	Minimum mycocidal concentration
MIC	Minimum inhibitory concentration
MBC	Minimum bactericidal concentration
MeCN	Acetonitrile
NCS	*N*-Chlorosuccinimide
NMR	Nuclear Magnetic Resonance
RCM	Ring-closing metathesis
SDS	Sodium dodecyl sulfate
SAR	Structure-activity relationship
SPPS	Standard solid-phase peptide synthesis
SUVs	Small unilamellar vesicles
SPAAC	Strain-promoted click reaction

TL	Temporin L
TA	Temporin A
TB	Temporin B
TFE	2,2,2-Trifluoroethanol
TEA	Triethylamine
THF	Tetrahydrofuran
TFA	Trifluoroacetic acid
TIS	Triisopropylsilane
ThT	Thioflavin T
TCF	T cell factor protein
UHPLC	Ultra-high Performance Liquid Chromatography
UV-Vis	Ultraviolet-visible
XTT	2,3-Bis(2-methyloxy-4-nitro-5-sulfophenyl)-2H-tetrazolium-5-carboxanilide

SUMMARY

Peptides are biological polymers that perform many hormonal and vital functions in humans. In the field of medicinal chemistry, peptides are recognized for being highly efficacious, relatively safe and well tolerated, but, suffering from pharmacokinetic drawbacks, they are mainly engaged as models. In the light of advances in the peptide-based drug discovery field, peptidomimetics are rather considered more drug-like molecules, endowed with improved pharmacokinetic properties and widely employed as powerful tools to probe the biological mechanism of several diseases and emerging therapeutic strategies.

This Ph.D. thesis, divided into two parts, **Part 1** and **Part 2**, describes the development of peptidomimetics toolbox designed *ad hoc* and synthesized to challenge antibiotic resistance and Wnt/β-catenin pathway involved in several types of cancer. Nowadays, these phenomena are the leading causes of increase in mortality rates worldwide, hence scientific research constantly works in order to progress the treatment strategies.

In particular, the studies disclosed in the **Part 1** were aimed at investigating the following issues:

- development of novel antimicrobial Temporin L analogues by means of innovative chemical modifications for tackling ESKAPE infections (**Chapter 2, 3, 5**).
- investigation of antimicrobial and anti-inflammatory activities of selected Temporin L derivatives in polymicrobial infections (**Chapter 4**).

In **Chapters 2** and **4**, the Ph.D. thesis will focus on the design and synthesis of antimicrobial peptidomimetics by applying local modifications consisting in the incorporation of non-native amino acids such as decorated prolines and D-amino acids, in order to improve SAR knowledge about antimicrobial behavior. **Chapter 3** describes a lipidation strategy by the conjugation of saturated fatty acids with

different carbon chain length in both N- and C-termini. The library of lipidated peptidomimetics was used to probe the self-assembling process, as boosting the interaction with the bacterial membranes, and fine-tune a more potent and broad-spectrum antimicrobial activity. **Chapter 5** focuses on the introduction of chemical restrictions to generate conformationally-reduced peptidomimetics that delineates the correlation between bioactivity and amphipathic α-helix structure of temporins.
In the **Part 2**, the studies reported have been addressed to develop peptidomimetics acting as inhibitors of β-catenin implicated in oncogenic activation of Wnt/β-catenin pathway. In **Chapter 2**, the Ph.D. thesis will focus on the design and synthesis of a library of stapled bicyclic peptidomimetics by using the hydrocarbon stapling chemistry and the head-to-tail cyclization, to induce conformational constrictions and increase the binding activity towards β-catenin. Finally**,** in **Chapter 3,** the strain-promoted click reaction was exploited as strategy to tether two inhibitors of β-catenin and increase the potency and selectivity of β-catenin inhibition.

PART I

Antimicrobial Peptidomimetics

ABSTRACT

Infections caused by ESKAPE pathogens are a huge challenge in both human and veterinary medicine. Among the antimicrobial peptides (AMPs), temporins represent encouraging candidates since they act through a different mode of action from conventional antibiotics. Despite the strong antimicrobial activity, the native Temporin L has not considered an efficacious alternative due to its cytotoxicity. In this scenario, our efforts have been addressed to the improvement of drug-like features of some Temporin L analogues, applying several synthetic approaches spanning from local modification and conformational constraints. Specifically, we performed local modifications consisting of the incorporation of D-amino acids or "decorated prolines" featured by appropriate functional groups (polar-, positively charged-, aliphatic- and aromatic groups) and lipidation strategy in order to improve antimicrobial activity and to preserve low cytotoxicity. In addition, we probed the correlation between α-helix secondary structure and antimicrobial activity using different side-chain to side-chain cyclization strategies. In particular, lactamization, the formation of disulfide bridge between cysteines, triazole formation by CuAAC click chemistry reaction, and ring closing metathesis were used to stabilize α-helical conformation and to increase the biological activity. Thanks to the application of these several synthetic strategies, we discovered novel Temporin L analogues with a high therapeutic index that have shown characteristics desired to be good candidates in the development of novel antimicrobial agents for topical applications.

CHAPTER 1

INTRODUCTION

1.1. ANTIBIOTICS HISTORY AT A GLANCE

The prompt emergence of resistant bacteria is endangering the efficacy of traditional antibiotics, which have always been considered a blessing to human civilization to their power to eradicate most of the bacterial infections, saving millions of people.[1,2] The beginning of the "modern antibiotic era" was associated with the names of Paul Ehrlich and Alexander Fleming.[3] In 1911, Paul Ehrlich discovered the synthetic produgs Salvarsan for the treatment of *Treponema pallidum*, the agent of syphilis.[4,5] Salvarsan became the cornerstone for the discovery of sulfa drugs by Gerhard Domagk, but they were largely superseded by penicillin discovered by Alexander Fleming in 1928.[6,7] However, the high production of β-lactamase enzyme in bacteria led to rapid destruction of penicillin, making it totally ineffective and developing the phenomena of penicillin resistance.[8] Thus, the period from the 1950s and 1960s was named the "golden era" for the discovery of several antibiotics able to bypass penicillin resistance.[9] During this "golden era", many academic institutions and major pharmaceutical companies in the United States and other countries were involved in the research of about 20 classes of antibiotics (Figure 1), like aminoglycosides (1940s), tetracyclines (1940s), macrolides (1950s), glycopeptides (1950s), cephalosporins (1960s), quinolones (1960s) and carbapenems (1980s).[10] Unfortunately, the resistance to these new classes of antibiotics spread very fast in this golden age (Figure 1). Despite recent commercialization for some of them, the last classes of antibiotics discovered are from the 1980s. Indeed, the last antibiotic discovered was daptomycin in 1986 and it was only approved by the US Food and Drug Administration in 2003.[11] This detail confirms that any new classes have been found after about 50 years. In fact, antibiotic therapy for the treatment of many bacterial infections currently consists of associations or improvements of existing molecules. For example, molecules recently discovered belong to already known classes, as tedizolid (oxazolidinones), dalbavancin (lipoglycopeptides), ceftaroline and ceftobiprole (cephalosporins).[12,13] Instead, examples of combinations of existing

molecules recently commercialized are ceftolozane/tazobactam or ceftazidime/avibactam.[14] The rapid rise of antibiotic resistance due to overuse and incorrectly prescribing of antibiotics has led to pharmaceutical industries to gradually leave the field altogether.[15] As a result, the rhythm of antibiotic discovery has slowed down and there is always an urgent need to identify novel molecules that potentially could combat the "bacteria killer" and eradicate hard-to-treat infections.

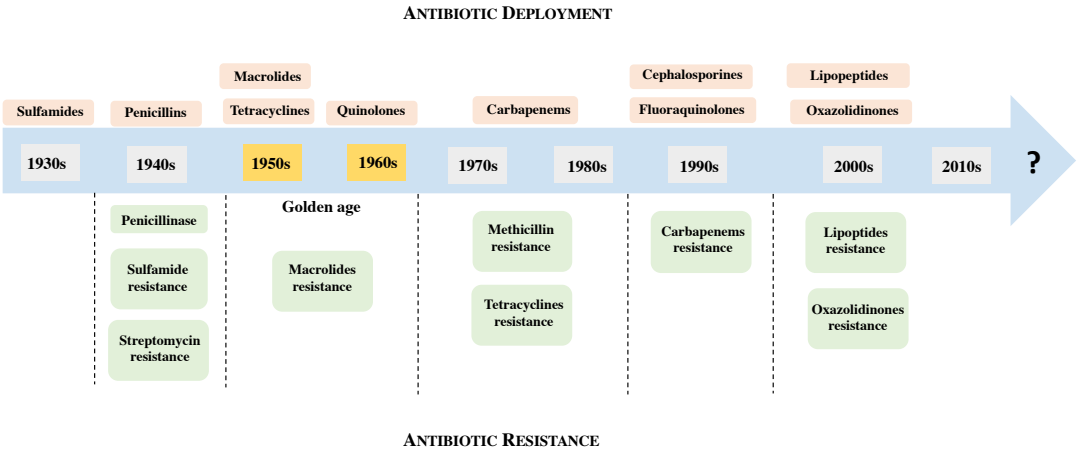

Figure 1. Developing antibiotic resistance: a timeline of key events.

1.2. ANTIBIOTIC RESISTANCE

As reported by the World Health Organization (WHO), in Europe every year an estimated 25000 patients die due to antibiotic resistance occurring in hospitals, in the community and through the food chain in Europe.[16,17] In the global priority pathogens list of antibiotic-resistant bacteria established by WHO, are included *Enterococcus* faecium, *Staphylococcus aureus*, *Klebsiella pneumoniae*, *Acinetobacter baumannii*, *Pseudomonas aeruginosa*, and *Enterobacter* species, referred to as "ESKAPE group".[18,19] The ESKAPE bugs have developed resistance against oxazolidinones, lipopeptides, macrolides, fluoroquinolones, tetracyclines, β-lactams and antibiotics that are the last line of defense, including carbapenems and

glycopeptides.[20] In general, bacteria may adapt to “antibiotic attack” through two major genetic mechanisms: *i)* mutations in chromosomal genes often associated with the mechanism of action of antibiotic; *ii)* acquisition of foreign DNA coding for resistance determinants by horizontal gene transfer (HGT).[21] The horizontal evolution can occur by a conjugation, a transduction or a transformation mechanism. Conjugation consists of a transfer of resistance plasmids containing resistance genes between bacteria by a conjugative pilus; transduction includes a transmission of DNA bacterial by a viral vector; while transformation involves an incorporation of exogenous DNA in bacterial genome.[22] These genetic resistance mechanisms include modification of target protein by disabling the antibiotic-binding but leaving intact the cellular functionality of target;[23] an inactivation of antibiotic by chemical covalent modifications;[24] an antibiotic efflux via pump that secrete antibiotic from the cell; a target bypass involving a formation of additional antibiotic targets or subunits that are not susceptible to binding of the antibiotic (Figure 2).[25] In addition, bacteria can protect themselves by self-assembling in biofilms, which are hydrated matrices composed of eDNA, proteins, and polysaccharides, in which bacterial cells are embedded and an exchange of genetic material between cells occurs very easily.[26] In biofilm communities, a slow or incomplete penetration of antibiotic and the transformation of bacterial cells in dormant cells which are less susceptible to antibiotics,[27] contribute to antibiotic resistance. Advances in genomics, system biology and structural biology have provided a lot of information related to events underpinning resistance, since a detailed understanding of resistance mechanisms could be the key to identify novel antibacterial agents, enable countering the resistance threat.

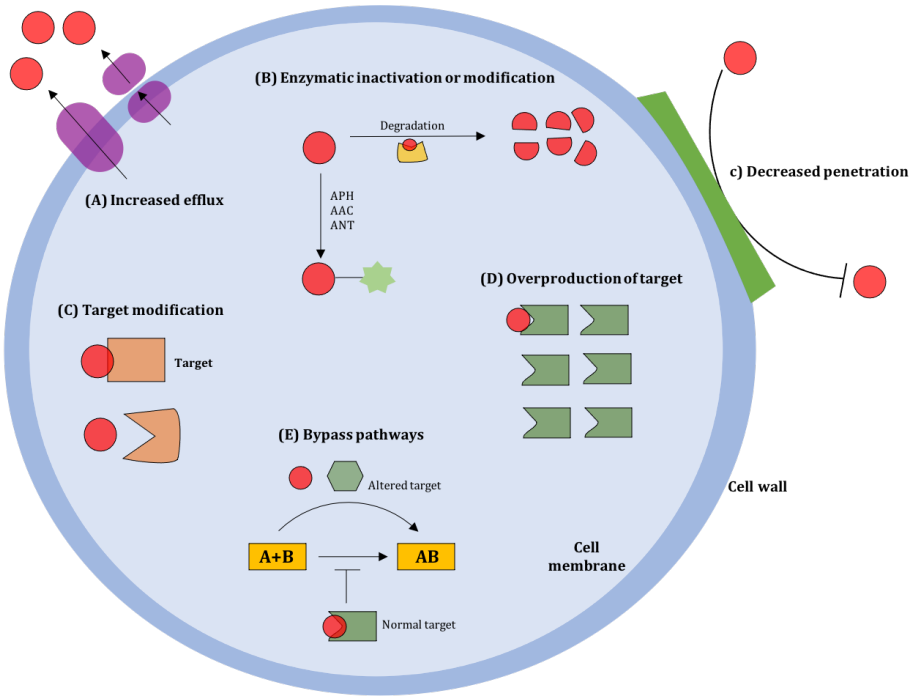

Figure 2. Mechanism of antibiotic resistance: **A)** Antibiotic efflux pumps remove the antibiotic from the cell before it can reach its target site. **B)** Antibiotic modification involving the addition of acetyl, phosphate, or adenyl groups to aminoglycosides by N-acetyl transferases (AAC), O-phosphotransferases (APH), and O-adenyltransferases (ANT). Antibiotic degradation involving a hydrolysis by β-lactamases. **C)** Target modification such as 23S rRNA or 16S rRNA methylation. **D)** Target bypass involves the generation of additional antibiotic targets or subunits that are not susceptible to binding of the antibiotic. **E)** Overproduction of target.[15,25]

1.3. The Antimicrobial Peptides (AMPs)

The speedy growth of bacterial resistance to conventional antibiotics has caused an inefficiency of traditional approaches for eradicating infections and in addition the lack of choice of antimicrobials for their treatment, emphasizes the urgent need to discover novel antibacterial strategies.[28] Antimicrobial peptides (AMPs) appear as a valid therapeutic option for the development of novel antibiotics classes.[29] AMPs are an abundant and varied group of molecules produced by many tissues and cell types in a variety of invertebrate, plant and animal species.[30] They can be divided in gene-encoded ribosomally synthesized peptides present in all organisms and in non-ribosomally synthesized peptide antibiotics produced by bacteria and fungi.[31,32,] Some non-ribosomally peptide antibiotics were clinically approved and widely used,

such as bacitracin, gramicidin S, polymyxin B, streptogramins as well as the two glycopeptide antibiotics vancomycin and teicoplanin.[33] Regarding ribosomally synthesized peptides are furtherly subdivided in eukaryotic AMPs and in defence peptides and proteins derived from bacteria, called bacteriocins.[34,35] In mammals, AMPs are an essential component of the innate immune system and represent the first line of immune biological defense.[36] In fact, they are also considered as effectors and regulators of the innate immune system, modulating profoundly the immune response through several mechanisms, for example, increasing the chemokine production and release by immune and epithelial cells and/or having an adjuvant activity in promoting adaptive immunity.[37]

Host-defense (antimicrobial) peptides (HDP) produced mostly by amphibian skin, derive from precursor peptides subjected to proteolytic activation steps.[38] They are typically amphipathic small peptides composed of 10–50 amino acids, have an overall net positive charge of +2 to +9 at physiological pH due to the presence of Lys and/or Arg residues, and have a substantial proportion (≥30%) of hydrophobic residues.[39] On the basis of their conformation, HDP are classified in four broad structural groups: *i)* α-helical peptides free of cysteine residues (*e.g.* magainins); β-sheet peptides stabilized by two to four disulfide bridges (*e.g.* human α- and β-defensins); loop peptides with one disulfide bridge (*e.g.* bactenecin); peptides characterized by extended structures rich in glycine, proline, tryptophan, arginine and/or histidine (*e.g.* indolicidin).[40] The main target for most HDP is bacterial membrane and their cationicity and amphiphilic nature are correlated to their activity.[40] The positively charged residues of AMPs determinate an accumulation at polyanionic microbial cell surfaces featured by lipopolysaccharide and teichoic acids in Gram-negative and Gram-positive bacteria, respectively. After crossing the outer membrane via self-promoted uptake, AMPs interact with acidic phospholipids (phosphatidylglycerol, phosphatidylethanolamine and cardiolipin) of the monolayer of cell membrane of both types of bacteria. The insertion of peptides into cell

membrane can cause a disruption of the physical integrity of bilayers by three different models, that is the barrel- stave, carpet and toroidal pore models.[41] In the carpet model, peptides interact with anionic phospholipid head groups and cover the membrane surface in a carpet-like manner.[42] When a critical threshold concentration is reached, peptides form toroidal transient holes in the membrane and the membrane ruptures in a detergent-like manner, resulting in micelle formation.[41,42] In the barrel stave model, hydrophobic peptide regions align with the lipid core region of bilayer and the hydrophilic peptide regions form the inner surface of pore channel.[43] Instead, in the toroidal-pore model, peptides aggregate and induce the lipid monolayers to bend incessantly through the pore, so that the water core is lined by both the inserted peptides and the lipid head groups.[43]

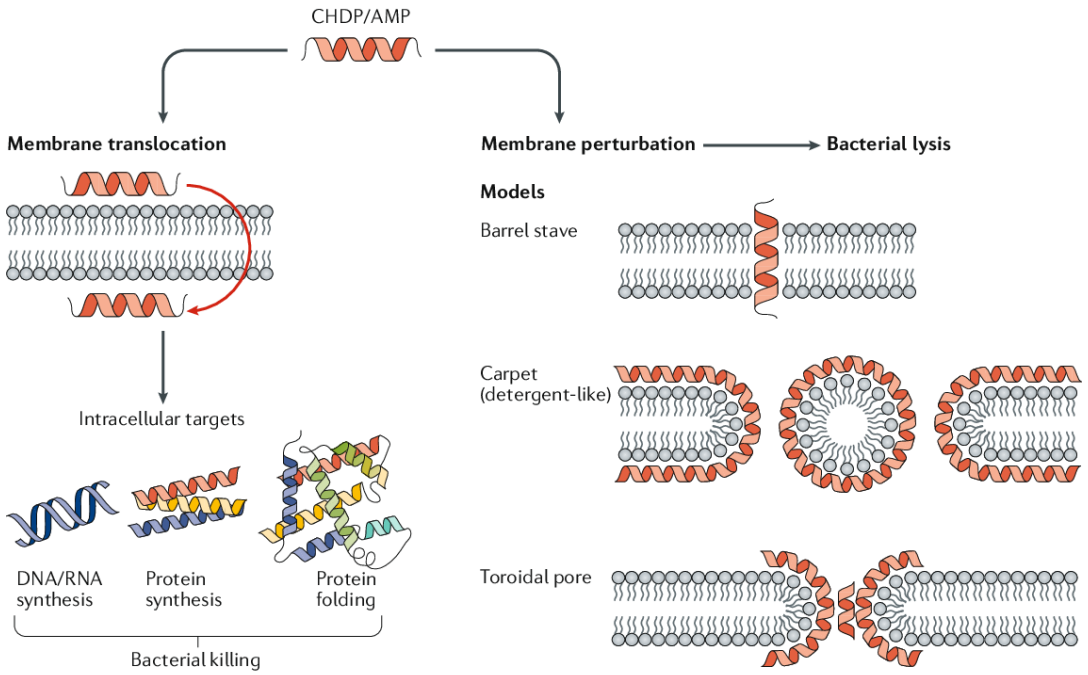

Figure 3. Models of mechanisms of antimicrobial host defence peptides.[46]

These two pore models differs from each other, because the pore is partly lined by lipid in toroidal model, while a cylindrical pore is completely lined by peptides in

barrel stave model,[44] but what drives the preference of AMPs for a certain models is not yet fully understood. In addition, a further mode of action of AMPs consists in crossing the bacterial membrane and binding to intracellular targets such as nucleic acids and/or proteins, killing bacteria by an arrest of cell processes such as replication, transcription or cell wall synthesis.[45] Exploiting this different mode of action of AMPs, an alternative route for the successful AMPs introduction may be their use in combination with conventional antibiotics in a synergistic mode of action. In a combined therapy, the disintegration of the bacterial membrane by AMP allows the antibiotic to enter the bacterial cell at higher concentrations and to interact with its specific intracellular targets, inducing bacterial cell death.[46]

Despite the mode of action of AMPs does not involve a specific target and so it is almost unlikely that bacteria can develop resistance, cases of AMP resistance have been reported anyway. Bacterial strategies which induce resistance to AMPs include bacterial cell envelope change as modifications in the polysaccharide layer and teichoic acid;[47] a production of bacterial proteins that can degrade or sequestrate peptides,[48] a removal of AMPs by an efflux system; and the formation of capsular polysaccharides hamper that capture the peptides.[49] Overall, unlike antibiotic resistance, the emergence of AMPs resistance is less recurrent and also less worrying, due to the lack of horizontal transmissions of resistance genes.

1.4. TEMPORINS

The amphibian skin is one of the richest source of ribosomally synthesized antimicrobial peptides (AMPs), especially the skin of the Rana genus which includes more than 250 species around the world.[50] Temporins, first isolated from the skin of the Asian frog *Rana erythraea*,[51] are known as vespa-like peptides because their sequence is similar to chemotactic peptides isolated from the venom of wasps of genus Vespa.[52] In 1996, a family of 10 temporins (from A to L) were identified from skin secretions of the European red frog *Rana Temporaria,* through a mild electrical

stimulation.[53] By a screening of a cDNA library prepared from the skin of *Rana temporaria* using the precursor of esculentin from *Rana esculenta* as probe, the biosynthetic precursor of temporins was identified.[51,53] This large peptide precursor made of 22 residues, contains a cysteine residue in position 22 representing the site of cleavage of the signal peptide in the pre-protemporins. The pro-sequence contains at the C-terminus an acidic propiece ending with the pair Lys-Arg, which represents a processing site for prohormone convertases for generating the mature sequence. The glycine residue flanking the carboxyl-terminus of the mature peptide, is recognized by peptidylglycine α-amidating monooxygenase for the formation of C-terminal amides.[54] Temporins are among the shortest amphipathic α-helical AMPs (10 to 14 amino acids) found in nature to date. Their derived composite consensus sequence is FLP(I/L)IASLL(S/G)KLL-NH_2 and their general amino acid type sequence is $X_1X_2X_3X_4X_5X_6Y_7X_8X_9Y_{10}Y_{11}{}^+X_{12}X_{13}$-$NH_2$, where X and Y indicate hydrophobic and hydrophilic residues, respectively, whereas Y^+ denotes charged amino acids.[55] X_2, X_3, X_9 and X_{13} are highly conserved amino acids and, since leucine is the most abundant amino acid in temporins, hydrophobic residues (Y) represent about 70% of the peptide sequence.[54,55] Temporins are C-terminally α-amidated, have a low net positive charge (from 0 to +3 at physiological pH) due to the presence of Lys and Arg residues in their sequence and adopt an α-helical conformation in a hydrophobic environment.[56] Temporins A (TA), B (TB), and L (TL) are the most studied among members of the temporin family. TA (Phe-Leu-Pro-Leu-Ile-Gly-Arg-Val-Leu-Ser-Gly-Ile-Leu-NH_2) and TB (Leu-Leu-Pro-Ile-Val-Gly-Asn-Leu-Leu-Lys-Ser-Leu-Leu-NH_2) show greater potencies against Gram-positive bacteria, including clinically isolated methicillin-resistant *Staphylococcus aureus*, vancomycin-resistant *Enterococcus faecium* and *E. faecalis* (with a minimal inhibitory concentration ranging from 2.5 to 20 μM) than against Gram-negative bacterial strains. These isoforms have also a strong activity against the human parasitic protozoan Leishmania, inducing severe damage to the plasma

membrane.[56] Differently, Temporin L (Phe-Val-Gln-Trp-Phe-Ser-Lys-Phe-Leu-Gly-Arg-Ile-Leu- NH_2) displays the strongest activity against fungi, yeasts, Gram-positive and is noticeably potent against Gram-negative species such as *Escherichia coli* D21 and *Pseudomonas aeruginosa* ATCC 15692, with a lethal concentration of 1.5 and 3.6 μM, respectively.[57,58] The hydrophobic residues, in particular the phenylalanine zipper motif made of Phe1, Phe5, Phe8 in TL, are involved in the initial binding to the Gram-positive membrane and the stabilization of peptide aggregates in the membrane, leading to the formation of large pores and consequential cell death. The killing activity of TL against Gram-negative bacteria is due to its strong affinity toward the lipopolysaccharide LPS, a component of the outer membrane.[59] Neutralizing the toxic effect of LPS during a Gram-negative infection may help to eradicate the risk of sepsis, which can lead to mortality. LPS is made of a variable and polyanionic polysaccharide portion and lipid A consisting of a disaccharide of phosphorylated glucosamines; both are involved in the interaction with TL through a mixture of hydrophobic and ionic bonds.[55,59] According to "self-promoted uptake model", these interactions permit TL to anchorage to the outer membrane, a loss of membrane integrity and a following increased permeability of peptide itself, reaching the cytoplasmic membrane.[60] A recent study using *E.coli* cells has showed that TL binds through a competitive inhibition mechanism the GTP binding site of FtsZ protein, involved in the first step of cell division process.[72] A high binding affinity was detected for TL toward FtsZ with a K_D value of 17.4 ± 0.8 nM. A morphologic investigation by a TEM analysis has displayed that in presence of TL, *E. coli* cells form elongated "necklace-like" structures absent in untreated cells, which are originated by a multitude of bacterial cells unable to divide. Instead, the weak activity of TA and TB against Gram-negative bacteria may be due to their oligomerization process in presence of the LPS, because oligomers have a large size and cannot diffuse efficiently through the cell wall; in contrast, TL is completely aggregated in aqueous solution adopting an α-

helical structure, but disaggregates when in contact with the LPS. A synergism study between these temporins in presence of the LPS, has demonstrated that TL prevents TA and TB oligomerization, making them able to cross it and to reach and permeate the inner bacterial membrane.[63] In fact, when TL was combined with TB in the same molar ratio, TL conserved its dimeric structure, while TB passed from oligomeric state to monomeric helical structure.[54] Unfortunately, TL has not proved to be a selective peptide, since TL interacts strongly with zwitterionic lipid bilayers of human erythrocytes and causes a dramatic hemolytic effect in comparison to minor hemolytic activity of TA and TB. A different molecular mechanism underlying antimicrobial and hemolytic activities of TL and TA was described by spectroscopic techniques (CD and NMR), using sodium dodecyl sulfate (SDS) and dodecylphospocholine (DPC) micelles, mimicking bacterial and eukaryotic membranes, respectively.[61,62]

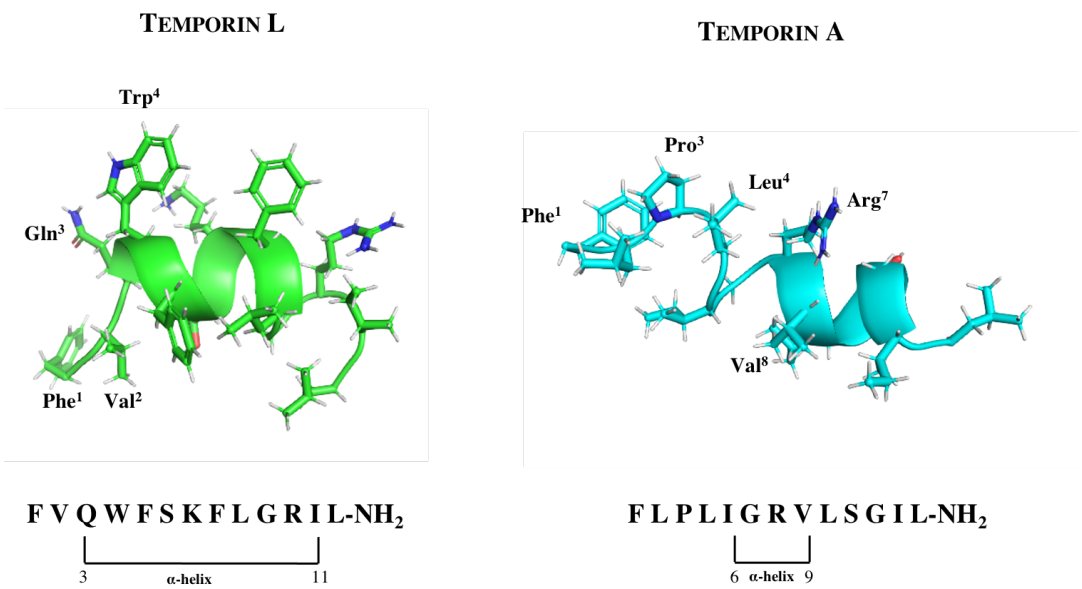

Figure 4. The secondary structures of TL (PDB 6GS5) and TA (PDB 2MAA) by NMR spectroscopy in SDS micelles and LPS, respectively.

TA interacts with SDS micelle adopting an amphipathic α-helix along central residues (6–9) and a β-turn centered on Pro[3]-Leu[4] at N-terminus; whereas TL

assumes a similar behavior but its α-helix extends along 3–11 residues and its N-terminus has a higher propensity to form helical structures (Figure 4).[63,64]

Both temporins exhibited a "dynamic peptide-lipid supramolecular pore" model in SDS micelles, consisting in binding to negatively charged phospholipids membrane surface and when a local high concentration of a peptide was reached, transient aqueous pores of variable sizes are formed. The considerable difference in hemolytic activity of TA and TL is correlated to their diverse conformational propensities in DPC micelles. TL assumes an α-helix conformation along its entire sequence, which allows the peptide to insert in a perpendicular orientation into micelle surface with its N-terminus located within the hydrophobic core, forming the staves of a barrel-like channel, as described in "barrel stave" model. Instead, the loss of α-helical structure along the entire sequence of TA in DPC, explains its inability to deeply insert into the hydrophobic core of micelles and to form barrel-like channel. This could be the reason why the lytic effect of TA on red blood cells is weaker in comparison to TL.[63,64] The proline residue in TA is responsible to the substantial difference observed between TL and TA secondary structures, since proline is well-known as a α-helix breaking amino acid and a β-turn inducer. In this context, a TL analogue, in which Gln^3 was replaced by Pro residue showed a hemolytic effect 2- to 5- fold lower than that of the native TL (at the 3-12 μM concentration range), since a breaking of α-helix and a β-turn centered on Pro^3 in N-terminal has conferred a high flexibility at N-terminus, which prevents to act via "barrel stave" mechanism in DPC micelles.[64] Therefore, TL cannot be considered as an efficacious alternative to traditional antibiotics because of its biological profile, but modifications of its chemical structure could contribute to challenge its drawbacks and to discover novel antibacterial agents with a high therapeutic index, referred to as the ratio between the concentration of hemolytic activity and antimicrobial activity.

1.5. REFERENCES

[1] S.B. Zaman, M.A. Hussain, R. Nye, V. Mehta, K.T. Mamun, N. Hossain. A Review on antibiotic resistance: alarm bells are ringing. Cureus. 2017, 9:e1403.
[2] S.B. Levy SB. From tragedy the antibiotic age is born . The Antibiotic Paradox. Springer, Boston, MA. 1992, pp 1–12.
[3] R.I. Aminov. A brief history of the antibiotic era: lessons learned and challenges for the future. Front. Microbiol. 2010, 1:134.
[4] M.I. Hutchings, A.W. Truman, B. Wilkinson. Antibiotics: past, present and future. Curr. Opin. Microbiol. 2019, 51, 72–80.
[5] P. Ehrlich, S. Hata. Die Experimentelle Chemotherapie der Spirilosen. Berlin: Julius Springer. 1910, pp 1–85.
[6] C.L. Ventola. The Antibiotic Resistance Crisis, Part 1: Causes and Threats. P T. 2015, 40, 277–283.
[7] J. Mahoney, R. Arnold, A. Harris. Penicillin treatment of early syphilis. A preliminary report. Verer. Dis. Inform. 1943, 24, 355–357.
[8] E.P. Abraham, E. Chain. An enzyme from bacteria able to destroy penicillin. Nature. 1940, 146:837.
[9] I. Chopra, L. Hesse, A. O'Neill. Discovery and development of new anti-bacterial drugs," in Pharmacochemistry Library, Vol. 32, Trends in Drug Research III, ed. H. van der Goot (Amsterdam: Elsevier). 2002, pp 213–225.
[10] E. Peterson, P. Kaur. Antibiotic resistance mechanisms in bacteria: relationships between resistance determinants of antibiotic producers, environmental bacteria, and clinical pathogens. Front. Microbiol. 2018, 9:2928.
[11] G. A. Durand, D. Raoult, G. Dubourg. Antibiotic discovery: history, methods and perspectives. Int. J. of Antimicrob. Agents. 2019, 53, 371–382.
[12] H.W. Boucher, G.H. Talbot, J.S. Bradley, J.E. Edwards , D. Gilbert, L.B. Rice, M. Scheld, B. Spellberg, J. Bartlett. Bad bugs, no drugs: no ESKAPE! An update from the Infectious Diseases Society of America. Clin. Infect. Dis. 2009, 48, 1–12.
[13] A.M. Slee, M.A. Wuonola, R.J. McRipley, I. Zajac, M.J. Zawada, P.T. Bartholomew, W.A. Gregory, M. Forbes. Oxazolidinones, a new class of synthetic antibacterial agents: in vitro and in vivo activities of DuP 105 and DuP 721. Antimicrob. Agents Chemother. 1987, 31, 1791-1797.
[14] D. Cluck, P. Lewis, B. Stayer, J. Spivey, J. Moorman. Ceftolozane-tazobactam: A new-generation cephalosporin. Am. J. Health Syst. Pharm. 2015, 72, 2135–2146.
[15] K. Lewis. Platforms for antibiotic discovery. Nat. Rev. Drug Discov. 2013, 12, 371–387.
[16] https:/www.euro.who.int.
[17] G.M. Rossolini, F. Arena, P. Pecile, S. Pollini. Update on the antibiotic resistance crisis. Curr. Opin. Pharmacol. 2014, 18, 56–60.
[19] Global priority list of antibiotic-resistant bacteria to guide research, discovery, and development of new antibiotics. https://www.who.int.

[20] L.B. Rice. Federal funding for the study of antimicrobial resistance in nosocomial pathogens: no ESKAPE. J. Infect. Dis. 2008, 197:1079–1081.
[21] D.M.P. De Oliveira, B.M. Forde, T.J. Kidd, P.N.A. Harris, M.A. Schembri, S.A. Beatson, D.L. Paterson, M.J. Walker. Antimicrobial resistance in ESKAPE pathogens. Clin. Microbiol. Rev. 2020, 33:e00181-19.
[22] J.M. Blair, M.A. Webber, A.J. Baylay, D.O. Ogbolu, L.J. Piddock. Molecular mechanisms of antibiotic resistance. Nat. Rev. Microbiol. 2015, 13, 42–51.
[23] A.J. Alanis. Resistance to antibiotics: are we in the post-antibiotic era?. *Arch. Med. Res*. 2005, 36, 697–705.
[24] J.M. Munita, C.A. Arias. Mechanisms of antibiotic resistance. *Microbiol. Spectr*. 2016 4:10.1128.
[25] M. Laws, A. Shaaban, K.M. Rahman. Antibiotic resistance breakers: current approaches and future directions. *FEMS Microbiol. Rev*. 2019, 43, 490-516.
[26] H.K. Allen, J. Donato, H.H. Wang, K.A. Cloud-Hansen, J. Davies, J. Handelsman. Call of the wild: antibiotic resistance genes in natural environments. *Nat. Rev. Microbiol*. 2010, 8, 251-259.
[27] R.M. Donlan. Biofilms: microbial life on surfaces. *Emerg. Infect. Dis*. 2002, 8, 881–890.
[28] T.K. Wood, S.J. Knabel, B.W. Kwan. Bacterial persister cell formation and dormancy. *Appl. Environ. Microbiol*. 2013, 79, 7116–7121.
[29] M.S. Zharkova, D.S. Orlov, O.Y. Golubeva, O.B. Chakchir, I.E. Eliseev, T.M. Grinchuk, O.V. Shamova. Application of antimicrobial peptides of the innate immune system in combination with conventional antibiotics—a novel way to combat antibiotic resistance?. Front. Cell. Infect. Microbiol. 2019, 9:128.
[30] K.A. Brogden. Antimicrobial peptides: pore formers or metabolic inhibitors in bacteria?. Nat. Rev. Microbiol. 2005, 3, 238-250.
[31] J. Wiesner, A. Vilcinskas. Antimicrobial peptides: the ancient arm of the human immune system. Virulence. 2010, 1, 440–464.
[32] E. Guaní-Guerra, T. Santos-Mendoza, S.O. Lugo-Reyes, L.M. Terán. Antimicrobial peptides: general overview and clinical implications in human health and disease. Clin. Immunol. 2010, 135, 1–11.
[33] W. Wohlleben, Y. Mast, E. Stegmann, N. Ziemert. Antibiotic drug discovery. Microb. Biotechnol. 2016, 9, 541-548.
[34] M. Papagianni. Ribosomally synthesized peptides with antimicrobial properties: biosynthesis, structure, function, and applications. Biotechnol. Adv. 2003, 21, 465-499.
[35] B.P. Cammue, M.F. De Bolle, H.M. Schoofs, F.R.Terras, K. Thevissen, R.W. Osborn, S.B. Rees, W.F. Broekaert. Gene encoded antimicrobial peptides from plants. Ciba Found Symp. 1994, 186, 91-101.
[36] H.G. Boman. Peptide antibiotics and their role in innate immunity. Annu. Rev. Immunol. 1995, 12, 61–92.

[37] R.E.W. Hancock, H.G. Sahl. Antimicrobial and host defense peptides as new anti-infective therapeutic strategies. Nature Biotech. 2006, 24, 1551–1557.
[38] M. Zasloff. Magainins, a class of antimicrobial peptides from Xenopus skin: isolation, characterization of two active forms, and partial cDNA sequence of a precursor. Proc. Natl. Acad. Sci. U S A. 1987, 84, 5449-5453.
[39] M. Zasloff. Antimicrobial peptides of multicellular organisms. Nature. 2002, 415, 389–395.
[40] N. Mookherjee, M.A. Anderson, H.P. Haagsman, D.J. Davidson. Antimicrobial host defence peptides: functions and clinical potential. Nat. Rev. Drug. Discov. 2020, 19, 311–332.
[41] R.M. Epand, C. Walker, R.F. Epand, N.A. Magarvey. Molecular mechanisms of membrane targeting antibiotics. Biochim. Biophys. Acta. 2016, 1858, 980-987.
[42] Y. Pouny, D. Rapaport, A. Mor, P. Nicolas, Y. Shai. Interaction of antimicrobial dermaseptin and its fluorescently labeled analogues with phospholipid membranes. Biochemistry. 1992, 31, 12416-12423.
[43] L. Yang, T.A. Harroun, T.M. Weiss, L. Ding, H.W. Huang. Barrel-stave model or toroidal model? A case study on melittin pores. Biophys. J. 2001, 81, 1475–1485.
[44] M. Mihajlovic, T. Lazaridis. Charge distribution and imperfect amphipathicity affect pore formation by antimicrobial peptides. Biochim. Biophys. Acta. 2012, 1818, 1274-1283.
[45] J. Wang, X. Dou, J. Song, Y. Lyu, X. Zhu, L. Xu, W. Li, A. Shan. Antimicrobial peptides: Promising alternatives in the post feeding antibiotic era. *Med. Res. Rev.* 2019, 39, 831–859.
[46] H. Jenssen, P. Hamill, R.E. Hancock. Peptide antimicrobial agents. *Clin. Microbiol. Rev.* 2006, 19, 491–511.
[47] A. Hollmann, M. Martinez, P. Maturana, L.C. Semorile, P.C. Maffia. Antimicrobial peptides: interaction with model and biological membranes and synergism with chemical antibiotics. *Front. Chem.* 2018, 6:204.
[48] S.A Loutet, R.S. Flannagan, C. Kooi, P.A. Sokol, M.A. Valvano. A complete lipopolysaccharide inner core oligosaccharide is required for resistance of Burkholderia cenocepacia to antimicrobial peptides and bacterial survival in vivo. J. Bacteriol. 2006, 188, 2073–2080.
[49] D.C. Nelson, J. Garbe, M. Collin. Cysteine proteinase SpeB from Streptococcus pyogenes—a potent modifier of immunologically important host and bacterial proteins. Biol. Chem. 2011, 392, 1077–1088.
[50] C.Y. Okumura, V. Nizet. Subterfuge and sabotage: evasion of host innate defenses by invasive gram-positive bacterial pathogens. Annu. Rev. Microbiol. 2014, 68, 439–458.
[51] J.M. Conlon, J. Kolodziejek, N. Nowotny. Antimicrobial peptides from ranid frogs: taxonomic and phylogenetic markers and a potential source of new therapeutic agents. *Biochim. Biophys. Acta.* 2004, 1696, 1–14.

[52] M. Simmaco, D. De Biase, C. Severini, M. Aita, G.F. Erspamer, D. Barra, F. Bossa. Purification and characterization of bioactive peptides from skin extracts of *Rana esculenta*. *Biochim. Biophys. Acta*. 1990, 1033, 318–323.
[53] M.L. Mangoni. Temporins, anti-infective peptides with expanding properties. *Cell. Mol. Life Sci*. 2006, 63, 1060–1069.
[54] M. Simmaco, G. Mignogna, S. Canofeni, R. Miele, M.L. Magoni, D. Barra. Temporins, antimicrobial peptides from the European red frog Rana temporaria. *Eur. J. Biochem*. 1996, 242, 788–792.
[55] M.L. Mangoni, A.D. Grazia, F. Cappiello, B. Casciaro, V. Luca. Naturally occurring peptides from *Rana temporaria*: antimicrobial properties and more. *Curr. Top. Med. Chem*. 2016, 16, 54-64.
[56] M.L. Mangoni, Y. Shai. Temporins and their synergism against Gram-negative bacteria and in lipopolysaccharide detoxification. *Biochim. Biophys. Acta*. 2009, 1788, 1610-1619.
[57] S.M. Romero, A.B. Cardillo, M.C. Martínez Ceron, S.A. Camperi, S.L. Giudicessi. Temporins: an approach of potential pharmaceutic candidates. *Surg. Infect. (Larchmt)*. 2020, 21, 309–322.
[58] A.K. Mahalka, P.K. Kinnunen. Binding of amphipathic α-helical antimicrobial peptides to lipid membranes: lessons from temporins B and L. *Biochim. Biophys. Acta*. 2009, 1788, 1600-1609.
[60] A.C. Rinaldi, M.L. Mangoni, A. Rufo, C. Luzi, D. Barra, H. Zhao, P.K. Kinnunen, A. Bozzi, A. Di Giulio, M. Simmaco. Temporin L: antimicrobial, haemolytic and cytotoxic activities, and effects on membrane permeabilization in lipid vesicles. *Biochem. J*. 2002, 368, 91–100.
[61] A. Giacometti, O. Cirioni, R. Ghiselli, F. Mocchegiani, F. Orlando, C. Silvestri, A. Bozzi, A. Di Giulio, C. Luzi, M.L. Mangoni, D. Barra, V. Saba, G. Scalise, A.C. Rinaldi. Interaction of antimicrobial peptide Temporin L with lipopolysaccharide *in vitro* and in experimental rat models of septic shock caused by Gram-Negative bacteria. *Antimicrob. Agents Chemother*. 2006, 50, 2478–2486.
[62] Y. Rosenfeld, D. Barra, M. Simmaco, Y. Shai, M.L. Mangoni. A synergism between temporins toward Gram-negative bacteria overcomes resistance imposed by the lipopolysaccharide protective layer. *J. Biol. Chem*. 2006, 281, 28565–28574.
[63] A. Di Somma, C. Avitabile, A. Cirillo, A. Moretta, A. Merlino, L. Paduano, A. Duilio, A. Romanelli. The antimicrobial peptide Temporin L impairs *E. coli* cell division by interacting with FtsZ and the divisome complex. *Biochim. Biophys. Acta Gen. Subj*. 2020, 1864:129606.
[64] A. Carotenuto, S. Malfi, M.R. Saviello, P. Campiglia, I. Gomez-Monterrey, M.L. Mangoni, L.M. Gaddi, E. Novellino, P. Grieco. A different molecular mechanism underlying antimicrobial and hemolytic actions of Temporins A and L. *J. Med. Chem*. 2008, 51, 2354–2362.

CHAPTER 2

CHEMICAL DECORATION OF PROLINE

This chapter is published in:

Buommino, E., Carotenuto, A., Antignano, E., **Bellavita, R.**, Casciaro, B., Loffredo, M.R., Merlino, F., Novellino, E., Mangoni, M.L., Nocera, F.P., Brancaccio, D., Punzi, P., Roversi, D., Ingenito, R., Bianchi, E., Grieco, P. The outcomes of decorated prolines in discovering novel antimicrobial peptides from Temporin-L. *ChemMedChem.* 14, 1283–1290 (2019).

CONTRIBUTIONS: Peptide synthesis.

2.1. TARGETING ESKAPE PATHOGENS

The uncontrollable growth of antibiotic resistance by superbugs, including the ESKAPE pathogens (*Enterococcus faecium, Staphylococcus aureus, Klebsiella pneumoniae, Acinetobacter baumannii, Pseudomonas aeruginosa, and Escherichia coli*), is the second cause of human mortality worldwide.[1,2] These resistant ESKAPE pathogens cause infectious diseases above all in hospitals, since their spread is very quickly in immune compromised-patients.[3] Among them, methicillin-resistant *Staphylococcus aureus* (MRSA) has become the leading pathogen in hospitals worldwide.[4] Vancomycin has long been considered the privileged drug for the treatment of MRSA infections, which can cause pneumonia and sepsis.[4] The methicillin resistance is conferred by expression of *mecA* gene encoding an altered penicillin binding protein PBP2a, which has a low affinity for all β-lactam antibiotics and enables the bacteria to synthesize cell-wall and to survive.[5] *Staphylococcus* strains isolated mainly from skin and mucosa of dogs is *Staphylococcus pseudointermedius*, which can cause skin infections and otitis externa along with *M. pachydermatis* yeast.[6] Methicillin-resistant *S. pseudointermedius* (MRSP) and MRSA infections are a huge challenge in veterinary medicine.[7] The close contact between household pets and their owners facilitates the transmission of MRSA and MRSP infections from household pets to owners and vice versa.[7] The presence of MRSP in food producing animals and in people working with food animals is considered a risk factor for human health, increasing the mortality rate in population.[8] In addition, antibiotic resistance developed by Gram-negative strains represents a demanding issue, since no novel class of drugs against Gram-negative strains has been introduced during the last four decades.[9,10] For example, *Escherichia coli* poses a large number of resistance genes that are the principal cause of treatment failures in both human and veterinary medicine.[11–13] The emergence of infections by ESKAPE pathogens (*e.g.* MRSA, MRSP, *E. coli, P. aeruginosa*) and the failure of antibiotics in their treatment has rung alarm bell in field of research,

leading to the discovery of novel antimicrobial agents such as antimicrobial peptides (AMPs). Among AMPs, temporins might represent an alternative to traditional antibiotics since act with a different mode of action from conventional antibiotics.[14] Herein, we performed a structure-activity relationship (SAR) study on interesting Temporin L (TL) analogue,[15] named [Pro^3]TL, with the aim to discover novel promising anti-infective agents in both human and veterinary medicine. Proline residue, existing in the majority of naturally occurring membrane-acting peptides, has a crucial role in their structures being a potent α-helix breaking amino acid and influences their biological activity.[16] The incorporation of a Pro residue may reduce the hemolytic activity, but may also facilitate membrane insertion as in antimicrobial peptide maculatin 1.1,[17] or may improve the antimicrobial activity as in AMP gaegurin peptide.[18] In the case of [Pro^3]TL, the replacement of glutamine in position 3 with the proline has induced a β-turn structure in N-terminal centered on Pro^3 (Figure 1), which has caused a drastic reduction in the hemolytic activity in comparison to TL.[19,20]

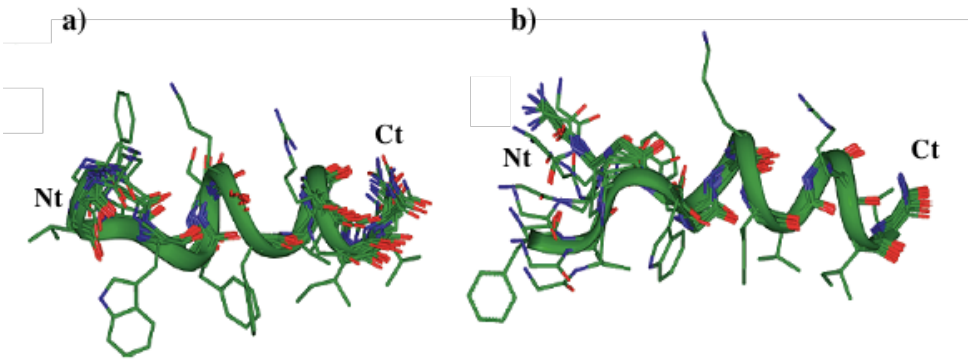

Figure 1. Superposition of the 20 lowest-energy conformers of Pro^3-TL in SDS (a), and Pro^3-TL in DPC (b). In SDS (a), Pro^3-TL showed an a-helix along residues 6–11 and a β-turn centered on Pro^3. In DPC (b), Pro^3-TL showed an a-helix along residues 6–13 and a β-turn centered on 3–5 residues in N-terminal. Heavy atoms are shown with different colors (carbon, green; nitrogen, blue; oxygen, red).[19]

Preserving the low toxicity of [Pro^3]TL, we performed a chemical decoration of proline residue using various chemical functionalities in position 4 of the ring,

modifying the physicochemical properties of [Pro^3]TL peptide and consequently its broad-spectrum antimicrobial activity. The antimicrobial activity of peptides **3–11** was evaluated both on human bacterial strains and on some veterinary bacterial strains. The hemolytic activity was investigated only for the most promising peptides. Conformational analysis by CD spectroscopy was performed for all compounds, while the NMR spectroscopy was carried out only for selected analogues.

2.2. Results and Discussions

2.2.1. Design

A previous SAR study on TL has led to the promising [Pro^3]TL analogue featuring a low hemolytic activity and a satisfactory antimicrobial activity.[15,19] In this study, we selected appropriate functional groups to perform a chemical decoration of proline residue in [Pro^3]TL analogue. Polar electronwithdrawing (fluoro, trifluoromethyl), apolar (methylthio), positively charged (amino), aliphatic (cyclohexyl), or aromatic (phenyl and benzyl) groups were chosen to yield peptides **3–11** (Table 1). A "chemical decoration" of Pro^3 with appropriate functional groups may cause an alteration of physicochemical properties such as hydrophilicity and hydrophobicity, affecting peptide interaction with bacterial membrane. For instance, the incorporation of aliphatic, apolar, and aromatic groups increases peptide hydrophobicity,[21] in contrast an amino group enhances peptide cationicity. In both cases, peptide-membrane interaction may be altered.[22,23] While a high net positive charge could reinforce peptide-membrane interaction, an excessive hydrophobicity could favor peptide aggregation with resultant reduced activity. Besides, an increase of hydrophobicity could promote the binding to mammalian membranes and reduce easily cell selectivity.[21] Therefore, our purpose was to perform a chemical decoration of [Pro^3]TL analogue to improve its broad-spectrum antimicrobial activity, but conserving simultaneously its low hemolytic activity.

Table 1. Antimicrobial activity of designed compounds **3–11**.

Peptides	decorated Pro[3] residue	Sequence
1	-	F V Q W F S K F L G R I L
2		F V **Pro** W F S K F L G R I L
3	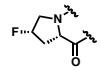	F V **(*cis*-4F-Pro)** W F S K F L G R I L
4		F V **(4,4diF-Pro)** W F S K F L G R I L
5	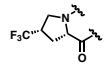	F V **(*cis*-4CF$_3$-Pro)** W F S K F L G R I L
6	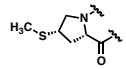	F V **(*cis*-4MeS-Pro)** W F S K F L G R I L
7	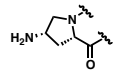	F V **(*cis*-4NH$_2$-Pro)** W F S K F L G R I L
8	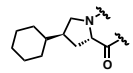	F V **(*trans*-4Chx-Pro)** W F S K F L G R I L
9	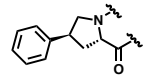	F V **(*trans*-4Ph-Pro)** W F S K F L G R I L
10	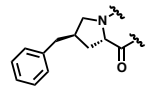	F V **(*trans*-4Bn-Pro)** W F S K F L G R I L
11	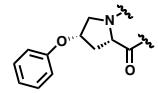	F V **(*cis*-4PhO-Pro)** W F S K F L G R I L

2.2.2. BIOLOGICAL ACTIVITY

Antibacterial activity on human strains. The antimicrobial activity of designed peptides **3–11** was evaluated against some reference bacterial and *Candida* strains in the broth microdilution assay to determine their MIC (Table 2).[24] All synthesized compounds displayed a good antimicrobial activity towards Gram-positive bacterial strains (*B. megaterium* BM11 and *S. epidermidis* ATCC 12228) with MICs values comparable to those of **1** and **2**. Notably, almost all compounds displayed a similar efficacy against *Candida albicans* ATCC 24433, as compound **2**. Peptide **3**, in which

the residue of Pro[3] was replaced with *cis*-4-fluoro-proline, showed a similar antibacterial activity as the parent peptide **2**, on both Gram-negative and Gram-positive bacterial strains. In addition, the activity towards *C. albicans* resulted to be 2-fold lower respect to TL. Peptides **4** and **5**, featuring by 4,4-difluoro-Pro and *cis*-trifluoromethyl-Pro, respectively, had the same behavior on both Gram-positive and Gram-negative strains. Their antimicrobial activity did not increase on Gram-positive strains in comparison to TL, but they resulted to be 2-fold less active than TL toward *P. aeruginosa* ATCC 27853, and their activity on *E. coli* ATCC 25922 was unchanged. Peptide **6,** characterized by the apolar methylthio group on Pro[3], conserved the same activity of peptides **4** and **5** on both Gram-negative and Gram-positive bacteria, but its activity towards *C. albicans* resulted to slightly improved respect to parent [Pro[3]]TL (**2**). Surprisingly, by replacing the Pro[3] with its *trans*-4-cyclohexyl-Pro derivative, the resulting peptide **8** showed a dramatic reduction in activity on *E. coli* ATCC 25922 and lost effect on *P. aeruginosa* ATCC 27853. In addition, the activity towards *C. albicans* resulted to be 2-fold lower than the parent peptide **2**. Finally, analogues **9–11**, all characterized by an aromatic-containing functionality in position 4 of the pyrrolidine ring, *trans*-4-phenyl-Pro (**9**), *trans*-4-benzyl-Pro (**10**), *cis*-4-phenoxy-Pro (**11**), respectively, resulted to be poorly active on *P. aeruginosa* ATCC 27853 (MIC 50 μM), while the activity on *E. coli* ATCC 25922 was 2-fold lower for compounds **10** and **11**, compared to both reference peptides TL (**1**) and [Pro[3]]TL (**2**). However, the anticandidal activity remained almost unchanged with respect to **2**, except for compound **10**, showing a MIC of 25 μM. The one exception of enhancement of activity against Gram-negative was highlighted by a decoration of Pro[3] residue with a positively charged amino group in peptide **7.** In fact, peptide **7** displayed a significant lower MIC (3.12 μM) on *E. coli* ATCC 25922, while conserved a similar activity against *P. aeruginosa* ATCC 27853 in comparison to TL. Furthermore, the anticandidal activity was slightly decreased with respect to **1**.

Table 2. Antimicrobial activity of designed compounds **3–11**.

	MIC values (μM)[a]				
Peptides	*E. coli* ATCC 25922	*P. aeruginosa* ATCC 27853	*B. megaterium* BM11	*S. epidermidis* ATCC 12228	*C. albicans* ATCC 24433
1	12.5	12.5	3.12	3.12	6.25
2	12.5	25.0	3.12	6.25	12.5
3	12.5	12.5	3.12	6.25	12.5
4	12.5	25.0	3.12	3.12	12.5
5	12.5	25.0	3.12	3.12	12.5
6	12.5	25.0	3.12	3.12	6.25
7	3.12	12.5	3.12	3.12	12.5
8	50.0	100	3.12	3.12	12.5
9	12.5	50.0	3.12	3.12	12.5
10	25.0	50.0	3.12	3.12	25.0
11	25.0	50.0	3.12	3.12	12.5

On the basis of these results, the net charge positive seemed to be crucial for the activity toward Gram-negative. In fact, the introduction of an amino group on Pro^3 conferred to peptide **7** a net positive charge of +4 in contrast to other peptides (+3), which promoted an increase of its activity on *E. coli* ATCC 25922 compared to native TL and lead compound [Pro^3]TL. Instead, the net positive charge did not affect the activity on Gram-positive bacteria, since all peptides showed a good activity towards Gram-positive strains.

Antimicrobial activity on veterinary bacterial strains. The activity of peptides **3–11** was evaluated on veterinary bacterial strains, such as *E. coli* and *P. mirabilis* (Gram-negative), *S. pseudintermedius* (Gram-positive), *M. pachydermatis* (yeast). The veterinary clinical isolates were first analyzed by disc diffusion test for the occurrence of antibiotic resistance, demonstrating a strong resistance to most common antibiotics used in the therapy of pet animals (data not shown).

Table 3. Antimicrobial activity of designed compounds **3–11** on veterinary strains.

	MIC values (μM)				
Peptides	*E. coli*	*Proteus mirabilis*	*MSSP*	*MRSP*	*M. pachydermatis*
1	12.5	>100	3.12	3.12	25
2	12.5	>100	3.12	3.12	25
3	>100	>100	1.56	1.56	25
4	12.5	25.0	3.12	3.12	12.5
5	>100	>100	>100	>100	25
6	12.5	>100	3.12	3.12	12.5
7	3.12	>100	6.25	6.25	25
8	>100	>100	3.12	3.12	25
9	>100	>100	3.12	6.25	12.5
10	>100	>100	3.12	3.12	25.0
11	>100	>100	1.56	1.56	12.5

Regarding the activity on Gram-negative strains, only compounds **6** and **7** were active on *E. coli*, in particular, compound **7** resulted in the most potent one with a MIC of 3.12 μM. On the contrary, all other synthesized compounds were inactive against *P. mirabilis* (MIC >100μM). Further interesting results were obtained on *S. pseudintermedius* all peptides, except for peptides **4** and **5**, showed a good activity as parent Pro^{3}TL (**2**). Specifically, compounds **3** and **11** displayed a strong activity against both MSSP and MRSP with a MIC of 1.56 μM. Additionally, the compounds were tested on the yeast *M. pachydermatis*. Good activity was shown for all compounds, especially for **6**, **9**, and **11** with a MIC of 12.5 μM. Overall, compound **11** showed the best activity on both *M. pachydermatis* and *S. pseudintermedius*. Because both strains can be etiological agents in canine pyoderma and otitis, compound **11** may be considered a potential lead compound for combined therapy in the care of pet animals. Taking into account the antimicrobial activity against reference strains and clinical isolates, the compounds **6**, **7**, and **11** showed a better

activity than compound **2** and for this reason they were selected for further characterization in the hemolysis assay.

Hemolytic activity versus human erythrocytes. The compounds with the best antimicrobial activity (**6**, **7** and **11**) were tested for their effect on circulating blood cells (*i.e.* erythrocytes) and the percentages of hemolysis are reported in Figure 2 and compared to those of the parent peptide (**2**).

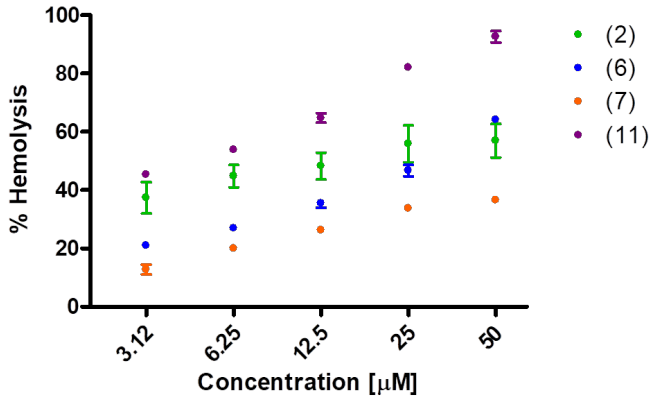

Figure 2. Hemolytic activity of compounds **6**, **7** and **11** compared to the parent peptide **2**. Percentages of hemolysis ± SEM were calculated with respect to the complete lysis of erythrocytes in distilled water.

Compound **11,** characterized by *cis*-4-phenoxy-Pro, showed a potent hemolytic effect even at low concentrations (> 40% at 3.12 or 6.25 μM), probably due to its high hydrophobic content that creates strong interactions with eukaryotic membranes. In comparison, compound **6** was found to be less hemolytic than compounds **11** and **2** at a concentration range from 3.12 to 25 μM, but more active than the parent peptide **2** at the highest concentration (*i.e.* 50 μM). Interestingly, compound **7** was less toxic than compound **2** ($p<0.01$) and all the other tested analogs at all concentrations tested. This makes peptide **7** the compound with the best biological profile.

2.2.3. STRUCTURAL STUDIES

CD analysis. To explore the conformational changes of TL analogues synthesized in this study, we performed CD spectroscopy studies in phosphate buffer (PB, pH 7.4), sodium dodecylsulphate (SDS), dodecylphosphocholine (DPC), and DPC/SDS 9:1 micelle solutions (Figure 3). These micelles were used as mimetics of bacterial, mammalian, and yeast membranes, respectively.[26,27]

Secondary structure content (Table 4) was evaluated from CD spectra by the Bestsel method.[28] CD spectra in PB revealed the prevalence of disordered conformers for all compounds characterized by a minimum close to 200 nm (Figure 3a and Table 4). For some analogues (**8**, **10**, and **11**) a relatively intense minimum at 228 and maximum at 190 nm were observed. These spectral features were associated by Bestsel prediction to an increase of the β-sheet and/or β-turn structures content (Table 4). In SDS, DPC, and DPC/SDS 9:1 membrane mimetic solutions, CD spectra indicated more structured peptides (Figures 3b–d).

In all cases, two minima close to 208 and 222 nm were obtained, indicating helical propensity (Table 4). Indeed, helical percentage of the peptides varied from 21 to 52% in SDS and from 24 to 60% in DPC/SDS according to Bestsel prediction (Table 4). Nonetheless, antibacterial activity on Gram-positive strains and antifungal activity were almost identical regardless of helical content. For example, peptides **7** (42.7% helix in SDS) and **8** (21.3% helix in SDS) had the same activity on both *B. megaterium* and *S. epidermidis* (Table 2). The relationships between the conformations of the synthesized peptides and the antibacterial activity on Gram-negative bacteria is more intriguing.

Table 4. Secondary structure* percentages of TL analogues.

Pept	PB solution				DPC solution				SDS solution				DPC/SDS Solution			
	h	*b*	*t*	*r*	*h*	*b*	*t*	*r*	*h*	*b*	*t*	*r*	*h*	*b*	*t*	*r*
1	12.7	31.5	14.2	41.5	62.2	2.0	9.5	26.4	47.7	8.7	11.0	32.6	60.5	3.7	11.1	24.7
2	9.6	19.1	18.7	52.7	42.8	16.2	11.2	29.8	45.6	3.4	15.0	36.0	43.2	14.5	12.7	29.5
3	11.9	25.1	16.3	46.7	42.2	9.9	12.8	35.2	42.0	10.9	14.3	32.8	43.5	8.4	13.8	34.3
4	12.3	26.9	16.2	44.5	40.2	17.1	11.0	31.7	43.5	5.9	12.0	38.6	41.0	16.5	11.2	31.3
5	15.3	17.9	14.8	51.9	39.5	13.4	11.3	35.9	51.7	2.8	12.4	33.1	40.9	14.5	11.9	32.7
6	0.0	51.7	13.1	35.2	42.6	8.1	12.4	36.9	44.1	2.3	16.1	37.5	45.3	5.1	13.0	36.7
7	14.9	14.5	16.1	54.5	44.3	16.1	12.0	27.5	42.7	9.4	12.8	35.2	45.1	15.2	11.5	28.2
8	6.1	36.7	16.1	41.0	25.0	13.4	13.5	48.2	21.3	15.8	13.6	49.3	24.4	21.2	12.3	42.1
9	13.3	31.0	16.1	39.7	28.8	17.9	13.4	39.9	32.3	6.7	14.7	46.3	26.5	15.2	16.6	41.7
10	4.8	35.8	18.0	41.3	39.4	6.1	12.9	41.6	30.9	4.2	14.3	50.6	35.8	12.5	12.4	39.3
11	5.5	22.1	27.6	44.8	51.8	6.8	10.8	30.6	48.4	4.2	12.7	34.8	49.9	8.0	13.9	28.2

*h helix, β beta-sheet, t turn, r random coil. Peptide **8** in LPS: h 1.6, β 41.3, t 13.9, r 43.2.

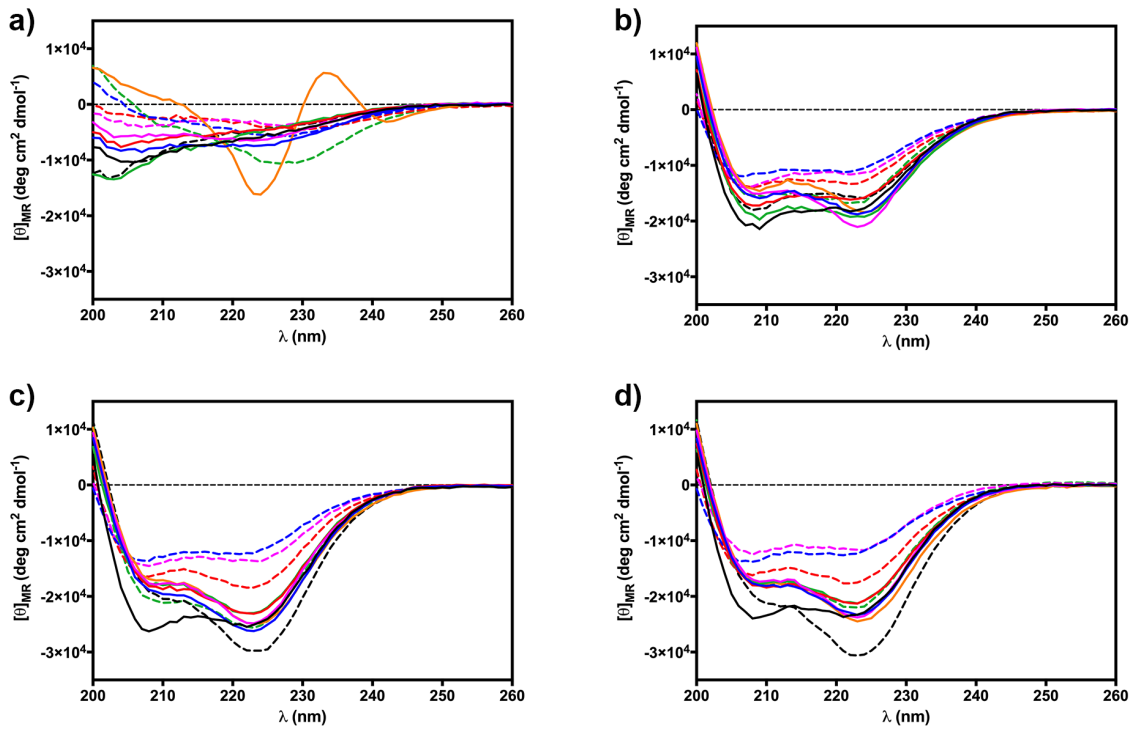

Figure 3. CD spectra of peptide **1** and its analogues **2**-**11** in PB a), SDS b), DPC c), and DPC/SDS 9:1 micelle solutions d). (**1**, black solid line; **2**, blue solid line; **3**, magenta solid line; **4**, red solid line; **5**, green solid line; **6**, orange solid line; **7**, black dashed line; **8**, blue dashed line; **9**, magenta dashed line; **10**, red dashed line; **11**, green dashed line).

Three peptides (**8**, **10**, and **11**) showed lower activity than the parent **2** against both the human Gram-negative bacteria tested (Table 2). Those peptides had different degrees of helical content in SDS (from 21 to 48%), hence, there is not a clear correlation between antibacterial activity and helical content. Interestingly enough, peptides **8**, **10**, and **11** showed a relatively high propensity to the β-sheet or turn formation in PB solution, which could indicate their tendency to aggregate in amyloid-like structures. It has been hypothesized that this aggregation tendency increased in contact with the external membrane of the Gram-negative bacteria, in particular, in the presence of lipopolysaccharides (LPS). This possibility was tested by acquiring the CD spectrum of peptide **8**, which was almost inactive against Gram-negative bacteria, in the presence of LPS micelles (Figure 4).

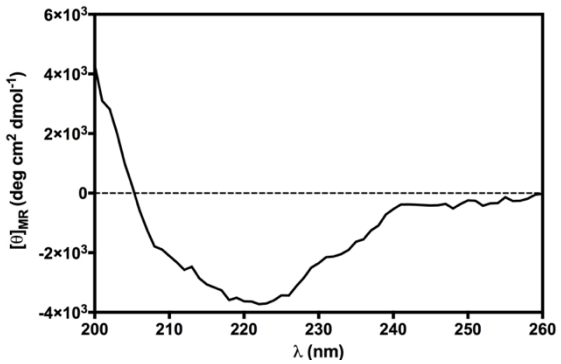

Figure 4. CD spectrum of peptide **8** (25 μM) in a 100 μM LPS solution.

The spectrum displayed a minimum at 220 nm and a maximum at 196 nm, and its deconvolution by Bestsel algorithm gave a β-sheet content higher than 40%, a situation often associated with amyloid-like peptide oligomers.[14] Therefore, peptide **8** inactivity against Gram-negative bacteria could be due to its oligomeric state induced by contact with LPS. The large size of the oligomer makes it more difficult for the peptide to diffuse through the cell wall into the target cytoplasmic membrane.[30] Notably, TL, in contrast to peptide **8**, was active against Gram-negative bacteria differently, because it showed a high helical propensity and disassembles in contact with LPS.[31] Compound **7** showed very high activity against

E. coli, being 4-fold higher than both its parent **2** and the native TL (**1**). Notably, the activity of peptide **7** against *E. coli* was also confirmed on the veterinary strain (Table 3). Considering the effect of the conformational propensities of the peptides on their hemolytic effect, peptide **11** showed the highest hemolytic effect (Figure 2) and also the highest helical content (Table 4) in the eukaryotic mimetic DPC solution. This result was in accordance with our previous result correlating peptide helicity in DPC with its hemolytic effect.[14] Peptides **2**, **6**, and **7** displayed similar helical content (Table 4). The lower hemolytic potency of peptide **7** could be tentatively explained by considering our previous result on the mechanism of the hemolytic action of TL (**1**) and its derivatives. In fact, studying the interaction between **1** and zwitterionic DPC micelles by NMR and MD simulations,[15,19] we found that **1** inserts into the micelle, perpendicular to the membrane, with the N terminus deeply buried in the micelle hydrophobic core, thus unveiling the barrel-stave mechanism.[19] The presence of a hydrophilic group on Pro^3 within the N-terminal region, such as in peptide **7**, probably prevented the peptide from exerting the above-described mechanism, thus explaining its low toxicity.

NMR analysis of peptides 7 and 8. Considering the very interesting antimicrobial activity of compound **7**, in particular against Gram-negative bacteria, and its low hemolytic effect, it was also investigated by NMR spectroscopy. Moreover, peptide **8**, which was almost inactive against Gram-negative, was also investigated by NMR for comparison. NMR spectroscopy was performed in SDS micellar solution. Complete ^{1}H NMR chemical shift assignments were effectively achieved for both peptides according to the Wüthrich procedure.[32] Peptide **7** in SDS solution exhibited NMR spectral features pointing to helical propensity. Structure calculation gave an ensemble of 20 structures (Figure 5a) satisfying the NMR-derived constraints (violations smaller than 0.10 Å). Backbone is well defined, with a RMDS = 0.34 Å. An inverse γ-turn centered on the amino-Pro^3 can be observed at the N-terminus followed by an α-helix from Trp^4 to Leu^{13} (Figure 5a). Interestingly, the peptide

assumes an amphipathic structure with a positive side (Figure 5a) and a hydrophobic side (lower side in Figure 5b). In particular, the *cis*-4-amino group on Pro^{3} points towards the other positively charged groups (Lys^{7} amino and Arg^{11} guanidinium groups) enlarging the charged peptide surface. Diagnostic NMR parameters observed for **8** also indicated conformational propensity toward helical or turn structures but with higher flexibility. Calculated structures, shown in Figure 5b, were less defined than those obtained for **7** (backbone heavy atoms RMSD=0.72 Å), which was in accordance with the CD result indicating a minor content of helix structure compared to **1**, **2**, and **7** (Table 4). A helix structure was observable from residue 5 to 12 in many structures of the ensemble (18/20), while the N-terminal region was in extended conformation. Notably, the cyclohexyl group was positioned near the phenyl rings of Phe^{1} and Phe^{5} forming a hydrophobic cluster. The overall structure was amphipathic with the cyclohexyl cluster oriented on the same side of Phe^{8}, Leu^{9}, and Ile^{12} (Figure 5b). However, the loss of the N-terminal helical segment, observed in **7** and **8**, did not affect the antimicrobial activity of the TL derivatives, as already demonstrated for peptide **2**.[15,19] In fact, the high flexibility of the N-terminal region of these peptides allowed an optimal orientation of the additional group on the proline for membrane interactions.

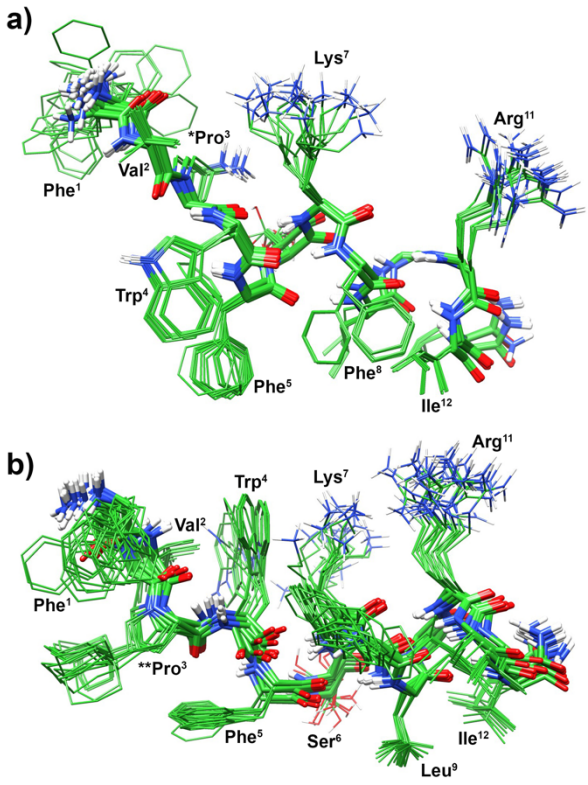

Figure 5. Superposition of the 20 lowest energy conformers of **7** (a, PDB ID code: 6QXB) and **8** (b, PDB ID code: 6QXC) in SDS. Structures were superimposed using the backbone heavy atoms. Only heavy backbone atoms are shown for clarity. Backbone atoms were evidenced as a ribbon. Heavy atoms are shown with different colors (carbon, green; nitrogen, blue; oxygen, red). *Pro: *cis*-4-amino proline. **Pro: *trans*-4-cyclohexyl proline.

This could explain the high activity against Gram-positive bacteria and good activity against fungi observed for all peptides (Table 2). In the same way, an optimal orientation of the positively charged amino group of **7** could explain its increased activity against many Gram-negative strains. In the same way, this flexibility at N-terminus of peptide **7** could also explain its increased activity against many Gram-negative strains. On the other hand, the reduction or loss of activity against Gram-negative bacteria observed in some of the novel peptides was likely due to peptide aggregation as stated above. In fact, the hydrophobic cluster found in the structure of peptide **8** (Figure 5b), but also predictable in other peptides such as **10** and **11**, could work as an aggregation point leading to oligomerization.

2.3. CONCLUSIONS

TL (**1**) has unique anti-yeast and anti-Gram-negative activity among the temporins. These activities were maintained by its analogue [Pro^3]TL (**2**), which also showed a reduced cytotoxicity against red blood cells. By decorating the Pro residue with several chemical functionalities (fluoro, trifluoromethyl, amino, cyclohexyl, phenyl and benzyl groups) in [Pro^3]TL (**2**), we have obtained interesting candidates for antimicrobial clinical studies. In particular, peptide **7** characterized by a *cis*-4-amino-Pro residue, showed an improved activity than the parent peptide **2** against human and veterinary Gram-negative bacterial strains. At the same time, it conserved the activity of **2** on Gram-positive bacteria and yeasts and a low toxicity on red blood cells. Peptide **11** was also interesting due to its activity against veterinary strains but, because of its toxicity, it could be considered as a starting point for further chemical modifications. More generally, we demonstrated that the decoration of Pro^3 on peptide **2** is a successful strategy to obtain active antimicrobial peptides, since the flexibility of the N-terminal peptide region allows an optimal orientation of additional group to establish strong membrane interactions and increase antimicrobial activity.

2.4. EXPERIMENTAL SECTION

2.4.1. CHEMISTRY

Materials. All N$^{\alpha}$-Fmoc-protected amino acids were purchased from NovaBiochem. Other non-natural N$^{\alpha}$-Fmoc-amino acids, namely Fmoc-l-Pro(4,4-diF2), Fmoc-l-Pro(*cis*-4-F), Fmoc-l-Pro(*cis*-4-CF_3), Fmoc-l-Pro(*cis*-4-OPh), Fmoc-l-Pro(*trans*-4-Bz), Fmoc-l-Pro(*trans*-4-Ph), Fmoc-l-Pro(*trans*-4-Chx), and Fmoc-l-Pro(*cis*-4-SMe), were purchased from Polypeptide Laboratories. Fmoc-l-Pro(*cis*-4-NHBoc) was purchased from 3B Scientific Corp. The Rink amide resin was purchased from

Chem-Impex. Coupling reagents were purchased as follows: N,N'-diisopropylcarbodiimide (DIC) from Sigma-Aldrich, ethyl cyano(hydroxyimino)acetate (Oxyma Pure) from Chem-Impex, 1-hydroxy-7-azabenzotriazole (HOAt) from CreoSalus. All were reagent grade acquired from commercial sources and used without further purification.

Peptide synthesis. The synthesis of peptides **1–11** was performed by solid-phase peptide synthesis (SPPS) using Fmoc/tBu chemistry. All peptides were assembled on a Rink amide PS resin 100–200 mesh, (0.2 mmol scale with 0.47 mmol × g^{-1} of loading). The synthesis of peptides **1** and **2** was performed manually using a Microwave CEM Accent instrument. Amino acids (3 equiv) were acylated using equimolar amounts of DIC and Oxyma as activators. Double coupling conditions: 75°C, 170 W, 15 min, then 90°C, 30 W, 110 min, were used for all amino acids. The synthesis of all other peptides was performed on a Liberty Blue microwave synthesizer (CEM corporation) using a 5-fold excess of amino acids and equimolar amounts of DIC and Oxyma. The synthesis proceeded on the synthesizer up to Trp^4, followed by acylation with the different pyrrolidine analogues for each sequence by manual synthesis using 3 equivalents of each amino acid and equimolar amounts of activators DIC and HOAt in DMF. The last two residues Val^2 and Phe^1 were acylated by double acylation with DIC and HOAt as activators. The final peptide resins were washed and dried with CH_2Cl_2, MeOH, and Et_2O. Peptide **1** and its analogues **2–11** were cleaved from the resin using a solution of TFA/TIS/phenol/H_2O (87:3:5:5, *v*/*v*/*v*) for 2 h. The resins were filtered, and peptide solutions were precipitated with MTBE. The peptide precipitates were centrifuged and washed with fresh MTBE. The peptide pellets were dried dissolved in 50:50 H_2O/CH_3CN and lyophilized. Purification of peptides was performed by preparative reversed phase chromatography on a Waters 2545 HPLC system equipped with a 2489 UV detector on a Waters XBridgeTM C18 preparative column (130 Å, 5μm, 150 × 50 mm) using

as eluents (A) 0.1% TFA in water and (B) 0.1% TFA in CH_3CN. All fractions with the highest purity were collected and lyophilized, obtaining peptides with a purity >95%. Purified peptides were characterized on an Acquity UPLC Waters chromatograph, using a Waters BEH130 C18 Acquity column (2.1 × 100 mm, 1.7 μm, at 45°C) for compounds **1–6** and an Aeris PEPTIDE XB-C18 100 Å column (2.1 × 100 mm, 2.6 μm, at 45°C) for compounds **7–11**, using as eluents (A) 0.1% TFA in water and (B) 0.1% TFA in CH_3CN, and by ESI on an Acquity SQ2 Mass Detector (Table 5).

Table 5. Analytical data of compounds **1–11.**

Cmpd#	R_t(min)	MW calcd	MW found
1	3.15	1640.01	1641.2
2	3.34	1609.00	1610.2
3	3.47	1626.99	1628.2
4	3.51	1644.98	1646.3
5	3.74	1677.00	1678.0
6	3.61	1655.09	1655.9
7	3.64	1624.02	1625.5
8	3.69	1691.15	1692.6
9	3.08	1685.10	1686.6
10	3.20	1699.13	1700.2
11	3.25	1702.10	1702.5

2.4.2. BIOLOGY

Antimicrobial assay. The MIC values were obtained by adapting the microbroth dilution method outlined by the Clinical and Laboratory Standards Institute, using sterile 96-well plates (Falcon NJ, USA). Aliquots (50 μL) of bacteria in mid-log phase at a concentration of 2×10^6 colony-forming units (CFU) per mL (5×10^4 CFU mL^{-1} for *C. albicans*) in culture medium (Mueller–Hinton, MH or Winge broth, WB, for *C. albicans*, and Sabouraud broth for *M. pachydermatis*) were added to 50 μL of MH/WB containing the peptide in serial 2-fold dilutions in water.[29] Peptide dilutions ranged from 0.1 to 100 μM. MICs were considered as

the peptide concentration at which 100% inhibition of microbial growth is visually observed after 18–20 h of incubation at 37°C (30°C for yeasts). Each MIC value is the average of at least three independent experiments.

Hemolytic assay. The hemolytic activity was measured on sheep red blood cells (OXOID, SR0051D).[20] Briefly, aliquots of erythrocyte suspension (1×10^8 cells mL^{-1}) in 0.9% (w/v) NaCl were incubated with serial 2-fold dilutions of the peptides in water for 40 min at 37°C with gentle shaking. The samples were then centrifuged for 5 min at 900×g and the absorbance of the supernatant was measured at 415 nm using a microplate reader (Infinite M200; Tecan, Salzburg, Austria). The complete lysis of red blood cells was measured by suspending erythrocytes in distilled water.

2.4.3. CONFORMATIONAL ANALYSIS

Circular dichroism spectroscopy. Circular dichroism spectra were recorded at 25°C using quartz cells of 0.1 cm path length with a JASCO J-710 CD spectropolarimeter (JASCO International Co. Ltd.). Measurements were run in the 260–185 nm spectral range, 1 nm bandwidth, 16 s response time, and 2 nm min-1 scanning speed. The concentration of peptides was 100 μM in 10 mM, sodium phosphate buffer (pH 7.4), SDS (20 mM), DPC (20 mM), or DPC/SDS (18/2 mM) micellar solutions.[29] The Bestsel algorithm was used to extract secondary structure content. A CD spectrum of peptide **8** was also acquired in LPS 100 μM.

NMR spectroscopy. The samples for NMR spectroscopy were prepared by dissolving the appropriate amount of peptides in 0.55 mL of 1H2O, 0.05 mL of 2H2O to obtain a concentration of 1–2 mM peptides and 200 mM [D25]SDS.[32] The NMR experiments were performed at pH 5.0. NMR spectra were recorded on a Varian Unity INOVA 700 MHz spectrometer equipped with a z-gradient 5

mm triple-resonance probe head. All spectra were recorded at a temperature of 25°C. One-dimensional (1D) NMR spectra were recorded in the Fourier mode with quadrature detection. Two-dimensional (2D) DQF-COSY, TOCSY, and NOESY spectra were recorded in the phase-sensitive mode using the method from States *et al*. Data block sizes were 2048 addresses in t2 and 512 equidistant t1 values. A mixing time of 80 ms was used for the TOCSY experiments. NOESY experiments were run with mixing times in the range of 100–200 ms. The qualitative and quantitative analysis of DQF-COSY, TOCSY, and NOESY spectra were obtained using the interactive program package XEASY.

The structure was determined by NOESY spetra that were collected with a mixing time of 100 ms. The NOE cross-peaks were integrated with the XEASY program and were converted into upper distance bounds using the CALIBA program incorporated into the program package CYANA. For each examined peptide, an ensemble of 200 structures was generated with the simulated annealing of the program CYANA.

2.5. REFERENCES

[1] J. Davies, D. Davies. Origins and evolution of antibiotic resistance. Microbiol. Mol. Biol. Rev. 2010, 74, 417 –433.

[2] S.C. Davies, T. Fowler, J. Watson, D.M. Livermore, D. Walker. Annual report of the chief medical officer: infection and the rise of antimicrobial resistance. Lancet. 2013, 381, 1606 – 1609.

[3] S. Maria-Neto, K.C. de Almeida, M.L. Macedo, O.L. Franco. Understanding bacterial resistance to antimicrobial peptides: from the surface to deep inside. Biochim. Biophys. Acta. 2015, 1848, 3078–3088.

[4] Y. Guo1, G. Song, M. Sun, J. Wang, Y. Wang. Prevalence and therapies of antibiotic-resistance in Staphylococcus aureus. Front. Cell. Infect. Mi. 2020, 10, 107.

[5] H.F. Chambers, F.R. DeLeo. Waves of resistance: Staphylococcus aureus in the antibiotic era. Nat. Rev. Microbiol. 2009, 7, 629–641.

[6] W. Kmieciak, E.M. Szewczyk. Are zoonotic *Staphylococcus pseudintermedius* strains a growing threat for humans?. Folia Microbiol (Praha). 2018, 63, 743–747.

[7] M.G. Papich. Antibiotic treatment of resistant infections in small animals. Vet. Clin. North Am. Small Anim. Pract. 2013, 43, 1091–1107.
[8] J.S. Weese, E. van Duijkeren. Methicillin-resistant *Staphylococcus aureus* and *Staphylococcus pseudintermedius* in veterinary medicine. Vet. Microbiol. 2010, 27, 418–429.
[9] R.J. Fair, Y. Tor. Antibiotics and bacterial resistance in the 21st century. Perspect. Medicin. Chem. 2014, 6, 25–64.
[10] R. Maviglia, R. Nestorini, M. Pennisi. Role of old antibiotics in multidrug resistant bacterial infections. Curr. Drug. Targets. 2009, 10, 895–905.
[11] K. Sen, T. Berglund, M.A. Soares, B. Taheri, Y. Ma, L. Khalil1, M. Fridge, J. Lu, R.J. Turner. Antibiotic resistance of *E. coli* isolated from a constructed wetland dominated by a crow roost, with emphasis on ESBL and AmpC containing *E. coli*. *Front. Microbiol*. 2019, 10:1034.
[12] Y. Sàenz, L. Brinas, E. Domínguez, J. Ruiz, M. Zarazaga, J. Vila, C. Torres. Mechanisms of resistance in multiple-antibiotic-resistant *Escherichia coli* strains of human, animal, and food origins. *Antimicrob. Agents. Chemiother*. 2004, 48, 3996–4001.
[13] L. Poirel, J.Y. Madec, A. Lupo, A.K. Schink, N. Kieffer, P. Nordmann, S. Schwarz. Antimicrobial resistance in *Escherichia coli*. Microbiol. Spectr. 2018, 6.
[14] M.L. Mangoni, A.C. Rinaldi, A. Di Giulio, G. Mignogna, A. Bozzi, D. Barra, M. Simmaco. Structure-function relationships of temporins, small antimicrobial peptides from amphibian skin. Eur. J. Biochem. 2000, 267, 1447–1454.
[15] A. Carotenuto, S. Malfi, M.R. Saviello, P. Campiglia, I. Gomez-Monterrey, M.L. Mangoni, L.M. Gaddi, E. Novellino, P. Grieco. A different molecular mechanism underlying antimicrobial and hemolytic actions of temporins A and L. J. Med. Chem. 2008, 51, 2354–2362.
[16] E. Azuma, N. Choda, M. Odaki, Y. Yano, K. Matsuzaki. Improvement of therapeutic index by the combination of enhanced peptide cationicity and proline introduction. ACS Infect. Dis. 2020, 6, 2271–2278.
[17] D. I. Fernandez, T.H. Lee, M.A. Sani, M.I. Aguilar, F. Separovic. Proline facilitates membrane insertion of the antimicrobial peptide maculatin 1.1 via surface indentation and subsequent lipid disordering. Biophys. J. 2013, 104, 1495–1507.
[18] J.Y. Suh, Y.T. Lee, C.B. Park, K.H. Lee, S.C. Kim, B.S. Choi. Structural and functional implications of a proline residue in the antimicrobial peptide gaegurin. *Eur. J. Biochem*. 1999, 266, 665–674.
[19] M.R. Saviello, S. Malfi, P. Campiglia, A. Cavalli, P. Grieco, E. Novellino, A. Carotenuto. New insight into the mechanism of action of the temporin antimicrobial peptides. *Biochemistry*. 2010, 49, 1477–1485.
[20] M.L. Mangoni, A. Carotenuto, L. Auriemma, M.R. Saviello, P. Campiglia, I. Gomez-Monterrey, S. Malfi, L. Marcellini, D. Barra, E. Novellino, P. Grieco.

Structure-activity relationship, conformational and biological studies of temporin L analogues. *J. Med. Chem.* 2011, 54, 1298–1307.
[21] Y. Chen, M.T. Guarnieri, A.I. Vasil, M.L. Vasil, C.T. Mant, R.S. Hodges. Role of peptide hydrophobicity in the mechanism of action of α-helical antimicrobial peptides. *Antimicrob. Agents Chemother.* 2007, 51, 1398–1406.
[22] M. Stark, L. Liu, C.M. Deber. Cationic hydrophobic peptides with antimicrobial activity. *Antimicrob. Agents Chemother.* 2002, 46, 3585–3590.
[23] M. Mahlapuu, J. Hakansson, L. Ringstad, C. Bjorn. Antimicrobial peptides: an emerging category of therapeutic agents. Front. Cell. Infect. Microbiol. 2016, 6, 194.
[24] F. Merlino, A. Carotenuto, B. Casciaro, F. Martora, M.R. Loffredo, R. Di Grazia, A.M. Yousif, D. Brancaccio, L. Palomba, E. Novellino, M. Galdiero, M.R. Iovene, M.L. Mangoni, P. Grieco. Glycine-replaced derivatives of [Pro3, DLeu9] TL, a temporin L analogue: evaluation of antimicrobial, cytotoxic and hemolytic activities. Eur. J. Med. Chem. 2017, 139, 750–761.
[25] E.C. Ledbetter, J.K. Starr. Malassezia pachydermatis keratomycosis in a dog. Med. Mycol. Case Rep. 2015, 10, 24–26.
[26] P. Grieco, A. Carotenuto, L. Auriemma, A. Limatola, S. Di Maro, F. Merlino, M.L. Mangoni, V. Luca, A. Di Grazia, S. Gatti, P. Campiglia, I. Gomez-Monterrey, E. Novellino, A. Catania. Novel α-MSH peptide analogues with broad spectrum antimicrobial activity. PLoS One. 2013, 8.
[27] P. Grieco, V. Luca, L. Auriemma, A. Carotenuto, M.R. Saviello, P. Campiglia, D. Barra, E. Novellino, M.L. Mangoni. Alanine scanning analysis and structure–function relationships of the frog-skin antimicrobial peptide temporin-1Ta. J. Pept. Sci. 2011, 17, 358–365.
[28] A. Micsonai, F. Wien, L. Kernya, Y.H. Lee, Y. Goto, M. Refrégiers, J. Kardos. Accurate secondary structure prediction and fold recognition for circular dichroism spectroscopy. Proc. Natl. Acad. Sci. U S A. 2015, 112, 3095-3103.
[29] P. Grieco, A. Carotenuto, L. Auriemma, M.R. Saviello, P. Campiglia, I. Gomez-Monterrey, L. Marcellini, V. Luca, D. Barra, E. Novellino, M.L. Mangoni, Biochim. The effect of d-amino acid substitution on the selectivity of temporin L towards target cells: identification of a potent anti-Candida peptide. Biophys. Acta. 2013, 1828, 652–660.
[30] M. Lindberg, J. Jarvet, U. Langel, A. Gräslund. Secondary Structure and Position of the Cell-Penetrating Peptide Transportan in SDS Micelles As Determined by NMR. Biochemistry. 2001, 10, 3141–3149.
[31] Y. Rosenfeld, D. Barra, M. Simmaco, Y. Shai, M.L. Mangoni. A synergism between temporins toward Gram-negative bacteria overcomes resistance imposed by the lipopolysaccharide protective layer. J. Biol. Chem. 2006, 281, 28565–28574.
[32] K. Wütrich in NMR of Proteins and Nucleic Acids, John Wiley & Sons, Inc, New York, 1986.

CHAPTER 3

PROMOTING SELF-ASSEMBLING BY LIPIDIC TAGS

This chapter is published in:

Bellavita, R., Falanga, A., Buommino, E., Merlino, F., Casciaro, B., Cappiello, F., Mangoni, M.L., Novellino, E., Catania, M.R., Paolillo, R., Grieco, P., Galdiero, S. Novel Temporin L antimicrobial peptides: promoting self-assembling by lipidic tags to tackle superbugs. Journal of Enzyme Inhibition and Medicinal Chemistry. 35, 1751–1764 (2020).

CONTRIBUTIONS: Peptide synthesis; fluorescence assays (Laurdan, Thioflavin T and ANTS/DPX assay); circular dichroism; protease stability assay.

3.1. PEPTIDE SELF-ASSEMBLING

Peptide self-assembly is driven by intra- and intermolecular interactions, involving hydrophobic, charged and aromatic residues for the organization in supramolecular structures.[1] The formation of highly stable assemblies is mainly driven by non-covalent interactions, although are known as weak interactions (2–250 kJ mol^{-1}).[2] Biomimetic peptide-based motifs, such as peptide amphiphiles and lipopeptides, are examples of molecules that can readily self-assemble without losing their activity, but interacting effectively with their biological target.[3] The self-assembling of amphipathic AMPs depends strongly on their amphiphilicity and their secondary structures. Generally, in water solution, AMPs could self-organize in aggregate with polar residues located on the surface of aggregate, while the apolar residues are localized in the core;[4] instead they can self-assemble smoothly in fibrillar amyloid-like nanostructure or helical bundles in membrane environments. This self-assembly might alter the interaction between AMPs and cell membranes and thus their activity could change.[4] However, the self-assembly confers some marked features,[5] such as cell selectivity towards bacterial membranes and not mammalian cells,[6] and high proteolytic stability because self-assembly protects their cleavage sites to proteases, increasing *in vivo* half-life.[2,5] Lipopeptides are a class of amphiphilic AMPs showing a strong self-assembly behavior.[7] They are composed of a hydrophobic moiety covalently attached, *e.g.* fatty acid or a sterol group, which acts as the driving force of the self-assembling process. Among AMPs, temporins have a strong tendency to aggregate in water; in fact temporin L (TL) has higher propensity to aggregate in water, forming a single aggregate as shown in a MD simulation.[9] In addition, an *in silico* study focused on the mechanism of action of TL, have shown that hydrophobic residues, in particular the phenylalanine zipper motif (Phe^1, Phe^5, Phe^8), are involved in the initial peptide binding to the Gram-positive cytoplasmic membrane and in the stabilization of peptide aggregates as tetramers inside the membrane, leading to the formation of large pores and consequential cell death.[10]

This phenylalanine zipper motif mediates also the TL self-assembling in monomer, dimer and trimer aggregates in Gram-negative bacterial membrane, but its mechanism does not seem to be membranolytic as for Gram-positive bacteria.[10] Unfortunately, TL also kills human erythrocytes at its antimicrobial concentration, and earlier structure-activity relationship studies (SAR) showed that this drawback is correlated to its a-helical content.[11–13] By previous SAR studies on TL, two analogue devoid of toxicity to human erythrocytes, [Pro^3,$DLeu^9$] and [Pro^3, $DLeu^9$, $DLys^{10}$],[14,15] were identified, but both compounds did not show an improved antimicrobial activity in comparison to TL. In our study, considering the intrinsic ability of TL to aggregate both in water and in inside the bacterial membrane, we designed a library of lipopeptides by addition of saturated fatty acids with different carbon chain length at N- or C-terminus of [Pro^3,$DLeu^9$] and [Pro^3,$DLeu^9$,$DLys^{10}$], in order to induce the self-assembling state to boost membrane binding and increase their antimicrobial activity, but preserving simultaneously their low cytotoxic activity. The increased hydrophobicity induced by fatty acids may facilitate the incorporation into lipid bilayers[16–18] and induce self-organization into micelles in the bacterial membrane.[19,20] Altogether these effects determine fluidization of bilayer and deformation of packing of the phospholipid acyl chain, causing typically large channel formation and cell death.[21] It is well-known that a too high hydrophobicity may cause cytotoxicity due to a robust binding to eukaryotic cell membranes, hence it is crucial to conserve an accurate hydrophilic/hydrophobic balance, in order that selectivity and specificity of self-assembled AMPs can be finely adjusted.[20] Moreover, the addition of long hydrophobic lipid tails confers the peptides self-organization that makes them also less sensitive to enzymatic degradation.[22] The designed compounds were characterized by means of antimicrobial assays against ATCC reference strains of *S. aureus*, *K. pneumoniae* and *P. aeruginosa* and cytotoxicity assay. The mechanism of action of the most promising peptides was studied by fluorescence assays such as Laurdan, Thioflavin T and leakage assays.

Their self-assembling in aqueous solution was calculated by critical aggregation concentration (CAC) and their conformational analysis was performed by CD spectroscopy. Additionally, the most active peptide was preliminarily evaluated for its activity against clinically isolated *S. aureus*, *K. pneumoniae* and *P. aeruginosa* strains, and finally, its biostability in human serum was assessed.

3.2. RESULTS AND DISCUSSIONS

3.2.1. DESIGN

In order to induce self-assembling properties to improve membrane binding and broad-spectrum antimicrobial activity, herein, we designed a library of lipopeptides by the addition of fatty acids of variable length at the N- and C-termini of peptides **1A** and **1B**. Valeric, heptanoic, undecanoic and tridecanoic acids were linked at the N-terminus of **1A** and **1B** (Table 1), to obtain, respectively, peptides **2A–5A** and **2B–5B**. After the first screening of biological activity, we designed peptide **C** featured by pentyl chain in para position of the Phe[1] aromatic ring preserving the net positive charge of +4 as the peptide **1B**, in order to investigate the activity towards Gram-negative strains. Besides, we investigated the effects of C-5 and C-7 hydrophobic lipid tails attached to the side chain of the ornithine residue at C-terminus of peptide **1B**, achieving peptides **D** and **E**.

Table 1. Lipopeptide sequences of [Pro^3, DLeu^9, DLys^{10}]TL (**1B**) and its reference peptide [Pro^3,DLeu^9] (**1A**).

Peptides	Lipidic tag (– R_1)	Sequence
1A	-	F V P W F S K F DL G R I L
2A	**$CH_3(CH_2)_3CO$-**	**R_1–**F V P W F S K F DL G R I L
3A	**$CH_3(CH_2)_5CO$-**	**R_1–**F V P W F S K F DL G R I L
4A	**$CH_3(CH_2)_9CO$-**	**R_1–**F V P W F S K F DL G R I L
5A	**$CH_3(CH_2)_{11}CO$-**	**R_1–**F V P W F S K F DL G R I L
1B	-	F V P W F S K F DL DK R I L
2B	**$CH_3(CH_2)_3CO$-**	**R_1–**F V P W F S K F DL DK R I L
3B	**$CH_3(CH_2)_5CO$-**	**R_1–**F V P W F S K F DL DK R I L
4B	**$CH_3(CH_2)_9CO$-**	**R_1–**F V P W F S K F DL DK R I L
5B	**$CH_3(CH_2)_{11}CO$-**	**R_1–**F V P W F S K F DL DK R I L
C	**[$CH_3(CH_2)_5CO$]-**	F[**R_1**] V P W F S K F DL DK R I L
D	**-[$NHCO(CH_2)_3CH_3$]**	F V P W F S K F DL DK R I L Orn[**R_1**]
E	**-[$NHCO(CH_2)_5CH_3$]**	F V P W F S K F DL DK R I L Orn[**R_1**]

3.2.2. EFFECT OF SELF-ASSEMBLING ON ANTIBACTERIAL ACTIVITY

The antimicrobial activity of lipopeptides (**1A–5A**, **1B–5B** and **C**, **D**, **E**) was initially assessed against the reference bacterial strains of *P. aeruginosa* ATCC 27853, *K. pneumoniae* ATCC BAA-1705 and *S. aureus* ATCC 25923 by evaluating their minimal growth inhibitory concentration (MIC). The MIC values are shown in Table 2. Peptide **1A** was active against all tested microorganisms with a stronger efficacy towards *S. aureus* (MIC of 6.25 μM), compared to 50 μM for both *P. aeruginosa* and *K. pneumoniae*. Peptide **1B** resulted to be active against all tested microorganisms with a stronger efficacy towards *S. aureus* (MIC of 6.25 μM), compared to 12.5 μM for *P. aeruginosa* and *K. pneumoniae*. Peptides **4A**, **5A**, **4B** and **5B** did not show any antimicrobial effect up to 100 μM, probably due to a reduction of positive charge from +3 to +2 in comparison to their parent peptide **1A**. The peptide **3B** featuring by

the heptyl chain showed the best activity on *S. aureus* (MIC of 3.12 μM), but displayed a weak activity on Gram-negative strains.

Instead, the peptide **2B** characterized by a pentyl chain has lost activity on Gram negative bacteria (50 μM), while a discrete activity was reported on *S. aureus* (12.5 μM). This reduction of activity of peptides **2B** and **3B** was probably due to a reduction of positive charge from +4 to +3 in comparison to their parent peptide **1B**.

Table 2. *In vitro* antimicrobial activity of compounds **1A-5A**, **1B-5B**, **C**, **D**, **E**

	MIC values (μM)[a]		
Peptides	*P. aeruginosa* ATCC 27853	*K. pneumoniae* ATCC BAA-1705	*S. aureus* ATCC 25923
1A	50	50	6.25
2A	>100	>100	12.5
3A	>100	>100	12.5
4A	>100	>100	>100
5A	>100	>100	>100
1B	12.5	12.5	6.25
2B	50	50	12.5
3B	25	50	3.12
4B	>100	>100	>100
5B	>100	>100	>100
C	25	6.25	6.25
D	>100	50	25
E	>100	50	25
Gentamicin	4	4	1
Imipenem	4	>8	0.5
Tobramycin	4	>4	1
Vancomycin	NA	NA	2

In fact, peptide **C** characterized by pentyl chain in *para* position of the Phe[1] aromatic ring and by a net positive charge of +4 as peptide parent **1B**, was able to preserve the same activity (6.25 μM) of **1B** on *S. aureus* and on *K. pneumoniae*. This means that the net positive charge of +4 plays a crucial role in maintaining a right

hydrophilic/hydrophobic balance to preserve the antimicrobial activity both against Gram-positive and Gram-negative strains. Peptides **D** and **E,** designed to investigate the effects of C5 and C7 hydrophobic lipids at C-terminus, respectively, were not effective against *P. aeruginosa* and have weak activity against *K. pneumoniae* (50 μM) and *S. aureus* (25 μM).

Table 3. In vitro antibacterial activity of peptides 1B and C against multidrug resistant clinical isolates. For the antibiotic, MIC values are expressed as μg/ml; NA, not applicable

	MIC values (μM)[a]								
Peptides	*Pa1*	*Pa2*	*Pa3*	*KpCR1*	*KpCR2*	*KpCR3*	*Sa1*	*Sa2*	*Sa3*
1B	12.5	12.5	12.5	12.5	12.5	12.5	12.5	12.5	6.25
C	25	25	25	12.5	12.5	12.5	12.5	12.5	12.5
Gentamicin	>4	>4	>4	1	>8	1	<1	<1	<1
Imipenem	>4	>4	>4	>8	>8	>8	8	>8	>8
Tobramycin	4	4	4	2	2	>4	1	<1	1
Vancomycin	NA	NA	NA	NA	NA	NA	2	1	2

By considering these biological results, the peptides **1B** and **C** were selected as the best and were further assessed against clinical strains of against carbapenem-, fluoroquinolones-, and gentamicin- resistant *P. aeruginosa*, carbapenemase resistant *K. pneumoniae* and methicillin resistant *S. aureus* (MRSA) clinical strains. As reported in Table 3 both peptides **1B** and **C** were able to efficiently inhibit the growth of all the tested clinical strains, with MIC values very close to those reported for reference strains.

3.2.3. LONG LIPIDIC TAILS INCREASE THE CYTOTOXICITY

The cytotoxic effect of the active compounds, **1B**, **2B**, **3B**, and **C**, was evaluated at the short-term against mammalian red blood cells after 40 min treatment at different concentrations. As reported in Figure 1A, peptides **1B**, **2B** and **C** showed a weak

hemolytic activity (lower than 20%) at 3.12 and 6.25 μM. Peptide **3B** showed the highest hemolytic potency (over 50%), especially at the highest concentrations used. It is clear that long hydrophobic tails as in peptide **3B** cause non-selective binding to the cell membrane and consequently stronger hemolytic activity. Interestingly, compounds **1B** and **C** had a similar hemolytic profile, with a percentage of lysed cells of about 30% at the highest concentrations tested (12.5 and 25 μM).

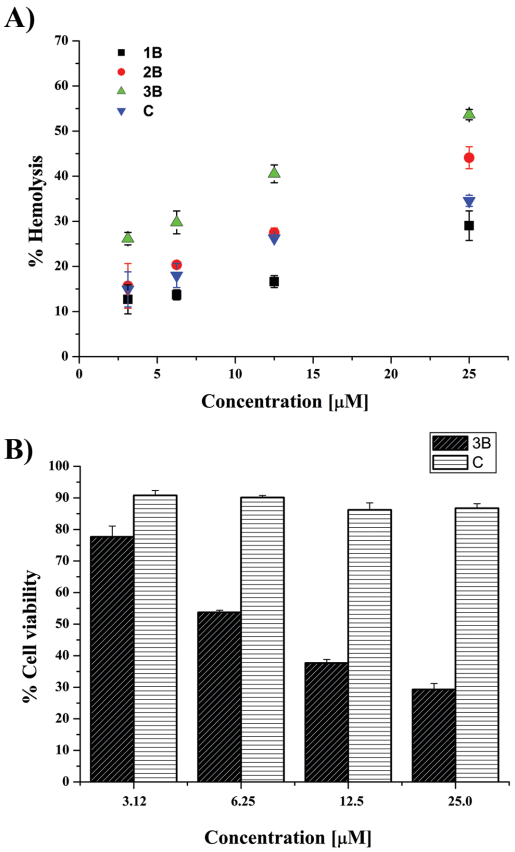

Figure 1. Panel A reports the effect of peptides **1B**, **3B**, **2B** and **C** at different concentrations on hemoglobin release from mammalian red blood cells after 40 minutes treatment. All data are expressed as a percentage with respect to the controls (erythrocytes treated with vehicle) and are the mean of three independent experiments ± standard error of the mean (SEM). Panel B reports the viability of peptide-treated HaCaT cells evaluated by MTT assay at 24h. All data are expressed as a percentage with respect to the untreated control cells and are the mean of three independent experiments ± standard error of the mean (SEM).

For long-term treatment (24 h), the cytotoxic effect of peptides **3B** and **C** was further investigated by the 3-(4,5-dimethylthiazol-2-yl)-2,5-diphenyltetrazolium bromide (MTT) assay on human keratinocytes (HaCaT cells) (Figure 1B). Compound **3B** was confirmed to be harmful causing a strong reduction in cell viability, about 50% already at 6.25 μM. However, note that peptide **C** showed a negligible cytotoxic effect even at the highest tested concentration (25.0 μM), resulting even less toxic than peptide **1B**, already shown in Merlino et al. (13.29% cytotoxicity for peptide **C** vs 28.22% for peptide **1B**, at 25.0 μM).[15]

3.2.4. AGGREGATION STUDIES

Critical Aggregation Concentration (CAC). The tendency to aggregate in water usually determines a significant reduction in antibacterial activity, which may be attributed to a reduced diffusion of the aggregates through the cell wall, due to their large size in comparison to the corresponding monomers as was previously demonstrated for other peptide sequences.[16,17] Nile red was used as a fluorescent probe to determine the ability of the designed peptides to self-assemble in the aqueous solution. The poor solubility of Nile red is responsible to its preference for hydrophobic binding sites and thus to a blue shift and hyperchromic effect. The change in the emission signal allows to ascertain the formation of the aggregates as well as to determine the concentration at which the aggregate forms (CAC).

In Figure 2 (panels A–D), the experiments performed at pH 7 (physiological condition) for all peptides are reported. In particular, the wavelength of Nile red maximum fluorescence emission is reported as a function of the concentration of single peptides.

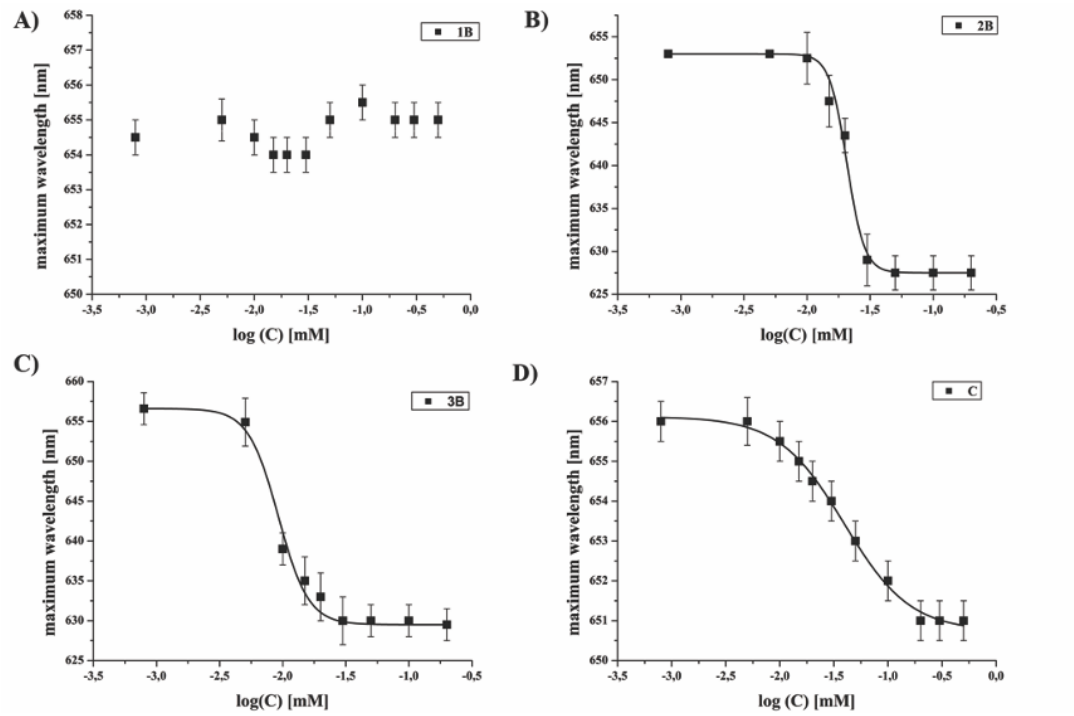

Figure 2. Wavelength corresponding to the maximum fluorescence emission of Nile red was plotted as a function of concentration of: **1B** (panel A), **3B** (panel B), **2B** (panel C), **C** (panel D) to determine their CAC. The measurements were repeated in triplicate.

For peptide **1B**, we were unable to observe any blue shift, indicating that this peptide is unable to aggregate under the range of concentrations investigated. On the contrary, the presence of lipids was sufficient to confer the hydrophobic driving force to promote peptide aggregation. The modified sequences containing the valeric (**2B**) and heptanoic (**3B**) acids at the N-terminus showed a significant ability to aggregate with a CAC, respectively, of 20.9 and 9.33 μM. That means that both peptides are active because are not aggregated at tested concentrations. Instead, probably, the peptides characterized by C11 or C13 hydrophobic lipid tails (**4A-5A**, **5A-5B**) are so completely aggregated in aqueous solution that were resulted to be not active at tested concentrations. Regarding the compound **C** has a high CAC (39.5 μM) indicating that the peptide is still able to aggregate and the presence of the positive charge on the N-terminal amino group reduced its aggregating ability.

3.2.5. OLIGOMERIZATION IN BACTERIAL MEMBRANE

The ability of designed peptides to oligomerize inside the membrane was investigated using Thioflavin T (ThT) as fluorescent probe (Figure 3).[18] The peptide aggregation was studied using liposomes (LUVs) mimicking the Gram-positive DOPG/CL (58/42) and Gram-negative membranes DOPG/DOPE/CL (63/23/12). We observed a dramatic increase of fluorescence as a function of concentration for all peptides, indicating a progressive phenomenon of aggregation in LUVs. In particular, at low peptide/lipid ratios, peptides **1B** and **C** produced a drastic increase of fluorescence, indicating that both peptides oligomerize significantly in liposomes. In fact, both peptides are able to oligomerize in the membrane monomeric at lower peptide/lipid ratios, but are monomeric in aqueous solution at the same condition of peptide/lipid ratios.

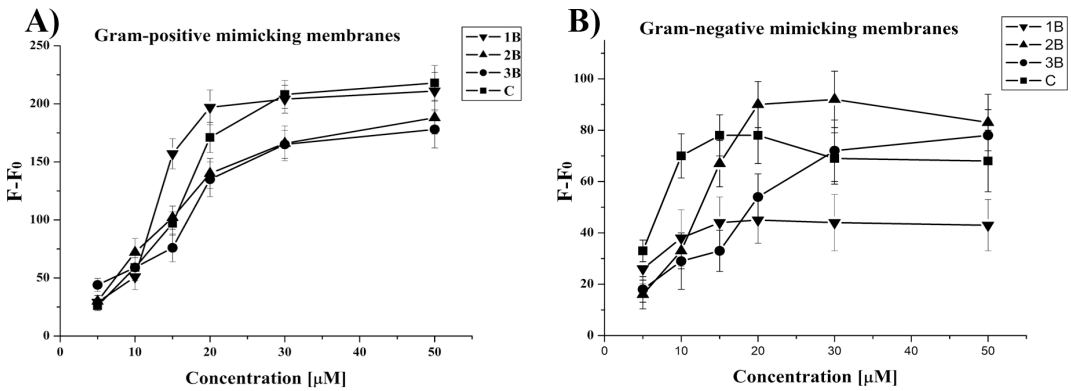

Figure 3. ThT aggregation as a function of the peptide/lipid ratio of **1B**, **3B**, **2B**, **C** in liposomes mimicking Gram-positive (A) and Gram-negative (B) membranes. The difference between the value of fluorescence after peptide addition (F) and the initial fluorescence in the absence of peptide (F_0) was reported on the x-axis.

Peptides **3B** and **2B** showed a lower aggregation at low peptide/lipid ratio while enhanced aggregation was observed at higher ratios as revealed by an increased fluorescence. These results are in agreement with those obtained in the other experiments; in fact, **2B** and **3B** are already aggregated in aqueous solution and thus they aggregate in membranes at a higher concentration as it is likely that they need first to disaggregate in the move between the two environments.

3.2.6. LIPOPEPTIDES INFLUENCES MEMBRANE FLUIDITY

The effect of the peptides **1B**, **2B**, **3B**, **C** on the fluidity of the bilayer was analyzed below and above the CAC using the fluorescent probe Laurdan.[19] Laurdan changes its emission when inserted in the gel phase membranes (440 nm) or in the liquid phase membranes (490 nm). The Generalized Polarization (GP) parameter, which is commonly used to quantify the change in the lipid fluidity, can be calculated from the emissions at 440 and 490 nm. LUVs mimicking Gram positive and Gram negative bacterial membranes were used. The emission spectra clearly indicated the presence of more fluid membranes at 25 °C; the reproducibility of the spectra after 24 h (data not shown) further supported that LUVs were stable and not leaky in the condition used for the experiments. The GP parameter allowed to quantify the effect of the peptide (Table 4).

Table. 4. Membrane fluidity evaluation using the generalized polarization (GP) value calculate as GP $=(I_{440}-I_{490})/(I_{440}+I_{490})$.

		Gram negative mimicking membranes	
Compound	**Unloaded LUVs**	**LUVs + 5 μM Cmpd**	**LUVs + 30 μM Cmpd**
1B	-0.07	0.09	0.11
2B	-0.07	-0.05	0.03
3B	-0.07	-0.07	0.07
C	-0.03	0.07	0.15
		Gram positive mimicking membranes	
Compound	**Unloaded LUVs**	**LUVs + 5 μM Cmpd**	**LUVs + 30 μM Cmpd**
1B	-0.18	-0.06	0.26
2B	-0.18	-0.14	-0.02
3B	-0.18	-0.18	-0.11
C	-0.23	-0.14	0.18

The GP parameter of the membranes mimicking Gram positive bacteria at 25 °C increased significantly for all tested peptides at 30 μM, indicating a shift towards

more ordered membranes. Interestingly, **1B** and **C** provided the highest increase. The fluidity of the membranes in the presence of peptides at 5 μM was not modified significantly, except for peptide **C**. For the Gram- negative mimicking membranes, we observe the same trend although we obtain fewer modifications.

3.2.7. LIPOSOMES LEAKAGE BY LIPOPEPTIDES

Since the mode of action of AMPs involves mostly a membrane disintegration induced by a formation of large pores, the ANTS/DPX assay was exploited to determine eventual leakage of liposomes mimicking Gram-positive and Gram-negative membranes in presence of the peptides **1B**, **2B**, **3B**, **C**.[19] In both tested conditions, we observed a significant leakage with all peptides, supporting pore formation as the primary mechanism of toxicity against bacteria (Figure 4). In particular, we observe higher leakage in presence of Gram-positive membranes; thus, membrane leakage resulted to be strongly dependent on the content of negatively charged lipids. This is in line with the biological data showing a greater activity against *S. aureus* (Figure 4). These data indicate that leakage is involved in the antimicrobial mechanism of these molecules. Leakage events are typical of AMPs; nonetheless, in order to have promising molecules to be developed for further applications it is important to have membrane perturbation not accompanied by hemolysis. The peptides **2B** and **3B** showed the highest leakage ability but also the highest hemolysis. They have lower CACs and are likely already aggregated when they induce the leakage of the membrane. On the contrary, **1B** presents the lowest leakage ability and its percentage of hemolysis is similar to **C**. This latter presents an intermediate ability to produce leakage of both Gram-positive and Gram-negative membranes and low hemolysis up to 25 μM. At this concentration, it is also below the CAC, indicating that it is not already aggregated when in contact with the membranes.

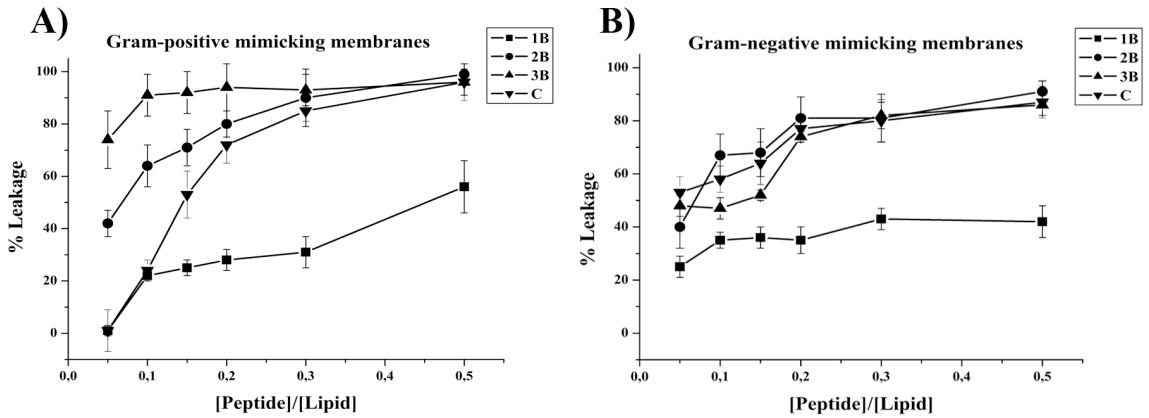

Figure 4. Peptide-promoted membrane leakage of compounds **1B**, **3B**, **2B**, **C** in LUVs mimicking Gram-positive (panel A) and Gram-negative (panel B) membranes. Percentage of leakage is reported as a function of the peptide/lipid ratio and each trace represents an average of three independent experiments.

3.2.8. HELICAL AGGREGATION IN BACTERIAL MEMBRANE

The molecular conformation of the peptides was investigated by far-UV CD spectroscopy, which is widely exploited for the determination of the secondary structure and for studying the formation of peptide assemblies in solution (Figure 5 panels A, B). In fact, changes in secondary structures compared to monomers often characterize self-assembly processes. We here determined the secondary structure in liposomes mimicking the Gram-positive and Gram-negative membranes at a concentration below the CAC obtained in aqueous solution, in order to better understand if peptides that were not aggregated in water solution could self-aggregate when in membrane environment. The data obtained clearly demonstrate that the peptides were monomeric with a random coil conformation in aqueous solution (data not shown). Moreover, they showed a significant ability to aggregate in membrane mimetic environments with a high tendency to give helical aggregates in both Gram-positive and Gram-negative membranes. In fact, we observe a helical conformation in Gram-positive membranes with two negative bands at about 208 and 222 nm.

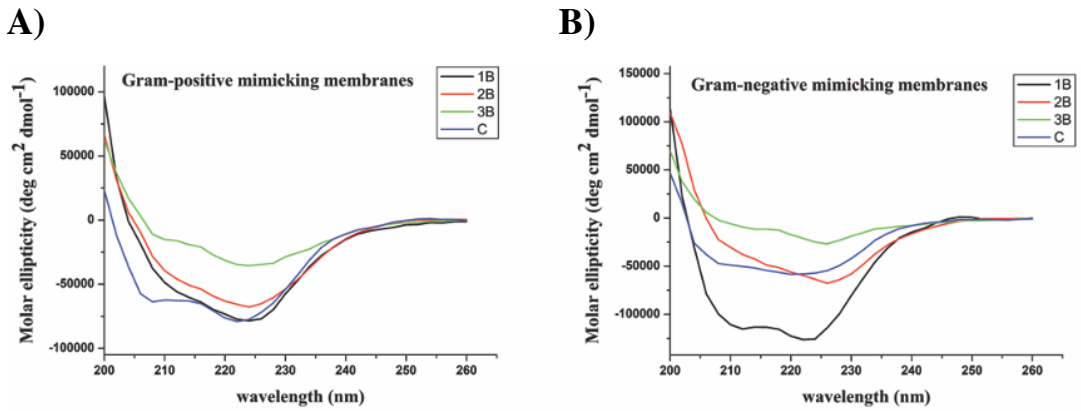

C)

Peptides	CAC (μM)	Gram –positive mimicking membranes $\theta_{222}/\theta_{208}$	Gram –negative mimicking membranes $\theta_{222}/\theta_{208}$
1B	-	2.0	1.3
2B	20.9	2.3	2.6
3B	9.33	3.1	10.3
C	39.5	1.2	1.2

Figure 5. Conformational characterization of the four peptides by CD spectroscopy in membranes mimicking Gram-positive (panel **A**) and Gram-negative (panel **B**) membranes. Panel **C** reports the critical aggregation concentration (CAC) calculated by a fluorescence assay with the fluorophore Nile red and the ratio of the ellipticities at 222 and 208 nm, which discriminates between monomeric and oligomeric states of helices for peptides **1B**, **2B**, **3B** and **C**.

The visual analysis of the spectra clearly indicates the presence of aggregates. To establish whether we were observing oligomerization processes which likely occur through self-assembly in the experimental condition used for our assays we determined the ratio of the ellipticities at 222 and 208 nm (Figure 5, panel C), which helps in discriminating between monomeric and oligomeric states of helices.[20] In our spectra, the ratio $\theta_{222}/\theta_{208}$ is always greater than 1.0, indicating a α-helical conformation in its oligomeric state; for a monomeric state the ratio $\theta_{222}/\theta_{208}$ would have been lower than 0.8.[21] Moreover, we performed experiments after centrifugation of the samples to get rid from solution of eventually precipitated peptides and as expected we did not observe any effect on the spectra. One of the

main features of peptides able to enter the bilayer is the change of conformation from random to helical.[22]

3.2.9. SELF-ASSEMBLING IMPROVES PROTEOLYTIC STABILITY

Peptide aggregation or ordered self-assembly might positively effect both on pharmacokinetic and pharmacodynamic proprieties of AMPs; in fact, it might reduce effectively their susceptibility to proteolytic degradation, increasing their half-life.[23] In this context, we probed the proteolytic human serum stability upon peptide incubation with 90% fresh human serum at 37 ± 1 °C within 120 min and the percentage of intact peptide was calculated by the peak area of the RP-HPLC performed on a Phenomenex Kinetex column (4.6 mm x 150 mm, 5 μm, C18) chromatograms using a linear gradient from 10 to 90% MeCN (0.1% TFA) in water (0.1% TFA) over 20 min (flow rate of 1 mL/min, and absorbance detection at 220 nm). Figure 6 reports the data obtained for peptide **1B** and **C**. As expected, peptide **1B**, our starting sequence is rapidly degraded and cleaved in fragments, notwithstanding the presence of D-amino acids. Chemical modifications in the sequence and formation of the self-assembled structures can significantly modify enzymatic degradation rates. As a matter of fact, we observed that peptide **C** is stable up to 1 h (Figure 6); while we observed partial degradation starting from 80 min even though a significant part of the active peptide is present. Clearly, the further addition of the hydrophobic tail in **C** and the formation of supramolecular assemblies can be used as a viable strategy to reduce protease susceptibilities of AMPs.

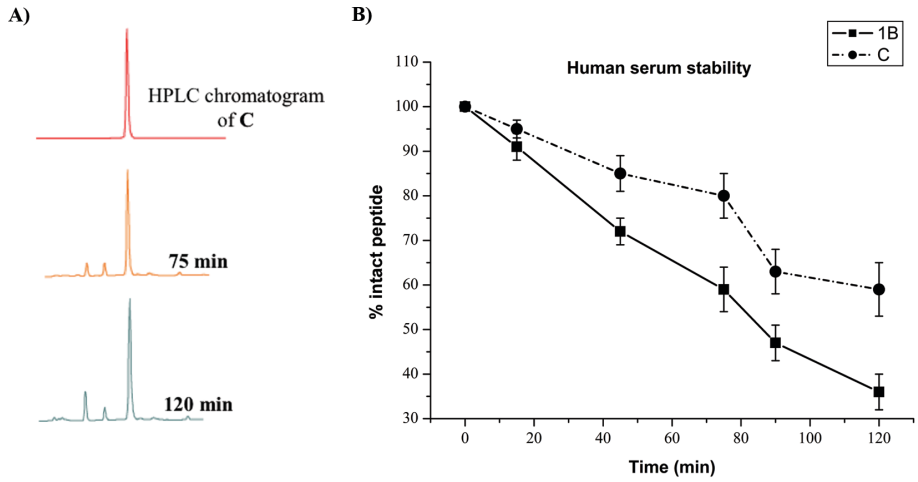

Figure 6. (Panel A) RP-HPLC analysis of peptide **C** in 90% human serum at 37 °C at different times (X, 75 and 120 min). The HPLC profile shows the results of one representative experiment out of at least three independent ones. (Panel B) Percentage of intact peptides **1B** and **C** detected at different time intervals after incubation in 90% fresh human serum (200 μM) at 37 ± 1 °C.

3.3. CONCLUSIONS

The obtained results clearly show that modification in the hydrophobicity and hydrophilicity may influence the self-aggregation in both water solution and in the bilayer. The most active peptide is monomeric in aqueous solution but is able to form molecular helical aggregates in the membrane environment of Gram-positive bacteria (Figure 7). In addition, it is also able to boost the membrane modifications which certainly are correlated to the affinity for the membrane and formation of pores. The hydrophilic/hydrophobic balance also helps to reduce hemolysis and toxicity. Interestingly, the same peptide (**C**) is the only one to show a higher activity against *K. pneumoniae*, conserving a good activity against *S. aureus*. The analysis of the data showed that also from a biophysical point of view the interaction of **C** with membrane mimicking Gram-negative bacteria is stronger compared to the other peptides. Nonetheless, it is interesting to note that the interaction is very different because the aggregation is less evident but the fluidity of the membrane changes more. The conformational change inside the membrane is clearly involving the presence of β-structures compared to helical aggregates in Gram-positive

membranes. We may hypothesize that the mechanism of interaction with Gram-positive and negative bacteria is completely different, involving different secondary structures although both leading to leakage of the membranes. Biological data on clinical strains further support the possible application of TL analogues as novel AMPs able to help in the fight against antibiotic resistant bacteria.

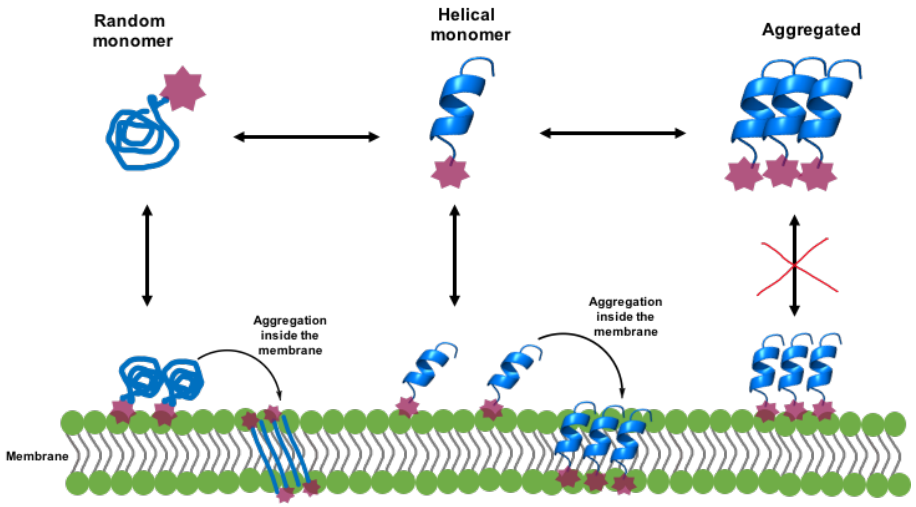

Figure 7. Schematic description of the hypothetical mechanisms involved in Temporin L coupled to lipid tags monomeric structures are involved in the membrane attachment, while self-aggregated peptides are present inside the membrane and both steps are influenced by the presence of lipid tags.

3.4. EXPERIMENTAL SECTION

3.4.1. CHEMISTRY

Materials. N^{α}-Fmoc-protected amino acids used were purchased from GL Biochem Ltd (Shanghai, China). Fatty acids used, such as tridecanoic, undecanoic, heptanoic, and valeric acids, were purchased by Sigma-Aldrich/Merck. Anhydrous solvents [*N*,*N*-dimethylformamide (DMF) and dichloromethane (DCM)], Rink amide resin, 1,3-dimethylbarbituric acid, tetrakis(triphenylphosphine)palladium(0) [$Pd(PPh_3)_4$], tin(II)chloride [$SnCl_2$], 2,2,2-trifluoroethanol (TFE) were purchased from Sigma-

Aldrich/Merck. Fmoc-Orn(Alloc)-OH, *N,N*-diisopropylethylamine (DIEA), piperidine, and trifluoroacetic acid (TFA) were purchased from Iris-Biotech GMBH. Phospholipids: 1,2-dioleoyl-sn-glycero-3-phosphoethanolamine (DOPE), 1,2-dioleoyl-sn glycero-3-phospho-(1′-rac-glycerol) sodium salt (DOPG), and cardiolipin (CL) sodium salt (Heart, Bovine) were purchased from Avanti Polar Lipids (Birmingham, AL, USA), Phosphate-buffered saline (PBS) tablets were bought by Life Technologies Corporation. 8-aminonaphtalene-1,3,6-trisulfonic acid, disodium salt (ANTS) and p-xylene-bis-pyridinium bromide (DPX) were purchased from Molecular Probes. Triton X-100 and the fluorescent probes Nile red, Thioflavin T and 6-dodecanoyl-*N,N*-dimethyl-2-naphthylamine (Laurdan) were purchased by Sigma-Aldrich-Merck. 3-(4,5-dimethylthiazol-2-yl)-2,5-diphenyltetrazolium bromide (MTT) and human serum from human male AB plasma, USA origin, sterile-filtered was obtained by Sigma-Aldrich-Merck.

Peptide Synthesis by US-SPPS. The synthesis of peptides **1A–5A, 1B–5B, C, D, E** was performed by using the ultrasound-assisted solid-phase peptide synthesis (US-SPPS) integrated with the Fmoc/*t*Bu orthogonal protection strategy.[24] Each peptide was assembled on a Rink amide resin (0.1 mmol from 0.72 mmol/g as loading substitution) as solid support in order to obtain amidated C-termini. In particular, the resin was first placed into a 10 mL plastic syringe tube equipped with Teflon filter, stopper and stopcock, and swollen in DMF on an automated shaker for 30 min at rt. Then, the Fmoc group of the rink amide linker was removed by treatment with 20% piperidine in DMF solution (0.5 + 1 min) by ultrasonic irradiation. The first coupling was carried out by adding a solution of N^{α}-Fmoc-amino acid, HBTU, HOBt (3-fold excess), and DIEA (6-fold excess) in DMF to the resin, thus the resulting suspension was irradiated by ultrasound waves for 5 min. After each coupling and Fmoc-deprotection reaction the resin was washed with DMF (3 × 2 mL) and DCM (3 × 2 mL) and Kaiser or Chloranil tests were employed as colorimetric assays to monitor

the progress of the synthesis, used for the detection of solid-phase bound primary and secondary amine, respectively. Subsequent Fmoc-deprotection and coupling steps were performed following the same procedures described above.

The introduction of lipid amidated tails for peptides **2A–5A, 2B–5B** was accomplished by reacting the released primary amine in *N*-terminal region with 3 equiv of valeric (**2A** and **2B**), heptanoic (**3A** and **3B**), undecanoic (**4A** and **4B**), tridecanoic (**5A** and **5B**), acids, respectively, HBTU/HOBt (3 equiv) as coupling/additive reagents, in presence of DIEA (6 equiv) in DMF/DCM (1:1 *v*/*v*), by ultrasonic irradiation for 15 min (Scheme 1A). Upon filtering and washings (3×2 mL of DMF; 3×2 mL of DCM) of the resin, the lipidation was ascertained by Kaiser test. Thus, peptides **2A–5A, 2B–5B** were released from the resin and simultaneously cleaved by their protecting groups by using a cocktail of TFA/TIS/H_2O (95:2.5:2.5 *v*/*v*/*v*) at rt for 3 h. Finally, the resins were removed by filtration and crudes were recovered by precipitation with cool anhydrous Et_2O as amorphous solids. As for the synthesis of peptide **C**, the Fmoc-Phe(4-NO_2) reagent was used in replacement of Fmoc-Phe residue in order to give the valeric acid amide in *para* position of the aromatic ring of the Phe[1] in N-terminal. More specifically, after the elongation of peptide sequence, the resin-bound peptide sequence carrying the Phe(4-NO_2) was treated with a 1M solution of $SnCl_2$ in DMF and the resulting suspension was gently shaken at rt for 12 h (Scheme 1B).[25] Such reaction was monitored by LC-MS analysis of the residue obtained from the cleavage of an aliquot of resin [5 mg treated with 1 mL of TFA/TIS/H_2O (95:2.5:2.5, v/v/v)], and by chloranil test, as colorimetric assay used to reveal resin-bound aromatic primary amines. Once the reduction of aromatic nitro group was ascertained, the coupling with valeric acid (3 equiv) was performed by adding HBTU (3 equiv), HOBt (3 equiv), and DIEA (6 equiv) to the resin, and the mixture was therefore stirred on automated shaker at rt for 2 h. The LC-MS analysis and chloranil test were repeated to confirm coupling had achieved >80% conversion.

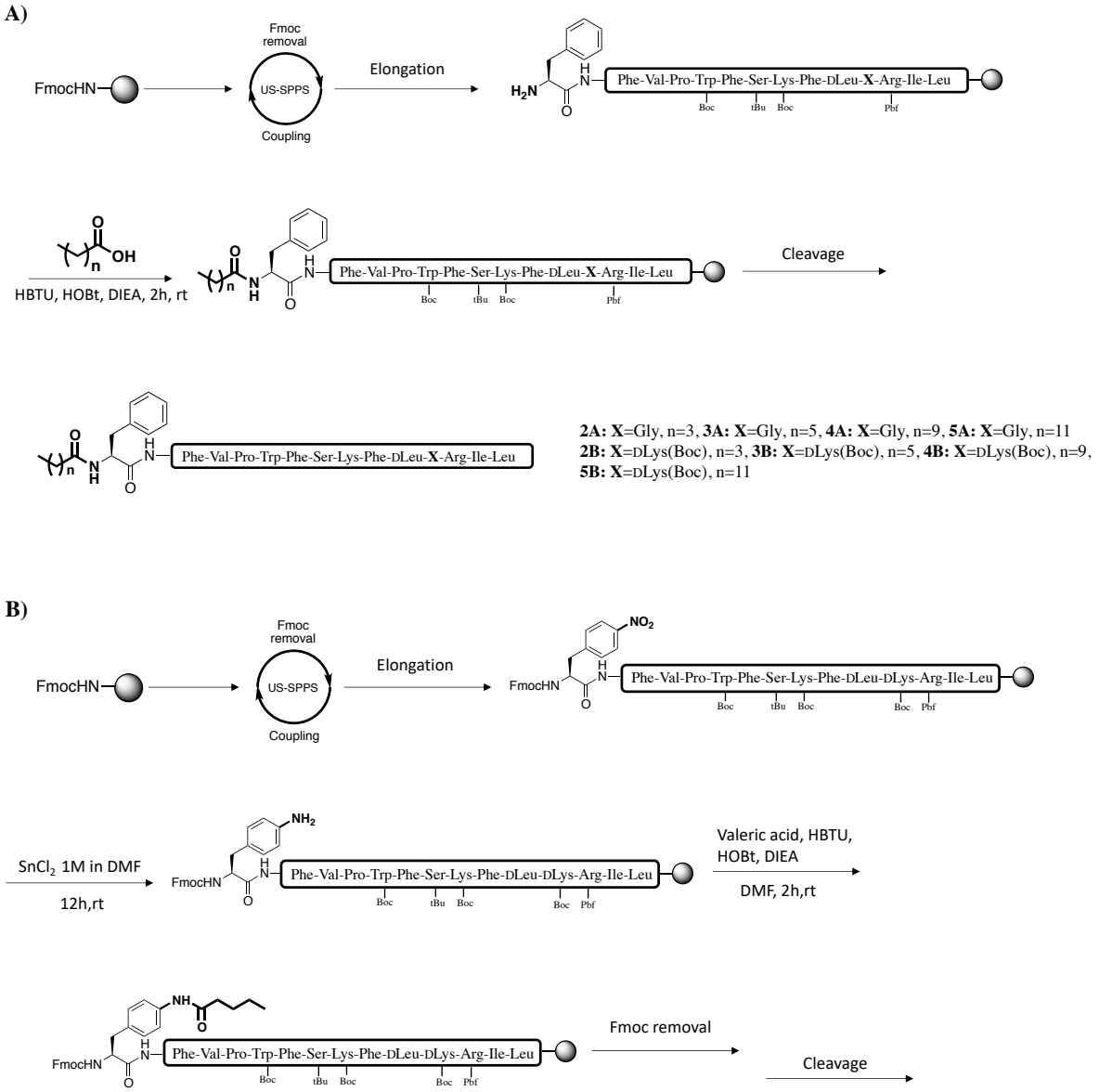

Scheme 1. **(A)** Synthesis of lipopeptides **2A–5A, 2B–5B. (B):** Synthesis of lipopeptide **C**.

Peptides **D** and **E** were otherwise obtained by the introduction of Orn(Alloc) residue at C-terminal. The ornithine allyl protecting group was removed in orthogonal condition with respect to the Fmoc/*t*Bu.[26] Specifically, the resin was treated with a

suspension of $Pd(PPh_3)_4$ (0.15 equiv) and 1,3-dimethylbarbituric acid (3 equiv) in DCM/DMF (3:2 *v*/*v*) and gently shaken for 1 h under argon (Scheme 2).

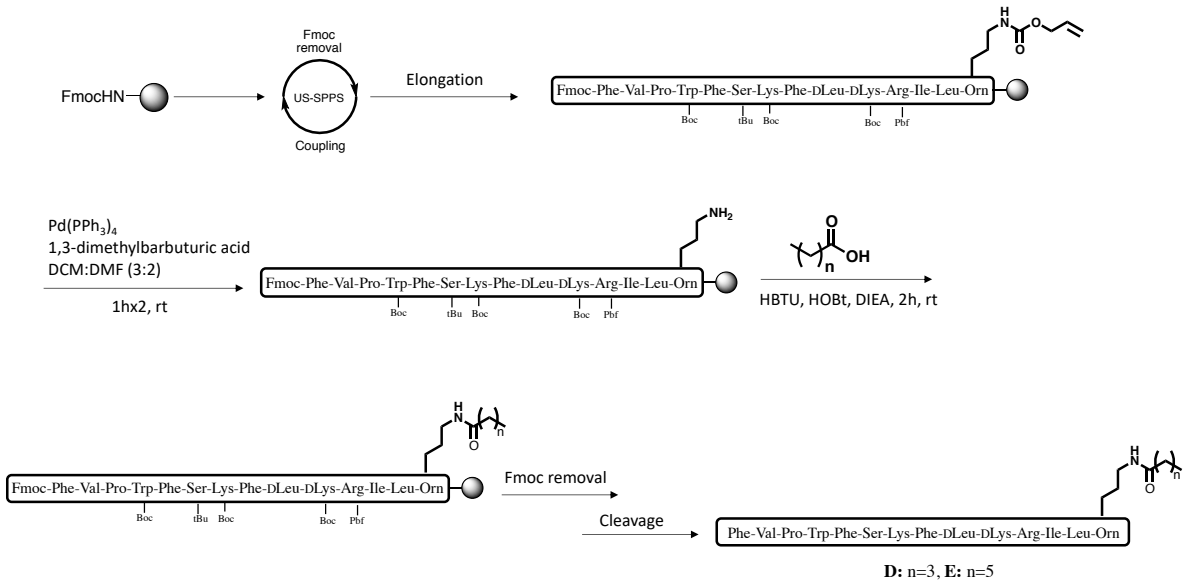

Scheme 2. Synthesis of lipopeptides **D** and **E**.

The resin was filtered and washed with DMF (3×2 mL) and DCM (3×2 mL), and the Alloc-deprotection procedure was repeated. After the complete removal was ascertained by Kaiser test and LC-MS, the heptanoic (3 equiv) or valeric (3 equiv) acids were coupled to the δ-amine group of Orn by following the same coupling procedure by ultrasonic irradiation as described above. The resin was filtered and washed with DMF (3×2 mL) and DCM (3×2 mL) and the lipidation was monitored by Kaiser test. Finally, the N-terminal Fmoc group was removed and the peptides were treated with a cleavage cocktail, consisting of TFA/TIS/H_2O (95:2.5:2.5 *v*/*v*/*v*), at rt for 3 h, to be released from the resin and cleaved by their protecting groups.

Analytical UHPLC (Shimadzu Nexera Liquid Chromatograph LC-30AD) analyses to assess critical synthetic steps as well as the purity of final compounds **1A–5A**, **1B–5B**, **C**, **D**, **E** were performed on a Phenomenex Kinetex reverse-phase column (C18, 5 μm, 100 Å, 150 × 4.6 mm) with a flow rate of 1 mL/min using a gradient of

MeCN (0.1% TFA) in water (0.1% TFA), from 10 to 90% over 20 min, and UV detection at 220 and 254 nm. Purification of peptides **1A–5A**, **1B–5B**, **C**, **D**, **E** was performed by RP-HPLC (Shimadzu Preparative Liquid Chromatograph LC-8A) equipped with a preparative column (Phenomenex Kinetex C18 column, 5 μm, 100 Å, 150 x 21.2 mm) using linear gradients of MeCN (0.1% TFA) in water (0.1% TFA), from 10 to 90% over 30 min, with a flow rate of 10 mL/min and UV detection at 220 nm. Final products were obtained by lyophilization of the appropriate fractions after removal of the MeCN by rotary evaporation. All compounds examined for biological activity were purified to >96%, and the correct molecular ions were confirmed by high-resolution mass spectrometry (HRMS) (Table 5).

Table 5. HRMS calculated and observed for peptides **2A–5A**, **2B–5B**, **C**, **D**, **E**.

Peptides	R_t(min)	m/z calcd	m/z found
2A	13.4	1694.0027	$[M+H/2]^+$=847.5036
3A	13.9	1722.0340	$[M+H/2]^+$=861.5185
4A	15.8	1778.0966	$[M+H/2]^+$ = 889.551
5A	15.2	1806.1279	$[M+H/2]^+$=903.5670
2B	12.7	1765.0762	$[M+2H/2]^+$=883.0450
3B	13.1	1793.1075	$[M+2H/2]^+$=897.0603
4B	14.9	1849.1701	$[M+H/2]^+$=925.0869
5B	14.3	1877.2014	$[M+2H/2]^+$=939.1046
C	12.6	1780.0871	$[M+H/2]^+$=890.5464
D	12.4	1879.1555	$[M+2H/2]^+$=940.0730
E	11.8	1907.1868	$[M+2H/2]^+$=954.0976

3.4.2. BIOLOGY

Bacterial strains and culture. *Staphylococcus aureus* ATCC 25923, *Pseudomonas aeruginosa* ATCC 27853 and *Klebsiella pneumoniae* ATCC BAA-1705 (carbapenemase producer) were obtained from the American Type Culture Collection (Rockville, MD). Clinical strains of *P. aeruginosa* (*Pa*1, *Pa*2 and *Pa*3), *K. pneumoniae* (*Kp*CR1, *Kp*CR2 and *Kp*CR3), and *S. aureus* (*Sa*1, *Sa*2 and *Sa*3) were isolated from bloodstream or pulmonary infections, and belong to a collection of bacterial strains established between 2010 and 2018 at the Department of

Molecular Medicine and Medical Biotechnologies (University Federico II, Naples) for research use. *Pa1, Pa2* and *Pa3* resulted resistant to carbapenems, fluoroquinolones, and gentamicin; *Kp*CR1, *Kp*CR2 and *Kp*CR3 were carbapenem-resistant since KPC carbapenemase producers; *Sa*1, *Sa*2 and *Sa*3 resulted MRSA strains. The antimicrobial susceptibility testing of all isolates was determined using Vitek II system and results were interpreted according to European Committee on Antimicrobial Susceptibility Testing (EUCAST version 9.0, 2019).

Antimicrobial susceptibility testing. Minimal inhibitory concentrations (MIC) of all the peptides were determined in Mueller–Hinton medium by the broth microdilution assay as described in Chapter 2.[27]

Cytotoxicity assay. The hemolytic assay was carried out following the procedures described in Chapter 2. The colorimetric MTT assay was performed to measure cellular metabolic activity in terms of cell viability.[27,28] Viable cells are able to reduce, by active mitochondrial dehydrogenases, the yellow salt MTT to purple formazan crystals. Briefly, 4×10^4 HaCaT cells, suspended in DMEMg supplemented with 2% FBS, were plated in each well of a 96-well microtiter plate. After overnight incubation, at 37 °C in a 5% CO_2 atmosphere, keratinocytes were treated for 24 h with fresh serum free medium containing the peptides **3B** and **C** at concentrations ranging from 3.12 ×μM to 25 μM. Afterward, the culture medium was replaced with Hank's buffer supplemented with 0.5 mg/mL MTT and the plate was incubated at 37°C and 5% CO_2 for 4 h. At the end, acidified isopropanol was employed to dissolve the formazan crystals. Cell viability was calculated, with respect to cells not treated with peptide, by absorbance measurements at 570nm using a microplate reader (Infinite M200; Tecan, Salzburg, Austria).[28] Colour solution changes are directly related to the number of viable, metabolically active cells.

Plasma stability assay. Human serum from human male AB plasma was acquired by Sigma-Aldrich-Merck. Water and MeCN were obtained from commercial suppliers and used without further purification. Analytical RP-UHPLC was performed on a Shimadzu Nexera equipped with a Phenomenex Kinetex column (C_{18}, 4.6 mm x 150 mm, 5 mm) and H_2O (0.1% TFA) and MeCN (0.1% TFA) as eluents. Serum stability was evaluated by modification of elsewhere described methods.[15,29] In particular, the human serum was allocated into a 1.5 mL eppendorf tube and temperature equilibrated at 37 ± 1 °C for 15 min. Peptides **1B, C** were dissolved in sterile water to prepare a stock solution of 2 mM and then mixed with the human serum to make a final concentration of 0.2 mM (90% serum). The resulting reaction solution was incubated at 37 ± 1 °C. Aliquots of the reaction solutions were taken at known time intervals (0 min, 15 min, 45 min, 75 min, 90 min, 120 min), subjected to serum proteins precipitation by addition of MeCN (double volume respect to the aliquot). The cloudy reaction sample was cooled (4 °C) for 15 min and then spun at 13000 rpm for 10 min to pellet the precipitated serum proteins. The supernatant was then analyzed by RP-UHPLC by using a linear elution gradient from 10 to 90% MeCN (0.1% TFA) in water (0.1% TFA) over 20 min. A flow rate of 1 mL/min was used, absorbance was detected at 220 nm, and the analysis was performed at room temperature.

3.4.3. CRITICAL AGGREGATION CONCENTRATION DETERMINATION

The solvatochromic fluorescent probe Nile red is widely used to determine the critical aggregation concentration (CAC) of self-assembling peptides. Nile red shows a blue shift with decreasing solvent polarity. Since Nile red is poorly soluble in water, there is a large preference to partition aggregates, which offer hydrophobic binding sites. Initially, 1 mM methanolic Nile red was prepared. Then, the methanolic Nile red was diluted with water in order to have a final concentration of 500 nM (solution A). The peptides **1B, 2B, 3B, C,** were prepared as follows:[30] peptide stock solutions

(0.4 mM) were prepared by dissolving the single peptides in water (**1B, C**) or tetrahydrofuran (**3B**, **2B**) and sonicating for 15 min. Different aliquots were taken to prepare solutions of each peptide at different concentrations (1, 5, 10, 15, 20, 30, 50, 100 and 200 μM). Then, all solutions were diluted with water, sonicated for 15 min and freeze-dried. Finally, the peptide powders were dissolved with the right volume of solution A and allowed to stand in the dark place for 1 h before measurement. Emission spectra for each solution were measured by a Cary Eclipse Varian spectrometer. Spectra were taken between 570 and 700 nm at a slit width of 5 nm, using an excitation wavelength of 550 nm and a 10 nm slit width. The measurements were performed in triplicate. The data were analyzed by plotting the maximum emission fluorescence corresponding wavelength (y) as a function of peptide concentration (x) and fitting with the sigmoidal Boltzmann equation:

$$y = \frac{\mathrm{A1} + A2}{1 + e^{(x - \frac{x0}{\Delta x})}} + A2$$

where the variables A_1 and A_2 correspond to the upper and lower limits of the sigmoid, x_0 is the inflection point of the sigmoid and Δx is the parameter, which characterizes the steepness of the function. The sigmoidal plot allows calculating the CAC value at x_0.

3.4.4. LIPOSOME PREPARATION

Large unilamellar vesicles (LUVs) and small unilamellar vesicles (SUVs) consisting of DOPG/CL (58/42 ratio in moles) and DOPG/DOPE/CL (63/23/12 ratio in moles), which mimic the Gram-positive membrane and Gram-negative membrane, respectively. LUVs were prepared using the extrusion method.[31] First, lipid films were prepared by dissolving an appropriate amount of lipids in chloroform and fluorescent probes was added when necessary, then dried under a nitrogen gas stream

and freeze-dried overnight. In all experiments, we used a final lipid concentration of 0.1 mM. For fluorescence experiments, buffer was added to dry lipid films and vortexed for 1 h; then the lipid suspension was freeze-thawed 6 times and extruded 10 times through polycarbonate membranes with 0.1 μm diameter pores to obtain LUVs. For circular dichroism measurements, peptide samples in SUVs were prepared.[32] Lipids were dissolved in chloroform and added to an equal volume of peptide solution dissolved in TFE containing appropriate peptide concentration. The samples were vortexed and lyophilized overnight. The dry samples were rehydrated with phosphate buffer 5mM, pH 7.4 for 1 h and sonicated for 30 min.

3.4.5. ANTS/DPX LEAKAGE ASSAY

The ANTS/DPX leakage assay was used to measure the ability of peptide to permeabilize and induce leakage of encapsulated dyes. After lipid films were prepared as previously described, ANTS (12.5 mM) and DPX (45 mM) were dissolved in 2mL water, were added to lipid films and then lyophilized overnight. The lipid films with encapsulated ANTS and DPX were hydrated with PBS 1X buffer, vortexed for 1h and then treated to obtain LUVs. The not encapsulated ANTS and DPX were removed by gel filtration using a Sephadex G-50 column (1.5 cm x 10 cm) at room temperature.[33] To start up the leakage experiment, a 2 mM peptide stock solution was prepared and LUVs were titrated with the peptide Samples were excited at 385 nm (slit width, 5 nm) and fluorescence emission was recorded at 512 nm (slit width, 5 nm). After the addition of peptide, we evaluated leakage of encapsulated ANTS through a change in fluorescence spectra of ANTS and DPX. In particular, leakage is associated to an increase in ANTS fluorescence at 512 nm. Complete release of ANTS was obtained by using 0.1% Triton X, which caused total destruction of liposomes. The percentage of leakage was calculated as % leakage $=(F_i-F_0)/(F_t-F_0)$, where F_0 represents the fluorescence of intact LUVs before the

addition of peptide, and F_i and F_t denote the intensities of the fluorescence achieved after peptide and Triton-X treatment, respectively.

3.4.6. LAURDAN ASSAY

Membrane fluidity was determined using LUVs containing the fluorescent probe Laurdan.[19] Laurdan was encapsulated into lipid films (0.1 mM) at a concentration of 0.001 mM. After lipid films with Laurdan were lyophilized, hydrated with PBS 1X buffer, pH= 7.4, and vortexed for 1h, they were freeze-thawed 6 times and extruded 10 times through polycarbonate membranes with 0.1 μm diameter pores, obtaining LUVs. The variation of fluidity membrane in presence of peptide was evaluated at 5 and 30 μM , under and above the CAC. The peptide, dissolved in water (2 mM peptide stock solution), was added to LUVs at specific P/L molar ratio and after 10 min the fluorescence spectra were recorded using a 1 cm path length quartz cell, thermostated at 25 °C. Spectra were corrected for the baseline signal. Laurdan emission spectra were recorded from 400 to 550 nm with λ_{ex} 365 nm in the absence or presence of peptide. Laurdan emission can shift from 440 nm, in the ordered phase, to 490 nm in the disordered phase. The Generalized Polarization (GP) is a parameter commonly used to quantify the change in the lipid fluidity. It was calculated as $GP = (I_{440} - I_{490}) / (I_{440} + I_{490})$, where I_{440} and I_{490} are the fluorescence intensities at the maximum emission wavelength in the ordered (λ_{em} 440 nm) and disordered (λ_{em} 490 nm) phases.[19]

3.4.7. PEPTIDE AGGREGATION

Peptide aggregation in bacterial membrane was assayed using fluorescent probe Thioflavin T (ThT). ThT associates rapidly with aggregated peptides giving rise to a new excitation maximum at 450 nm and an enhanced emission at 482 nm.[33] Lipid films were hydrated with 100 mM NaCl, 10 mM Tris-HCl, 25 μM Tht buffer, pH= 7.4 and then treated as described above to obtain LUVs. Each peptide was dissolved

in sterile water to prepare a 2 mM peptide stock solution and LUVs were titrated with a peptide concentration of 5, 10, 15, 20, 30, 50 μM. Fluorescence was measured before and after the addition of peptide into the cuvette using a Varian Cary Eclipse fluorescence spectrometer at 25 °C. Samples were excited at 450 nm (slit width, 10 nm) and fluorescence emission was recorded at 482 nm (slit width, 5 nm). Aggregation was quantified according to the equation, $\%A = (F_f - F_0)/(F_{max} - F_0) \times 100$, where F_f is the value of fluorescence after peptide addition, F_0 the initial fluorescence in the absence of peptide and F_{max} is the fluorescence maximum obtained immediately after peptide addition.

3.4.8. CD Spectroscopy

CD spectra were recorded at room temperature on a Jasco J-715 spectropolarimeter in a 1 cm quartz cell under a constant flow of nitrogen gas. The spectra are an average of 3 consecutive scans from 260 to 190 nm, recorded with a band width of 3 nm, a time constant of 16 s, and a scan rate of 10 nm/min. Spectra were recorded and corrected for the blank. A solution of 8 μM of peptide with SUVs consisting of DOPG/CL (58/42 ratio in moles) was prepared, as reported above, and then hydrated with phosphate buffer 5 mM.[20] Instead, a solution of 8 μM of peptide with SUVs consisting of DOPG/DOPE/CL (63/23/12 ratio in moles) was prepared and hydrated with phosphate buffer 5 mM. Each spectrum was converted the signal to mean molar ellipticity.

3.5. References

[1] A.W. Simonson, M.R. Aronson, S.H. Medina. Supramolecular peptide assemblies as antimicrobial scaffolds. *Molecules*. 2020, 25:2751.
[2] L. Lombardi, A. Falanga, V. Del Genio, S. Galdiero. New hope: self-assembling peptides with antimicrobial activity. *Pharmaceutics*. 2019, 4:166.
[3] A. Levin, T.A. Hakala, L. Schnaider, G.J.L. Bernardes, E. Gazit, T.P.J. Knowles. Biomimetic peptide self-assembly for functional materials. *Nat. Rev.Chem*. 2020, 4, 615–634.

[4] S.M. Häffner, M. Malmsten. Influence of self-assembly on the performance of antimicrobial peptides. *Curr. Opin. Colloid Interface Sci.* 2018, 38, 56–79.
[5] F. Sun, X.R. Zhou, S.Z. Luo, L. Chen. Role of peptide self-assembly in antimicrobial peptides. *J. Pept. Sci.* 2015, 21, 530–539.
[6] R.N. Mitra, A. Shome, P. Paul, P.K. Das. Antimicrobial activity, biocompatibility and hydrogelation ability of dipeptide-based amphiphiles. *Org. Biomol. Chem.* 2009, 7, 94–102.
[7] A. Makovitzki, D. Avrahami, Y. Shai. Ultrashort antibacterial and antifungal lipopeptides. *Proc. Natl. Acad. Sci. U.S.A.* 2006, 103, 15997–6002.
[8] Y. Hu, M.N. Amin, S. Padhee, R.E. Wang, Q. Qiao, G. Bai, Y. Li, A. Mathew, C. Cao, J. Cai. Lipidated peptidomimetics with improved antimicrobial activity. *ACS Med. Chem. Lett.* 2012, 3, 683–686.
[9] A. Farrotti, P. Conflitti, S. Srivastava, J. Kanti Ghosh, A. Palleschi, L. Stella, G. Bocchinfuso. Molecular dynamics simulations of the host defense peptide temporin L and its Q3K derivative: an atomic level view from aggregation in water to bilayer perturbation. *Molecules*. 2017, 22: 1235.
[10] G. Manzo, P.M. Ferguson, C.K. Hind, M. Clifford, V.B. Gustilo, H. Ali, S.S. Bansal, T.T. Bui, A.F. Drake, R.A. Atkinson, J.M. Sutton, C.D. Lorenz, D.A. Phoenix, A.J. Mason. Temporin L and aurein 2.5 have identical conformations but subtly distinct membrane and antibacterial activities. *Sci Rep*. 2019, 9: 10934.
[11] Mangoni ML, Carotenuto A, Auriemma L, M.R. Saviello, P. Campiglia, I. Gomez-Monterrey, S. Malfi, L. Marcellini, D. Barra, E. Novellino, P. Grieco. Structure–activity relationship, conformational and biological studies of Temporin L analogues. *J. Med. Chem*. 2011, 54, 1298–1307.
[12] Saviello MR, Malfi S, Campiglia P, M.R. Saviello, S. Malfi, P. Campiglia, A. Cavalli, P. Grieco, E. Novellino, A. Carotenuto. New insight into the mechanism of action of the temporin antimicrobial peptides. *Biochemistry*. 2010, 49, 1477–1485.
[13] A. Carotenuto, S. Malfi, M.R. Saviello, P. Campiglia, I. Gomez-Monterrey, M.L. Mangoni, L. M. Gaddi, E. Novellino, P. Grieco. A different molecular mechanism underlying antimicrobial and hemolytic actions of temporins A and L. *J. Med. Chem*. 2008, 51, 2354–2362.
[14] P. Grieco, A. Carotenuto, L. Auriemma, M.R. Saviello, P. Campiglia, I. Gomez-Monterrey, L. Marcellini, V. Luca, D. Barra, E. Novellino, M.L. Mangoni. The effect of d-amino acid substitution on the selectivity of temporin L towards target cells: identification of a potent anti-Candida peptide. *Biochim Biophys Acta*. 2013, 1828, 652–660.
[15] Merlino F, Carotenuto A, Casciaro B, F. Martora, M.R. Loffredo, A. Di Grazia, A.M. Yousif, D. Brancaccio, L. Palomba, E. Novellino, M. Galdiero, M.R. Iovene, M.L. Mangoni, P. Grieco. Glycine-replaced derivatives of [Pro^{3},DLeu^{9}]TL, a temporin L analogue: evaluation of antimicrobial, cytotoxic and hemolytic activities. *Eur. J. Med. Chem*. 2017, 139, 750–761.

[16] S.Y. Lau, A.K. Taneja, R.S Hodges. Synthesis of a model protein of defined secondary and quaternary structure. Effect of chain length on the stabilization and formation of two-stranded alpha-helical coiled-coils. *J. Biol. Chem.* 1984, 259, 13253–13261.
[17] A. Makovitzki, J. Baram, Y. Shai. Antimicrobial lipopolypeptides composed of palmitoyl Di- and tricationic peptides: *in vitro* and *in vivo* activities, self-assembly to nanostructures, and a plausible mode of action. *Biochemistry*. 2008, 47, 10630–10636.
[18] A. Falanga, R. Tarallo, G. Vitiello, M. Vitiello, E. Perillo, M. Cantisani, G. D'Errico, M. Galdiero, S. Galdiero. Biophysical characterization and membrane interaction of the two fusion loops of glycoprotein B from herpes simplex type I virus. *PLoS One*. 2012, 7:e32186.
[19] M. Amaro, F. Reina, M. Hof, C. Eggeling, E. Sezgin. Laurdan and Di-4-ANEPPDHQ probe different properties of the membrane. *J. Phys. D. Appl. Phys.* 2017, 50, 134004–134004.
[20] S.Y. Lau, A.K. Taneja, R.S Hodges. Synthesis of a model protein of defined secondary and quaternary structure. Effect of chain length on the stabilization and formation of two-stranded alpha-helical coiled-coils. *J. Biol. Chem.* 1984, 259, 13253–13261.
[21] A. Hollmann, M. Martínez, M.E. Noguera, M.T. Augusto, A. Disalvo, N. C. Santos, L. Semorile, P.C. Maffía. Role of amphipathicity and hydrophobicity in the balance between hemolysis and peptide–membrane interactions of three related antimicrobial peptides. *Colloids Surf. B. Biointerfaces*. 2016, 141, 528–536.
[22] J.M.A Blair, M.A Webber, A.J. Baylay, D.O. Ogbolu, L.J.V. Piddock. Molecular mechanisms of antibiotic resistance. *Nat. Rev. Microbiol*. 2015, 13, 42–51.
[23] E. Grimsey, D.W.P. Collis, R. Mikut, K. Hilpert. The effect of lipidation and glycosylation on short cationic antimicrobial peptides. *Biochim. Biophys. Acta Biomembr*. 2020, 1862:183195.
[24] F. Merlino, S. Tomassi, A.M. Yousif, A. Messere, L. Marinelli, P. Grieco, E. Novellino, S. Cosconati, S. Di Maro. Boosting Fmoc solid phase peptide synthesis by ultrasonication. *Org. Lett*. 2019, 21, 6378–6382.
[26] R.A. Scheuerman, D. Tumelty. The reduction of aromatic nitro groups on solid supports using sodium hydrosulfite ($Na_2S_2O_4$). *Tetrahedron Lett*. 2000, 41, 6531–6535.
[26] F. Merlino, Y. Zhou, M. Cai, A. Carotenuto, A.M. Yousif, D. Brancaccio, S. Di Maro, S. Zappavigna, A. Limatola, E. Novellino, P. Grieco, V.J. Hruby. Development of macrocyclic peptidomimetics containing constrained α,α-dialkylated amino acids with potent and selective activity at human melanocortin receptors. *J. Med. Chem*. 2018, 61, 4263–4269.
[27] A. Di Grazia, F. Cappiello, A. Imanishi, A. Mastrofrancesco, M. Picardo, R. Paus, M.L. Mangoni. The frog skin derived antimicrobial peptide esculentin-1a(1-

21)NH2 promotes the migration of human HaCaT keratinocytes in an EGF receptor-dependent manner: a novel promoter of human skin wound healing?. *PLoS One*. 2015, 10:e0128663.
[28] E. Buommino, A. Carotenuto, I. Antignano, R. Bellavita, B. Casciaro, M.R. Loffredo, F. Merlino, E. Novellino, M.L. Mangoni, F.P. Nocera, D. Brancaccio, P. Punzi, D. Roversi, R. Ingenito, E. Bianchi, P. Grieco. The outcomes of decorated prolines in the discovery of antimicrobial peptides from Temporin-L. *Chem. Med. Chem*. 2019, 14, 1283–1290.
[29] M.E. Mercurio, S. Tomassi, M. Gaglione, R. Russo, A. Chambery, S. Lama, P. Stiuso, S. Cosconati, E. Novellino, S. Di Maro, A. Messere. Switchable protecting strategy for solid phase synthesis of DNA and RNA interacting nucleopeptides. *J. Org. Chem*. 2016, 81, 11612–11625.
[30] L. Lombardi, Y. Shi, A. Falanga, E. Galdiero, E. de Alteriis, G. Franci, I. Chourpa, H.S. Azeyedo, S. Galdiero. Enhancing the potency of antimicrobial peptides through molecular engineering and self-assembly. *Biomacromolecules*. 2019, 20, 1362–1374.
[31] M.J. Hope, M.B. Bally, G. Webb, P.R. Cullis. Production of large unilamellar vesicles by a rapid extrusion procedure. Characterization of size distribution, trapped volume and ability to maintain a membrane potential. *Biochim. Biophys. Acta*. 1985, 812, 55–65.
[32] R.A. Parente, S. Nir, F.C. Jr. Szoka. Mechanism of leakage of phospholipid vesicle contents induced by the peptide GALA. *Biochemistry*. 1990, 29, 8720–8728.
[33] A. Falanga, R. Tarallo, G. Vitiello, M. Vitiello, E. Perillo, M. Cantisani, G. D'Errico, M. Galdiero, S. Galdiero. Biophysical characterization and membrane interaction of the two fusion loops of glycoprotein B from herpes simplex type I virus. *PLoS One*. 2012, 7:e32186.

CHAPTER 4

TEMPORIN L ANALOGUES WITH DUAL ACTIVITY IN POLYMICROBIAL INFECTIONS

This chapter is published in:

1. Bellavita, R., Raucci, F., Merlino, F., Piccolo, M., Ferraro, M.G., Irace, C., Santamaria, R., Iqbal, A.J., Novellino, E., Grieco, P., Mascolo, N., Maione, F. Temporin L-derived peptide as a regulator of the acute inflammatory response in zymosan-induced peritonitis. *Biomedicine and Pharmacotherapy*. 123, 109788 (2020).

2. Bellavita, R., Vollaro, A., Catania, M.R., Merlino, F., De Martino, L., Nocera, F.P., Della Greca, M., Lembo, F., Grieco, P., Buommino, E. Novel antimicrobial peptide from Temporin L in the treatment of *Staphylococcus pseudintermedius* and *Malassezia pachydermatis* in polymicrobial inter-kingdom infection. *Antibiotics.* 9, 530 (2020).

3. PATENT PENDING

Inventors: Mascolo Nicola, Maione Francesco, Carotenuto Alfonso, Novellino Ettore, Merlino Franesco, **Bellavita Rosa**, Buommino Elisabetta, Grieco Paolo. **Title:** Temporin L analogues with anti-inflammatory and antimicrobial activity. **Application:** P021300IT-01/lm. **Date:** 19/06/2019.

CONTRIBUTIONS: Peptide synthesis.

4.1. POLYMICROBIAL INFECTIONS

Polymicrobial diseases are acute and chronic diseases caused by interactions between pathogens, including bacteria, viruses, fungi and parasites.[1] These physical interactions depend on several factors, such as range of environmental, pathogen and host factors. In polymicrobial infections, one microorganism could generate a niche, which favours the infection and colonisation of other pathogens and consequently the genesis of infection.[2] A polymicrobial infection associated to a bacterial-fungal interaction could be triggered by a reduction of fungal viability due to a transfer of bacterial secretions with a fungicide activity in the local environment, or by a transmission of toxins directly into fungal cell.[2] The interaction between *Staphylococcus pseudintermedius* and *Malassezia pachydermatis* are an example of bacteria-fungal interaction implicated in zoonotic diseases (*e.g.* otitis externa) easily transmitted from dogs to their owners.[3,4] *S. pseudintermedius* is not a common zoonotic pathogen in humans, but an opportunistic pathogen typically involved in skin and ear infections in dogs and cats.[5] The *M. pachydermatis* yeast inhabits prevalently the skin mycobiota of dogs and normally behave as "good citizen" in dogs, but can become a highly troublesome pathogen provoking ceruminous otitis externa and a "seborrhoeic" dermatitis.[6]

Today, over 60% of western families possess a pet, in most of cases a dog. A pet has a precious role in human life, because can increase the physical activity of owners reducing cardiovascular events and can help to owners suffering depression and mental stress.[7] Despite there are numerous benefits on psychosocial and physical health of their owners, many zoonotic pathogens are transmitted by dogs. Immunocompromised individuals and children are main individuals at risk in getting zoonoses infections. Generally, otitis caused by *Malassezia* is normally treated with topical or systemic azole therapy, often with miconazole—chlorhexidine shampoos or oral itraconazole or ketoconazole.[8] Recently, the emergence of azole resistance and the high toxicity of some antifungal drugs after a long treatment, have prompted

an increased interest in alternative topical antifungal drugs.[9,10] A promising alternative might be antimicrobial peptides (AMPs) such as temporins, since they have a considerable antimicrobial activity, especially towards fungal pathogens and Gram-positive bacteria.[11–13] Previously, an encouraging temporin L analogue, named [Pro^3,DLeu^9] (**1**), endowed with an efficient antifungal activity against *Candida albicans* and devoid of cytolytic effects *in vitro*, was identified.[14] This TL analogue was considered as a lead for our structure-activity relationship (SAR) study, in which the role of Gly in position 10 was explored by replacement with different amino acids, yielding peptides **2–11**.[15] On the basis of preliminary outcomes related their activity on Gram-positive and Gram-negative strains,[15] herein, the antifungal activity of peptides **2–11** was tested on *M. pachydermatis*. After a first screening of all compounds, only the most interesting was further evaluated for its antimicrobial activity on *S. pseudintermedius*, with the aim to discover novel agents effective against polymicrobial infections. The treatment of *S. pseudintermedius–M. pachydermatis* polymicrobial infection requires generally a therapy of antibacterial agents and anti-inflammatory drugs due to inflammatory process associated with it. In this regard, our aim was to get a novel molecule with a dual activity capable to eradicate successfully both polymicrobial infection and inflammation correlated to it. In view of the capacity of temporins to inhibit inflammatory process interfering with the expression of IL-6 controlling the level of pro-inflammatory cytokines (TNF-α and INF-γ),[16–18] we investigated a potential anti-inflammatory effect of the most potent peptide on both *M. pachydermatis* and *S. pseudintermedius*. In this study, we used an *in vivo* model of inflammation caused by intraperitoneal sub-lethal dose of zymosan and we elucidated the cellular and molecular profiles responsible for the mode of action.

4.2. RESULTS AND DISCUSSIONS

4.2.1 DESIGN

To understand the influence of cationic and hydrophobic residues on biological activity of native TL, a SAR study was previously performed by my research group. By the replacement of Gln^3 with a proline and Leu^9 with its D-enantiomer, analogue [Pro^3,DLeu^9] (**1**) endowed with an effective antimicrobial activity and devoid of cytotoxicity, was identified.[12] In our study, [Pro^3,DLeu^9] (**1**) was used as template for better understanding the role of Gly in position 10 by modifying the helical conformation at C-terminal region. In the past,[19] taking into consideration the high helical propensity of a leucine residue,[19] the Gly^{10} switching was already investigated by a Leu scanning. TL analogue with a leucine in position 10, had completely lost its antimicrobial efficacy and in addition had a strong hemolytic activity.[20] In the light of this result, we designed a library of peptides (**2–11**) in which the Gly^{10} was replaced by amino acid with different chemical proprieties (Table 1). Amino acids as proline, hydroxyproline (Hyp) and 2-aminoindane-2-carboxylic acid (Aic) were chosen to evaluate the impact of a α-helix breaker in C-terminal on antimicrobial activity, while the influence of Gly^{10} replacement on membrane interactions was investigated by amino acids containing a positive charge and an indole ring in their side chain (Lys and Trp, respectively) and a hydrophobic side chain such as norleucine. Additionally, L and D isomers were used to all amino acids, except for the non-chiral Aic. Preliminary results showed that most of compounds **2–12** showed a good activity towards Gram-positive and Gram-negative strains and all compounds were endowed with high anticandidal activity (Table 1).[15] Additionally, only peptides **9** and **10** showed a negligible toxicity against keratinocytes, in particular the data revealed a reduction in cell viability of about 30% *versus* 57% of **1** at a high concentration of 25 μM.[15]

Table 1. Preliminary results on some Gram-positive (*S. aureus* and *S. epidermidis*) and Gram- negative (*E. coli* and *P. aeuruginosa*) strains.[15]

		MIC values (μM)[a]				
Peptides	**Sequence**	*E. coli* D 21	*P. aeruginosa* ATCC 27853	*S. aureus Cowan I*	*S. epidermidis* ATCC 12228	*C. albicans* ATCC 10231
1	F V P W F S K F DL **Gly[10]** R I L	12.5	50	12.5	6.25	3.12
2	F V P W F S K F DL **Pro[10]** R I L	25	50	3.12	3.12	1.56
3	F V P W F S K F DL **DPro[10]** R I L	50	>50	>50	25	3.12
4	F V P W F S K F DL **Hyp[10]** R I L	25	50	6.25	6.25	3.12
5	F V P W F S K F DL **DHyp[10]** R I L	25	>50	>50	50	3.12
6	F V P W F S K F DL **Nle[10]** R I L	25	50	3.12	3.12	3.12
7	F V P W F S K F DL **DNle[10]** R I L	25	50	3.12	3.12	3.12
8	F V P W F S K F DL **Lys[10]** R I L	12.5	12.5	6.25	3.12	1.56
9	F V P W F S K F DL **DLys[10]** R I L	12.5	12.5	12.5	3.12	1.56
10	F V P W F S K F DL **Trp[10]** R I L	25	>50	3.12	1.56	3.12
11	F V P W F S K F DL **DTrp[10]** R I L	25	50	3.12	1.56	3.12
12	F V P W F S K F DL **Aic[10]** R I L	>50	>50	1.56	1.56	6.25

In the light of these promising results, we explored the effectiveness of all compounds **2–12** in the treatment of polymicrobial infection caused by an *M. pachydermatis*– *S. pseudintermedius* interaction and in inflammation associated with it. In our design, we considered the opportunity to gain a molecule with a dual activity, that is capable to act on two different targets and eradicate simultaneously two different infectious processes.

4.2.2. BIOLOGICAL STUDIES ON *M. PACHYDERMATIS* AND *S. PSEUDINTERMEDIUS*

Antimicrobial Susceptibility of M. Pachydermatis. The minimum inhibitory concentration (MIC) values of tested compounds against *M. pachydermatis* are reported in Table 2. Peptide **9** showed the highest inhibitory properties with a MIC value of 6.25 μM. Peptides **8** and **11** inhibited the yeast growth at a MIC value of

12.5 μM, while the other compounds were not as effective. The minimum mycocidal concentration (MMC) of peptide **9** causing ≥3log10 reduction in colony count from the starting inoculum, was 6.25 μM. The MMC/MIC ratio of 1 indicated a mycocidal activity of peptide **9**.

Table 2. In vitro antifungal activity. Minimum inhibitory concentration (MIC), minimum mycocidal concentration (MMC) and MMC/MIC ratios for peptides evaluated against *M. pachydermatis*.

Peptides	Sequence	MIC Values (μM)	MMC Values (μM)	MMC/MIC Ratio
1	F V P W F S K F DL **Gly^{10}** R I L	25	100	4
2	F V P W F S K F DL **Pro^{10}** R I L	25	100	4
3	F V P W F S K F DL **DPro^{10}** R I L	25	100	4
4	F V P W F S K F DL **Hyp^{10}** R I L	25	100	4
5	F V P W F S K F DL **DHyp^{10}** R I L	25	100	4
6	F V P W F S K F DL **Nle^{10}** R I L	25	100	4
7	F V P W F S K F DL **DNle^{10}** R I L	25	100	4
8	F V P W F S K F DL **Lys^{10}** R I L	12.5	25	2
9	F V P W F S K F DL **DLys^{10}** R I L	6.25	6.25	1
10	F V P W F S K F DL **Trp^{10}** R I L	25	100	4
11	F V P W F S K F DL **DTrp^{10}** R I L	12.5	25	2
12	F V P W F S K F DL **Aic^{10}** R I L	25	100	4

Resistance acquisition test. To evaluate if the yeast acquired resistance to peptide **9** after a prolonged treatment, *M. pachydermatis* was subcultured through serial passaging in the presence of a sublethal peptide **9** concentration (3.12 μM). After 1 generation subculture, peptide **9** reduced cell growth, affecting only in part yeast cell vitality (Table 3); however, after 15 yeast subcultures (about 2 months treatment), *M. pachydermatis* was no more able to replicate in the presence of peptide **9**.

Table 3. Resistance acquisition tests to 3.12 μM of peptide **9**. Each experiment is the result of three independent experiments performed in triplicate.

Strains	Log10 CFU/mL After 1 Generation Subculture Including Pept 9	Log10 CFU/mL After 15 Generation Subcultures Including Pept 9
M. Pachydermatis **Untreated**	8.10 ± 0.21	8.26 ± 0.29
M. Pachydermatis **+ Pept 9**	5.80 ± 0.25	2.10 ± 0.12

Antimicrobial susceptibility of S. pseudintermedius. To investigate the efficacy of peptide **9** in the treatment of *S. pseudintermedius–M. pachydermatis* polymicrobial infection, two strains of *S. pseudintermedius,* isolated from auricular swabs of dogs suffering from otitis externa, were used. The strains were characterized for their pattern of antibiotic susceptibility as previously reported.[20] One strain resulted in oxacillin resistant (MRSP) and the other oxacillin susceptible (MSSP).

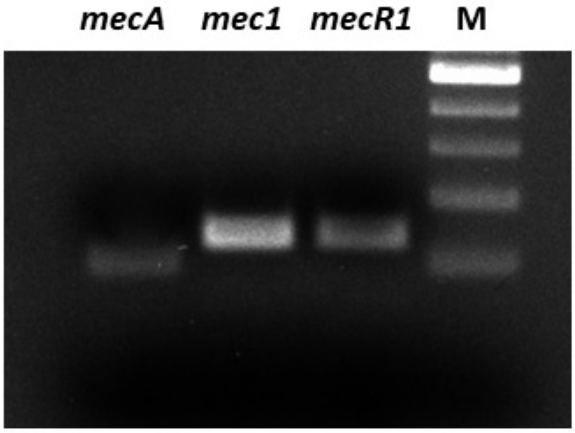

Figure 1. Detection of genes from mec operon in methicillin-resistant *S. pseudintermedius* (MRSP) strain. M: 100bp ladder marker (BiotechRabbit).

Both the MSSP and the MRSP strains were screened for the presence of *mecA*, *mec1*, *mecR1* genes by PCR. The results showed in Figure 1 are relative to MRSP strain, the only one that demonstrated to possess the *mecA* operon. The antimicrobial activity of peptide **9** against MRSP and MSSP strains is shown in Table 4. Peptide **9** exhibited a significant MIC value at 1.56 μM for MSSP and 6.25 μM for MRSP. As expected, oxacillin treated MRSP showed a MIC value four times higher than MSSP strain. Minimum bactericidal concentration (MBC) was also calculated and resulted in 3.12 μM for MSSP and 12.5 μM for MRSP. The MBC/MIC ratio values are reported in Table 4.

Table 4. MIC, minimum bactericidal concentration (MBC), MBC/MIC ratio, and FIC_{index} values (μM) of peptide **9** on selected bacterial strains. N.d.= not determined. Each experiment is the result of three independent experiments performed in triplicate.

Strains	MIC	MBC	Oxacillin	Vancomycin	MBC/MIC Ratio	FIC_{index}
MSSP	1.56	3.12	<5	<1.4	2	n.d.
MRSP	6.25	12.5	25	<1.4	2	0.37

To confirm the bactericidal or bacteriostatic activity of peptide **9** we performed the time kill assay at the MIC value (Table 5). Peptide **9** inhibited bacterial growth already at 1 h. After 6h treatment, a dramatic decrease in cell growth was observed. However, the number of both MSSP and MRSP cells increased 24h after peptide **9** treatment. These results supported a bacteriostatic activity of peptide **9**, because it is likely that a critical bactericidal concentration is not reached on all cell membranes, causing the death of some bacteria (highest cell membrane accumulation) and only cell growth arrest of others (low accumulation).[21]

Influence of Peptide 9 on MecA Gene Expression. Quantification data obtained by RT-PCR were normalized to the reference gene for 16S rRNA. The results showed that the mode of action of peptide **9** was not implicate in a regulation of mecA gene expression, but in a membranolytic process involving a membrane interaction, followed by an aggregation in membrane and then a disintegration of membrane by pore formation as shown in Bellavita et al.[22] On the basis of this study on membrane interaction, we hypothesize a similar mechanism of action of peptide **9** on MSSP and MRSP.

Synergistic study between peptide 9 and oxacillin. The synergism between peptide **9** and oxacillin was determined using the checkerboard technique. Oxacillin and peptide **9** were used alone and in combination against MRSP planktonic cells. Oxacillin and peptide **9** MICs value were 25 μM and 6.25 μM, respectively. The highest synergistic interaction against MRSP was obtained in the wells with the best

combination values of 1.56 μM peptide **9** (1/4 MIC) and 3.1 μM oxacillin (1/8 MIC). The FIC index, equal to 0.37, confirmed the synergistic effect of peptide **9** and oxacillin (Table 4). This enhanced susceptibility of MRSP to oxacillin by peptide **9** is correlated to its capacity to induce membrane leakage, consisting in a pore formation and resultant penetration of oxacillin in bacterial cell.[22]

Table 5. Time-kill assay of peptide **9** against methicillin-susceptible *S. pseudintermedius* (MSSP) and MRSP. Each experiment is the result of three independent experiments performed in triplicate.

Strains	**Log_{10}CFU/mL**					
	0 h	1 h	2 h	4 h	6 h	24 h
MSSP untreated	5.50 ± 0.21	5.74 ± 0.21	5.80 ± 0.25	5.87 ± 0.19	7.10 ± 0.31	9.8 ± 0.31
MSSP + cmpd 9	5.45 ± 0.25	0.60 ± 0.12	0.58 ± 0.32	0.89 ± 0.15	0.46 ± 0.15	4.97 ± 0.30
MRSP untreated	5.30 ± 0.21	5.37 ± 0.32	5.84 ± 0.28	5.91 ± 0.29	6.85 ± 0.25	9.36 ± 0.25
MRSP+ cmpd 9	5.30 ± 0.18	2.47 ± 0.18	2.38 ± 0.19	1.30 ± 0.21	0.77 ± 0.12	4.86 ± 0.28

***Peptide 9 reduces MSSP and MSRP biofilm viability*.** Biofilm formation, well-known as the main virulence factor in staphylococcal skin infections, can be divided into five stages: initial reversible attachment (**1**), irreversible attachment (**2-3**), maturation (**4**) and dispersion. In a recent study, TL (precursor of peptide **1**) proved to be an effective agent able to affect *P. aeruginosa* PAO1 and methicillin-resistant *S.aureus* (MRSA) biofilms, inhibiting the biofilm attachment stage.[23] In this context, we investigated the capacity of peptide **9** to inhibit MSSP and MRSP biofilm formation in initial reversible attachment, using crystal violet (CV) assay. Peptide **9** was tested at sub-MIC concentrations ranging from 0.095 to 0.78 μM for 24h. The max concentration used (0.78 μM) did not affect planktonic growth, which represents first stage of the biofilm reversible attachment. Quantification of crystal violet staining by measurement of OD595 showed the ineffectiveness of peptide **9** on MSSP and MSRP biofilm formation at each tested concentration (Figure 2).

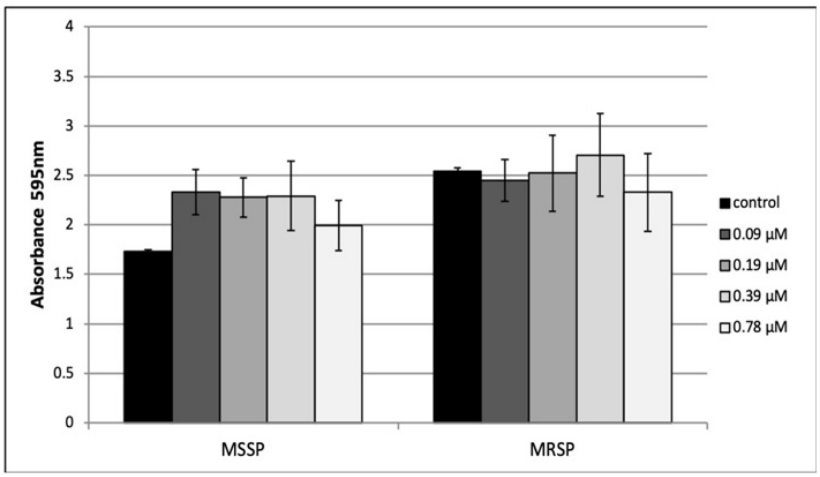

Figure 2. Effect of sub-MIC peptide **9** concentrations on MSSP and MRSP biofilm formation assessed by crystal violet assay. Experiments were performed in triplicate in three independent experiments.

In addition, mature biofilm displays antimicrobial resistance offering a favorable living environment for the growth of resistant bacteria. In this context, the activity of peptide **9** was also evaluated on biofilm maturation. One-day-old-biofilms of both MSSP and MRSP strains were incubated with peptide **9** at a concentration of 4X MIC, 2X MIC and 1X MIC for 24 h. Crystal violet results revealed that peptide **9** did not affect the biomass of both treated biofilms at concentrations up to 25 µM (Figure 3, upper panel). On the contrary, XTT assay clearly demonstrated that peptide **9** caused a significant decrease of both MSSP and MSRP biofilm viability compared to the corresponding untreated control (Figure 3, bottom panel). It was able to reduce biofilm viability of MRSP at 6.25 and 12.5 µM, by 38% and 52%, respectively, and 38% for MSSP at 12.5 µM.

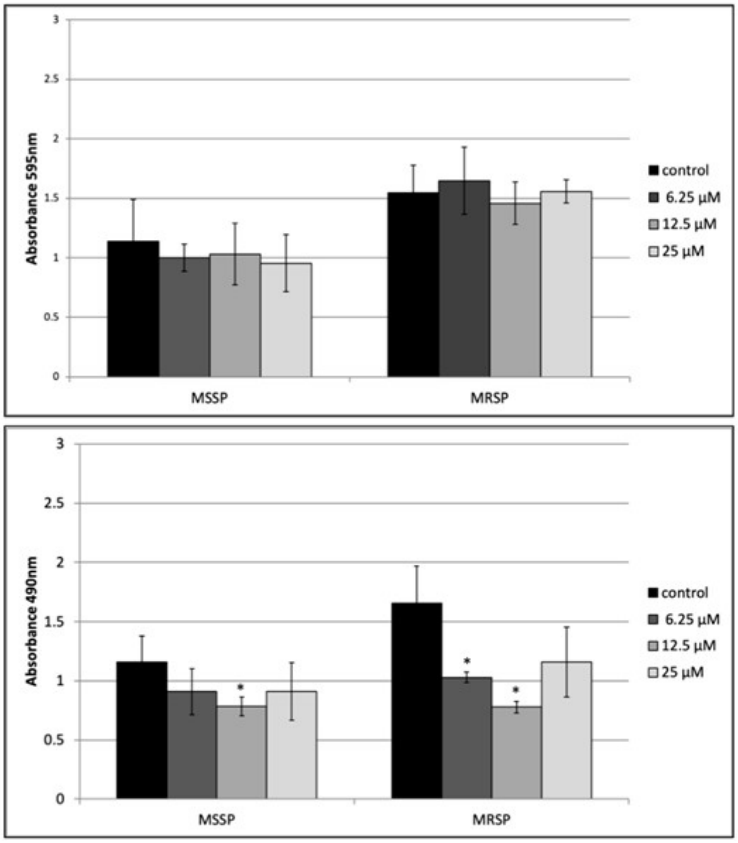

Figure 3. Peptide **9** activity on MSSP and MRSP mature biofilm assessed by crystal violet assay (upper panel) and XTT assay (bottom panel). Experiments were performed in triplicate in three independent experiments.

Additionally, the effect of peptide **9** on the mature biofilm of MRSP was observed by confocal microscopy at 12.5 µM, the dose at which we observed the maximal eradicating effect. Images of treated biofilm showed some red zone representing cells within biofilm that were killed or damaged by peptide **9** (Figure 4). Similarly to TL, peptide **9** can interact with the extracellular matrix of biofilm by its positive charges distributed in the peptide sequence, facilitating transition through this environment and improving its antimicrobial activity.[23]

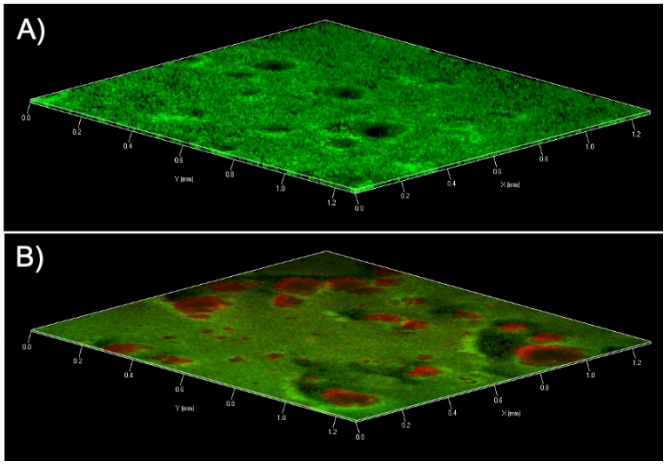

Figure 4. Peptide **9** effects on MRSP mature biofilm assessed by Confocal laser microscopy. (A) Untreated biofilm; (B) treated biofilm (12 μM).

4.2.3. *IN VITRO* AND *IN VIVO* ANTI-INFLAMMATORY STUDIES

With the discovery of the effectiveness of peptide **9** in the treatment of *S. pseudintermedius–M. pachydermatis* polymicrobial infection, we investigated a potential anti-inflammatory activity of peptide **9** to eradicate simultaneously polymicrobial infection and inflammation generally associated with it.

Macrophages biological response to treatments in vitro. First, we evaluated the activity of peptide **9** and its parent peptide (**1**) on the growth and proliferation of macrophages J774 *in vitro* to identify the lower micromolar range to allow a safe animal experimentation. As reported in Figure 5, the concentration effect curves did not show interference with cell growth and proliferation up to the concentration of 20 μM after 4 (A) and 24 h (B) of treatment with both peptides and anti-inflammatory reference drugs, *i.e.* Diclofenac and Betamethasone. However, at 25 μM a slight interference with cell viability was found for both peptides. Indeed, the calculated IC_{50} values of both peptides were higher than 80 μM after 4 h and 24 h of treatment. These values were similar to those measured for betamethasone and diclofenac (~85 and ~200 μM respectively), herein used as reference drugs.

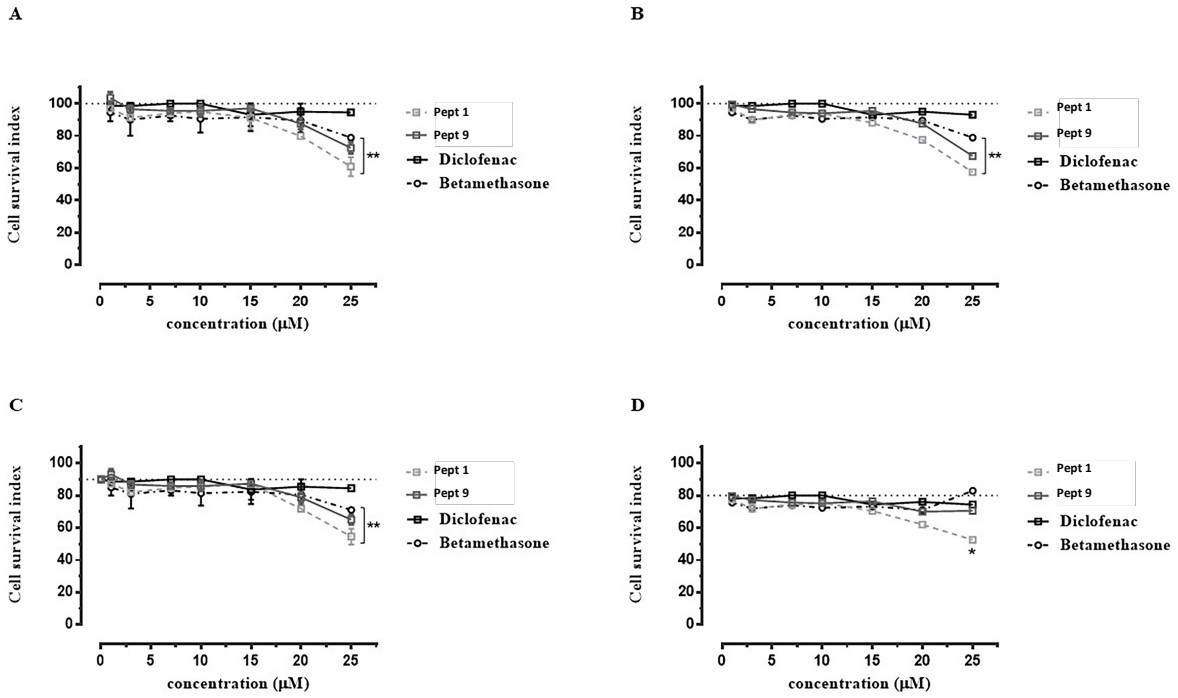

Figure 5. Bioactivity profile of peptides in J774 macrophages. Cell survival index, evaluated by MTT assay, on murine macrophage cell line, following 4 (A) and 24 h (B) of treatment with selected concentrations (1→25 μM) of peptide **1** and **9**. Anti-inflammatory positive control incubations were carried out by equivalent concentrations of Diclofenac and Betamethasone. Data are expressed as percentage of untreated control cells and are reported as mean of five independent experiments ± S.E.M. *P≤0.05, **P≤0.01, vs. control cells.

In another set of experiments cells were pretreated with zymosan (100 ng/ml) followed by peptide **1** and **9** for 4 (Figure 5C) and 24 h (Figure 5D), with the same range of concentrations. Although we observed a small reduction in cell vitality after zymosan treatment, the effect of both peptides was similar to that observed in "non-stimulated" conditions.

Anti-inflammatory effect of peptides 1 and 9 in zymosan-induced peritonitis in mice. In light of the safety of peptide **1** and **9** evidenced through *in vitro* evaluations on J774 macrophages, we investigated the role of both peptides in an *in vivo* model of inflammation that allowed for the characterization of leukocyte recruitment and local inflammatory mediator production. Mice were subjected to i.p. injection of 500

mg/kg zymosan, in the presence or absence of peptide **1** and **9** (1–10 mg/kg dissolved in PBS).

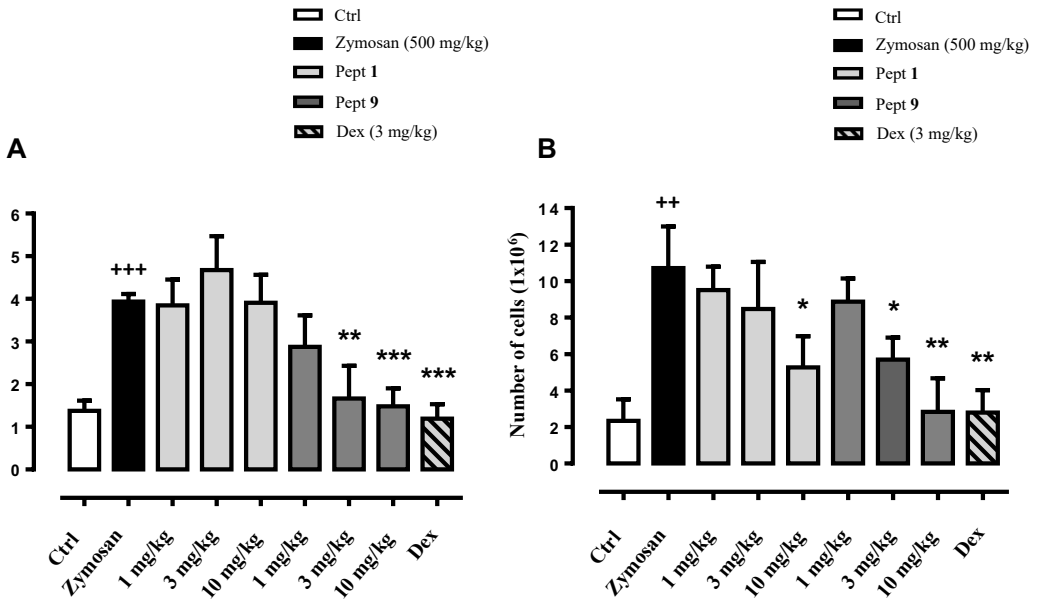

Figure 6. Anti-inflammatory effect of temporin-derived peptides in zymosan-induced peritonitis in mice. Mice (n=7) were injected intraperitoneally with 500 mg/kg zymosan, with 500 mg/kg zymosan and 1–10 mg/kg of peptides **1** and **9** or 500 mg/kg zymosan and 3 mg/kg of dexamethasone (Dex). At 4 (A) and 24 h (B) after zymosan injection, peritoneal essudate from each mouse was recovered and total cell number (expressed as 1×10^6 and normalized to exudate levels) was evaluated. Results are expressed as mean ± S.E.M. ++P≤0.01,+++P≤0.005 vs. ctrl group, *P≤0.05, **P≤0.01 and ***P≤0.005 compared to zymosan-treated mice.

As internal control, i.p injection of PBS alone without zymosan and i.p. injection of Dex (3 mg/kg) post zymosan administration were also assessed. As shown in Fig. 6A, zymosan injection elicited a strong leucocyte recruitment at 4h (~4.5×10^6) which was significantly reduced after peptide **9** administration at a dose of 10 mg/kg (P≤0.05). At this time-point the effect of peptide **1** (1–10 mg/kg) was not significant compared to mice injected with peptide **9** and Dex (P≤0.005).

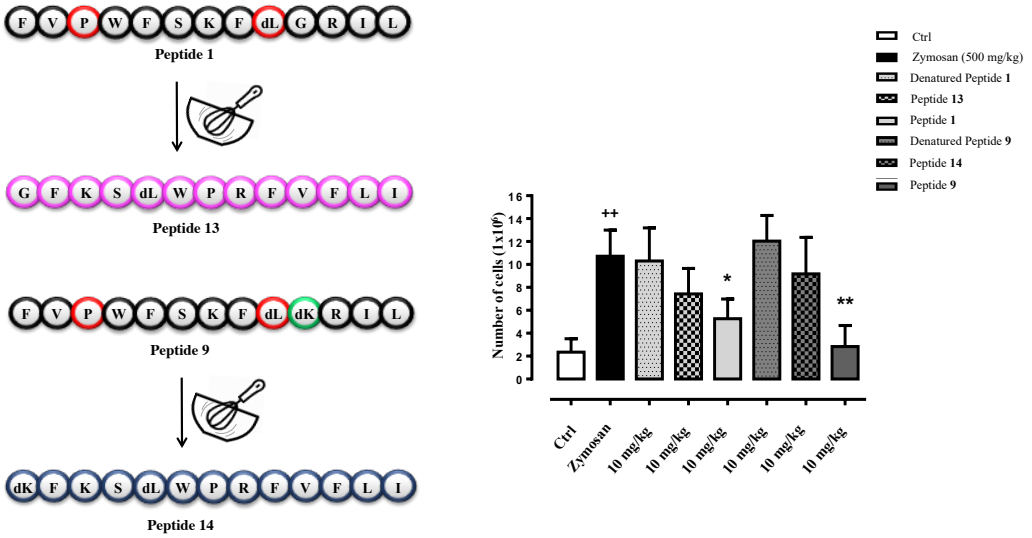

Figure 7. A) Peptide **13** and **14** represent scrambled sequence of peptide **1** and **9**, respectively. **B)** Effect of denatured and scrambled temporin-derived peptides in zymosan-induced peritonitis in mice. Mice (n=7) were injected intraperitoneally with 500 mg/kg zymosan, with 500 mg/kg zymosan and 10 mg/kg of peptides **1** and **9** or 500 mg/kg zymosan and peptides (**1** and **9**) denatured and scrambled (peptides **13** and **14**) (10 mg/kg). At 24 h post injection, peritoneal essudate from each mouse was recovered and total cell number (expressed as 1×10^6 and normalized to exudate levels) was evaluated. Results are expressed as mean ± S.E.M. ++P≤0.01 compared vs. ctrl group, *P≤0.05 and **P≤0.01 vs. zymosan treated mice.

Conversely, after 24 h both peptides at 10 mg/kg significantly reduced (P≤0.05 and P≤0.01 respectively for peptide **1** and **9**) leukocyte infiltration (~11×10^6 after zymosan injection) with a profile, for peptide **9**, comparable to Dex (P≤0.01). Interestingly, peptide **9** also displayed significant effects at a lower dose of 3 mg/kg (P≤0.05) (Fig. 6B). Other experimental groups also included mice that received zymosan with peptide **1** and **9** at the highest dose (10 mg/kg) inactivated by denaturation or peptides **13** and **14** with scrambled aminoacidic assembly (Figure 7). As shown in Figure 7B, both peptides at 24 h did not display any significant inhibitory effects on leukocyte recruitment, highlighting the hypothesis that only "selected peptides sequence" elicited observed anti-inflammatory effects.

Modulation of cellular inflammatory infiltrates. Zymosan, a polysaccharide cell wall component derived from *Saccharomyces cerevisiae*,[24] has been reported to elicit a multiple organ failure and a massive recruitment of innate immunity cells in

the peritoneal cavity, mainly characterized by neutrophils and monocytes.[25] The production of pro-inflammatory cytokines, such as IL-1, IL-6, TNF-α,[26,27] and of prostaglandin metabolites[28] is high in the pathophysiology of zymosan-induced shock. TNF-α plays a pivotal role characterized by the release of IL-1 and IL-6 that orchestrate neutrophil, macrophage, and fibroblast accumulation to the site of inflammation.[29,30] This scenario is supported by the CC chemokine MCP-1, as one of the most potent chemotactic factors for monocyte migration to the site of tissue injury.[31] On the other hand, IL-10 is an anti-inflammatory cytokine that mainly suppresses inflammatory response by increasing anti-inflammatory factors and inhibiting the activation and function of T cells and monocytes.[32]

To test the effects of an acute systemic administration of peptide **1** and **9**, we administered these peptides with the same dose (10 mg/kg) that evoked the optimal inhibition of leukocyte recruitment to the peritoneum. A single administration of zymosan into the peritoneal cavity causes a transient infiltration of leukocytes that becomes evident between 4–24 h and declines by 48h. All mice were sacrificed 24 h after zymosan administration. A single injection of zymosan (500 mg/kg) i.p caused a significant increase of the levels of TNF-α, IL-6, IL-10 and MCP-1 after 24h, compared to the control group (Fig. 8A, B, C and D respectively). Interestingly, peptide **1** at 10 mg/kg significantly ($p \leq 0.05$) reduced the levels of TNF-α (Fig. 8A) and IL-6 (Fig. 8B). The levels of IL-10 (Fig. 8C) and MCP-1 (Fig. 8D) remained unaffected. Similarly, peptide **9**, at the same dose, also reduced ($p \leq 0.01$) the levels of TNF-α (Fig. 8A) and IL-6 (Fig. 8B), but a reduction was also observed in ($p \leq 0.05$) MCP-1 (Fig. 8D). Injection of the positive control Dex (3 mg/kg) decreased the values of mentioned cyto-chemokines (Fig. 8A, B, C and D) with a profile comparable to peptide **9**.

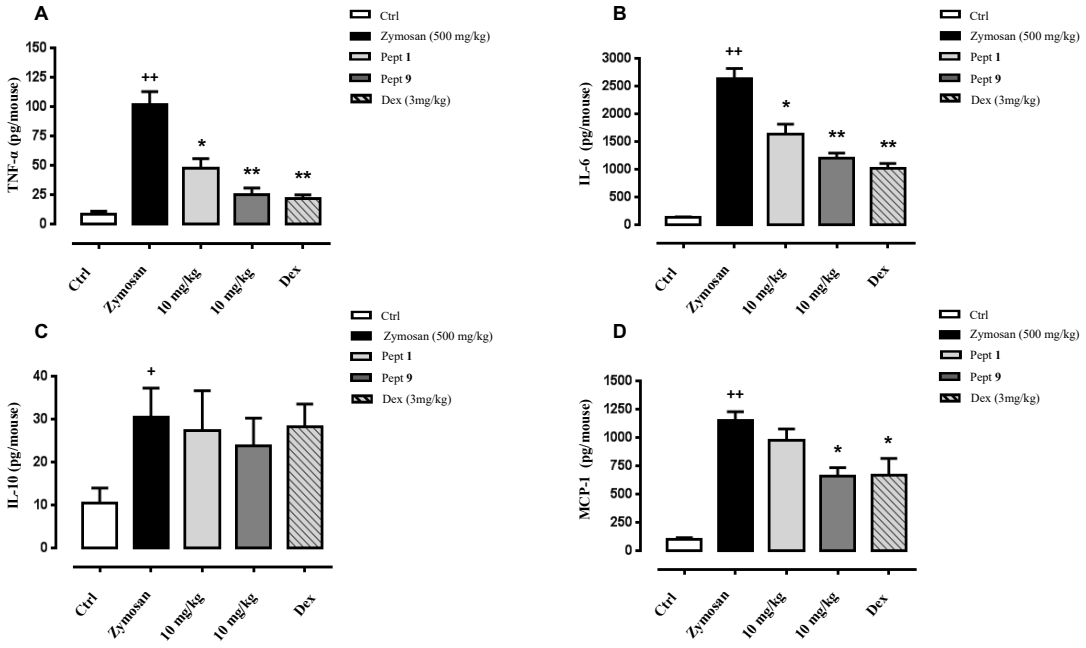

Figure 8. Cyto-chemokines analysis of collected peritoneal exudates. Analysis of collected peritoneal exudates identified heightened levels of the classical pro-inflammatory cyto-chemokines TNF-α (A), IL-6 (B), IL-10 (C), and MCP-1 (D) in the peritoneal cavity of mice from zymosan groups (n=7). Significant differences were found in relative levels after peptides **1** and **9** administration (n=7). Results (normalized to exudate levels) are expressed as mean ± S.E.M. +P≤0.05 and++P≤0.01 vs. ctrl group, *P≤0.05 and **P≤0.01 vs. zymosan-treated mice.

Based on these results, we selected the most active temporin L-derived peptide (peptide **9**) to investigate the phenotype of inflammatory leukocytes recruited to the peritoneal cavity. Leucocytes collected at 24h time-point post zymosan injection were stained with an anti-B220, anti-F480, anti-GR1, anti-CD115 antibodies and then analyzed by flow cytometry. We did not observe any significant difference in terms of neutrophils (GR1+ cells) and macrophages (F4/80+ cells) reduction after peptide **9** treatment (data not shown). However, to identify potential differences in monocyte subpopulations, total cells were gated on their totality (Fig. 9A, gate R1) and singlet (Fig. 9B, gate R2) for the identification of B220– population (Fig. 9C, gate R3) followed by GR1 and F480 expression (Fig. 9D–F). Double high positive population for these markers (Gate R4, 9.05 ± 0.32, 41.20 ± 2.78 and 31.70 ± 2.55 of double high positive population respectively for Ctrl, zymosan and zymosan+

peptide **9**; Figure 9J) were then further interrogated for CD115 (Figure 9G–I) as its expression level is commonly correlated with the degree of maturation of inflammatory monocytes. Our results show that in zymosan-injected mice, most cells recovered were B220–/GR1hi-F480hi/CD115+ (10.70 ± 1.14 compared to 2.70 ± 0.24 of Ctrl) with a significant lower expression in peptide **9**-treated group (3.24 ± 1.41) (Figure 10K). These values were strengthened by a low percentage of positive cells found in the staining for the isotype control antibodies.

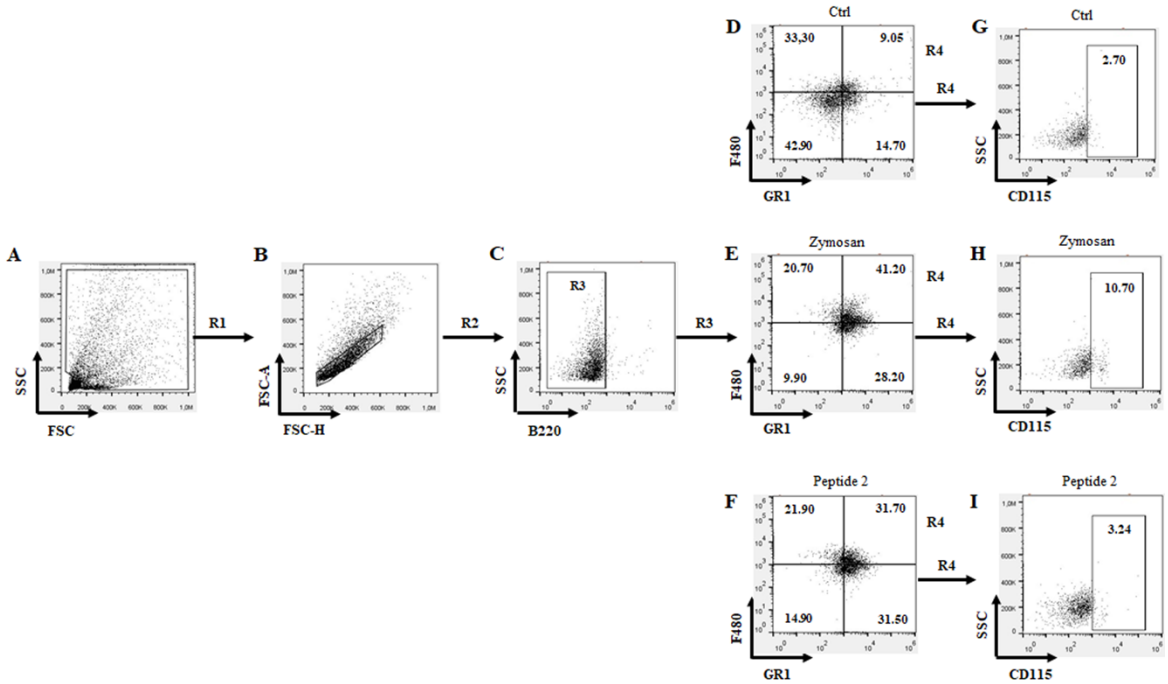

Figure 9. Flow cytometry strategy applied to identify the modulation of inflammatory monocytes in zymosan and zymosan+peptide **9**-treated group. Cells obtained at 24 h time-point post zymosan injection in all experimental conditions were washed and stained with the following panel of antibodies: anti-B220, anti-F480, anti-GR1 and anti-CD115. Specifically, to identify potential differences in monocyte subpopulations, total cells were gated for their totality (A, gate R1) and singlet (B, gate R2) to identify B220– population (C, gate R3) followed by GR1 and F480 expression (D-F). Double high positive population for these markers (gate R4) was then further interrogated for CD115 (G-I) The numbers in the dot plots indicated the percentage of positively stained cells after gating strategy. FACS plots are representative of seven samples with similar results. Results (normalized to exudate levels) are presented as mean ± S.E.M (J and K) of n=7 mice per group. +++P≤0.001 vs. ctrl group, *P≤0.05 and **P≤0.01 vs. zymosan-treated mice.

4.3. CONCLUSIONS

In conclusion, we discovered, for the first time, an analogue of TL native with a dual activity that is capable to wipe up inter-kingdom infection caused by *S. pseudintermedius* and *M. pachydermatis* interaction and inflammatory process associated to it. Peptide **9** contrasted the growth of both *S. pseudintermedius* and *M. pachydermatis*, it did not cause yeast drug resistance and increased the susceptibility of oxacillin against MRSP, not inhibiting the mecA gene expression but inducing a membrane disintegration. The use of peptide **9** may provide novel avenues of possible therapeutic strategies to combat inter-kingdom infections and inflammation, since it showed a notable anti-inflammatory activity *in vivo* in response to zymosan-induced peritonitis, modulating the recruitment of inflammatory monocytes. Therefore, the topical treatment using peptide **9** as drugs in otitis externa in dogs and in wound infections in humans caused by zoonotic microorganisms, might be a valid alternative to traditional therapies.

4.4. EXPERIMENTAL SECTION

4.4.1. CHEMISTRY

Peptides synthesis by US-SPPS. The synthesis of peptides was performed by using the ultrasound-assisted solid-phase peptide strategy (US-SPPS) combined with the orthogonal Fmoc/tBu chemistry, as described in Chapter 3.[33] Each peptide was assembled on a Rink amide resin (0.1 mmol from 0.64 mmol/g of loading substitution), as solid support. First, Fmoc group was deprotected by treatment with a solution of 20% piperidine in DMF (0.5 + 1 min) and the coupling reactions were performed using Fmoc-amino acid (3 equiv,), HBTU (3 equiv), HOBt (3 equiv) and DIEA (6 equiv), 5 min. Finally, peptides were purified and characterized by RP-HPLC using linear gradients of MeCN (0.1% TFA) in water (0.1% TFA), from 10 to 90% over 20 min (Table 6). All compounds examined for biological activity were purified to >96%.

Table 6. Analytical data of peptides **2–14.**

Peptides	Sequence	R_t(min)	MS Found	MS Calcd
2	F V P W F S K F DL **Pro^{10}** R I L	13.28	1649.25	1649.03
3	F V P W F S K F DL **DPro^{10}** R I L	12.81	1648.82	1649.03
4	F V P W F S K F DL **Hyp^{10}** R I L	12.98	1664.97	1665.03
5	F V P W F S K F DL **DHyp^{10}** R I L	12.61	1665.13	1665.03
6	F V P W F S K F DL **Nle^{10}** R I L	13.41	1665.72	1665.03
7	F V P W F S K F DL **DNle^{10}** R I L	13.49	1665.66	1665.03
8	F V P W F S K F DL **Lys^{10}** R I L	12.52	1680.54	1680.09
9	F V P W F S K F DL **DLys^{10}** R I L	12.52	1680.41	1680.09
10	F V P W F S K F DL **Trp^{10}** R I L	13.49	1738.85	1738.13
11	F V P W F S K F DL **DTrp^{10}** R I L	13.60	1737.98	1738.13
12	F V P W F S K F DL **Aic^{10}** R I L	14.19	1711.51	1711.10
13	G F K S DL W P R F V F L I	12.72	1608.42	1607.93
14	DK F K S DL W P R F L I	11.41	1680.41	1681.02

4.4.2 BIOLOGY

Microbial Strains and Culture. *M. pachydermatis* was cultured onto Sabouraud dextrose agar with chloramphenicol (Oxoid Ltd, London, UK) at 30 °C.[34] Veterinary clinical strains of *S. pseudintermedius* were isolated from auricular swabs of dogs suffering from otitis externa and processed at the Microbiology Laboratory of the Department of Veterinary Medicine and Animal Production, University of Naples "Federico II" (Italy). *S. pseudintermedius* strains were plated on blood agar base supplemented with 5% sheep blood and on mannitol-salt agar, and incubated aerobically at 37 °C for 24–48 h.[35]

Molecular Analysis. Genomic DNA extraction was performed by using GenUp Bacteria gDNA kit (BiotechRabbit, Berlin, Germany) according to the manufacturer's instructions. All the isolates were tested for genes of the mec operon using the polymerase chain reaction (PCR).[ref]

Resistance Acquisition Tests . To evaluate if the yeast acquired resistance to the drug, after a continued treatment, *M. pachydermatis* was subcultured with a sub lethal concentration of peptide **9** (1/2 MIC). Briefly, a final 3.12 μM peptide **9**

concentration was added to yeast inoculum suspension equivalent to 1–3 × 10^6 CFU/mL in Sabouraud dextrose broth (SB) and incubated 72 h at 30 °C (inoculum 1). After this period, optical density was measured and a new yeast subculture with 3.12 μM of peptide **9** was prepared starting from inoculum 1 (inoculum 2). Three days after, optical density was again recorded and a new inoculum in presence of peptide **9** prepared. This was repeated until evident yeast death was observed.

Antimicrobial Activity Assay. MIC of all compounds was determined in Sabouraud Dextrose broth with 1% tween 80 (SB) medium, for *M. pachydermatis*, and Mueller–Hinton broth (MH), for *S. pseudintermedius*, by the broth microdilution assay (BMD) in 96-well microtiter plates, as previously reported.[36]

Killing Rate. Bacterial suspension (10^5 CFU/mL) was added to microplates along with peptide **9** at 6.25 μM MIC concentration.[37] Plates were incubated at 37 °C on an orbital shaker at 120 rpm. Viability assessments were performed at 0, 2, 4, 6 and 24 h by plating 0.01 mL undiluted and 10-fold serially diluted samples onto Mueller–Hinton plates in triplicate. After overnight incubation at 37 °C, bacterial colonies were counted and compared with counts from control cultures.

Checkerboard Method. The interaction between peptide **9** and oxacillin against MRSP was evaluated by the checkerboard method. Briefly, twofold serial dilutions of oxacillin distributed in horizontal rows of 96-well microtiter plate were cross-diluted vertically by twofold serial dilutions of peptide **9** to at least double the MIC. The peptide **9** tested concentration ranging from 0.19 to 12.5 μM and Oxacillin from 1.25 to 25 μM (0.5 to 10 μg/mL). Microtiter plates were inoculated with bacteria at an approximate concentration of 10^5 × CFU/mL and incubated at 37 °C for 24 h. MIC values of the combinations were determined as the lowest concentrations that completely inhibited bacterial growth, recorded as optical density at 595 nm. To evaluate the effect of the combination treatment, the fractional inhibitory

concentration (FIC) index for each combination was calculated as follows: FIC index = FIC of peptide **9** + FIC of oxacillin, where FIC of peptide **9** (or oxacillin) was defined as the ratio of MIC of peptide **9** (or oxacillin) in combination and MIC of peptide **9** (or oxacillin) alone. The FIC index values were interpreted as follows: ≤0.5, synergistic; >0.5 to ≤1.0, additive; >1.0 to ≤2.0, indifferent; and >2.0, antagonistic effects.[38]

Biofilm study. Anti-biofilm activity of peptide **9** was examined by the crystal violet assay previously described with minor modifications.[39] Microtiter plates were inoculated with bacteria at a final density of 10^6 CFU/mL and treated with peptide **9** ranging from 0.095 to 0.78 μM. Control cells were grown in the absence of peptide **9**. After 24 h incubation at 37° C, the amount of biofilm formed in the wells was measured by crystal violet staining and the absorbance of the solution was measured at 595 nm. Biofilms were allowed to form in each well of a 96-well microtiter plate, as described by Stepanovic.[40] Cells biofilms were exposed to 200 μl of peptide **9** at the final concentration ranging from 6.25 to 25 μM and the plate was further incubated for 24 h at 37 °C. At the end of the experiment crystal violet-staining was performed to assess biofilm mass.

Quantitation of Metabolic Activity of Mature Biofilm by XTT Assay. The metabolic activity of MSSP and MRSP mature biofilms was quantified by the XTT [2,3-bis(2-methyloxy-4-nitro-5-sulfophenyl)-2H-tetrazolium-5-carboxanilide] (Roche Diagnostics, Germany) reduction assay. The assay was conducted as previously described with some modifications.[41] XTT (150 μL) was added to biofilms in each well and the plates were incubated for 40 min at 37 °C in the dark. The reduction of the tetrazolium salt by cellular dehydrogenase into orange formazan dye was photometrically measured at 490 nm. The medium was set as negative control. Viability values for each well were compared to controls.

Confocal Laser Scanning Microscopy (CLSM). CLSM was used to confirm the effect of peptide **9** on mature biofilm respect the controls. MSRP were grown in chambered cover glass (μ Slide 4 well; ibidi GmbH, Germany) in a static condition for 24 h. Peptide **9** was added on a 1-day-old biofilm at 12.5 μM. After 24 h, biofilms were rinsed with PBS and stained by using a LIVE/DEAD® BacLight Bacteria Viability stains (Life Technologies, Italy). After the staining, the images were observed using a LSM 700 inverted confocal laser-scanning microscope (Zeiss, Italy).

4.4.3. *IN VITRO* ASSAYS

Cell viability. Murine macrophage cell line, J774, was cultured in Dulbecco's modified Eagle's medium supplemented with 10 % fetal bovine serum (FBS, Cambrex, Verviers, Belgium), L-glutamine (2 mM, Sigma, Milan, Italy), penicillin (100 units/ml, Sigma) and streptomycin (100 μg/ml, Sigma), and cultured in a humidified 5 % carbon dioxide atmosphere at 37 °C. The cells were treated for 4 and 24 h, with a range of concentrations (1 → 25 μM) of peptide **1** and **9**. Positive control incubations were carried out by equivalent concentrations of Diclofenac and Betamethasone. In another set of experiments cell were pre-treated with zymosan (100 ng/ml) followed by peptide **1** and **9** for 4 and 24 h, with the same range of concentrations. Biological activity of peptides was investigated by the estimation of a "cell survival index", arising from the combination of cell viability evaluation with cell counting. Cell viability was evaluated using MTT assay, which measures the level of mitochondrial dehydrogenase activity using the yellow 3-(4,5-dimethyl-2-thiazolyl)- 2,5-diphenyl-2H-tetrazolium bromide (MTT, Sigma) as substrate.[42]

Flow cytometry. Cells collected from the peritoneal cavities were first washed with PBS and then re-suspended in FACS buffer (PBS containing 1 % FCS and 0.02 % NaN_2) containing CD16/CD32 FcγIIR blocking antibody (clone 93; eBioscience, Wembley, UK) for 30 min at 4 °C. Thereafter, cells were labelled for 60 min at 4 °C

with the following conjugated antibodies (all from BioLegend, London, UK): GR1 (1:300; clone RB6-8C5), F480 (1:300; clone BM8), B220 (1:200; clone RA3-6B2), CD115 (1:200; clone AFS98).[43] Flow cytometry was performed on BriCyte E6 flow cytometer (Mindray Bio-Medical Electronics, Nanshan, China) using MRFlow and FlowJo software operation.

Enzyme-linked immunosorbent assay (ELISA). The levels of TNF-α, IL-6, IL-10 and MCP-1 in the peritoneal exudates at 24h were measured using commercially available enzyme-linked immunosorbent assay kit (ELISA kits, eBioscience Co., San Diego, CA, USA) according to the manufacturer instructions.[44]

4.4.4. *IN VIVO* STUDY

Induction of peritonitis in mice. To examine the anti-inflammatory action of peptide **1** and **9**, mice were randomly divided into different groups: control group (Ctrl), model group (Zymosan), zymosan+peptides (1, 3 and 10 mg/kg) groups (peptide **1** and **9**), and zymosan+dexamethasone (3 mg/kg) group (Dex). Animals received the peptides or Dex intraperitoneally (i.p.) 30 min after i.p. injection of zymosan (500 mg/kg).[45] Peritonitis was induced by administering 500 mg/kg of zymosan dissolved in PBS and then boiled before the i.p. injection (0.5 mL) at selected time points (4 and 24 h).[46] Peritoneal exudates were collected and then cell number of lavage fluids was determined by TC10 automated cell counter (Bio-Rad, Milan, Italy) using disposable slides, TC10 trypan blue dye (0.4 % trypan blue dye w/v in 0.81 % sodium chloride and 0.06 % potassium phosphate dibasic solution) and a CCD camera to count cells based on the analyses of captured images. The remaining lavage fluids were centrifuged at 3000 rpm for 20 min at 4 °C and supernatants frozen at –80 °C for further ELISA analysis.[47]

Statistical analysis. The results obtained were expressed as the mean ± SEM. Statistical analysis was performed by two-way ANOVA followed by Dunnett's posttest when comparing more than two groups. Statistical analysis was performed by using GraphPad Prism 7.0 software (San Diego, CA, USA).[48]

4.5. REFERENCES

[1] K.A. Brogden, J.M. Guthmiller, C.E. Taylor. Human polymicrobial infections. *Lancet*. 2005, 365, 253-255.
[2] A.Y. Peleg, D.A. Hogan, E. Mylonakis. Medically important bacterial–fungal interactions. *Nat. Rev. Microbiol*. 2010, 8, 340–349.
[3] E. Chryssanthou, U. Broberger, B. Petrini. *Malassezia pachydermatis* fungaemia in a neonatal intensive care unit. *Acta Paediatr*. 2001, 90, 323–327.
[4] J. Bannoehr, L. Guardabassi. *Staphylococcus pseudintermedius* in the dog: taxonomy, diagnostics, ecology, epidemiology and pathogenicity. *Vet. Dermatol*. 2012, 23, 253–266.
[5] A.A. Ferran, J. Liu, P.L. Toutain, A. Bousquet-Mélou. Comparison of the *in vitro* activity of five antimicrobial drugs against *Staphylococcus pseudintermedius* and *Staphylococcus aureus* biofilms. *Front. Microbiol*. 2016, 7:1187.
[6] J. Guillot, R. Bond. Malassezia yeasts in veterinary dermatology: an updated overview. *Front. Cell. Infect. Microbiol*. 2020, 10:79.
[7] I. Ghasemzadeh, S.H. Namazi. Review of bacterial and viral zoonotic infections transmitted by dogs. *J. Med. Life*. 2015, 8, 1–5.
[8] A.M.P. Oliveira, J.S.P. Devesa, P.B. Hill. *In vitro* efficacy of a honey based gel against canine clinical isolates of *Staphylococcus pseudintermedius* and *Malassezia pachydermatis*. *Vet. Dermatol*. 2018, 29, 180-e65.
[9] T. Holm, J. Bruchmann, A. Scheynius, U. Langel. Cell-penetrating peptides as antifungals towards *Malassezia Sympodialis*. *Lett. Appl. Microbiol*. 2012, 54, 39–44.
[10] N. Al-Sweih, S. Ahmad, L. Joseph, S. Khan, Z. Khan. *Malassezia pachydermatis* fungemia in a preterm neonate resistant to fluconazole and flucytosine. *Med. Mycol. Case Rep*. 2014, 5, 9–11.
[11] M.L. Mangoni, A.C. Rinaldi, A.D. Giulio, G. Mignogna, A. Bozzi, D. Barra, M. Simmaco. Structure-function relationships of temporins, small antimicrobial peptides from amphibian skin. *Eur. J. Biochem*. 2000, 267, 1447–1454.
[12] M.L. Mangoni. Temporins, anti-infective peptides with expanding properties. *Cell*. Mol. *Life Sci*. 2006, 63, 1060–1069.
[13] M.L. Mangoni, Y. Shai. Temporins and their synergism against Gram-negative bacteria and in lipopolysaccharide detoxification. *Biochim. Biophys. Acta Biomembr*. 2009, 1788, 1610–1619.
[14] P. Grieco, A. Carotenuto, L. Auriemma, M.R. Saviello, P. Campiglia, I. Gomez-Monterrey, L. Marcellini, V. Luca, D. Barra, E. Novellino, M.L. Mangoni. The effect

of d-amino acid substitution on the selectivity of temporin L towards target cells: identification of a potent anti-Candida peptide. *Biochim. Biophys. Acta Biomembr.* 2013, 1828, 652–660.
[15] F. Merlino, A. Carotenuto, B. Casciaro, F. Martora, M.R. Loffredo, A. Di Grazia, A.M. Yousif, D. Brancaccio, L. Palomba, E. Novellino, M. Galdiero, M.R. Iovene, M.L. Mangoni, P. Grieco. Glycine-replaced derivatives of [Pro^{3},DLeu^{9}]TL, a temporin L analogue: evaluation of antimicrobial, cytotoxic and hemolytic activities. *Eur. J. Med. Chem.* 2017, 139: 750–761.
[16] M. Zaiou. Multifunctional antimicrobial peptides: therapeutic targets in several human diseases. *J. Mol. Med.* 2007, 85, 317–329.
[17] R. Capparelli, A. Romanelli, M. Iannaccone, N. Nocerino, R. Ripa, S. Pensato, C. Pedone, D. Iannelli. Synergistic antibacterial and anti-Inflammatory activity of Temporin A and modified Temporin B *in vivo*. *PLoS One*. 2009, 4:e7191.
[18] C.N. Serhan. Novel lipid mediators and resolution mechanisms in acute inflammation:to resolve or not? *Am. J. Pathol.* 2010, 177, 1576–1591.
[19] M.L. Mangoni, A. Carotenuto, L. Auriemma, M.R. Saviello, P. Campiglia, I. Gomez-Monterrey, S. Malfi, L. Marcellini, D. Barra, E. Novellino, P. Grieco. Structure-activity relationship, conformational and biological studies of temporin L analogues. *J. Med. Chem.* 2011, 54, 1298–1307.
[20] E. Buommino, A. Carotenuto, I. Antignano, R. Bellavita, B. Casciaro, M.R. Loffredo, F. Merlino, E. Novellino, M.L. Mangoni, F.P. Nocera, D. Brancaccio, P. Punzi, D. Roversi, R. Ingenito, E. Bianchi, P. Grieco. The Outcomes of decorated prolines in the discovery of antimicrobial peptides from Temporin-L. *Chem. Med. Chem.* 2019, 14, 1283–1290.
[21] S. Gottschalk, L.E. Thomsen. The Interaction of antimicrobial peptides with the membrane and intracellular targets of Staphylococcus aureus Investigated by ATP leakage, DNA-binding analysis, and the expression of a LexA-controlled gene, recA. *Methods Mol. Biol.* 2017, 1548, 297–305.
[22] R. Bellavita, A. Falanga, E. Buommino, F. Merlino, B. Casciaro, F. Cappiello, M.L. Mangoni, E. Novellino, M.R. Catania, R. Paolillo, P. Grieco, S. Galdiero. Novel temporin L antimicrobial peptides: promoting self-assembling by lipidic tags to tackle superbugs. *J. Enzyme Inhib. Med. Chem.* 2020, 35, 1751–1764.
[23] D. Brancaccio, E. Pizzo, V. Cafaro, E. Notomista, F. De Lise, A. Bosso, R. Gaglione, F. Merlino, E. Novellino, F. Ungaro, P. Grieco, M. Milanga, F. Quaglia, A. Miro, A. Carotenuto. Antimicrobial peptide Temporin-L complexed with anionic cyclodextrins results in a potent and safe agent against sessile bacteria. *Int. J. Pharm.* 2020, 584, 119437.
[24] E.J.U. Von Asmuth, J.G. Maessen, C.J. van der Linden, W.A. Buurman. Tumor necrosis factor alpha and interleukin 6 in zymosan-induced shock model. *Scand. J. Immunol.* 1991, 34, 197–206.

[25] S. Cuzzocrea, A. Filippelli, B. Zingarelli, M. Falciani, A.P. Caputi, F. Rossi. Role of nitric oxide in a non-septic shock model induced by zymosan in the rat. *Shock*. 1997, 7, 351–358.
[26] E.J.U. Von Asmuth, J.G. Maessen, C.J. van der Linden, W.A. Buurman. Tumor necrosis factor alpha and interleukin 6 in zymosan-induced shock model. *Scand. J. Immunol*. 1991, 34, 197–206.
[27] M.J. Jansen, T. Hendriks, M.T.E. Vogels, J.W.M. van der Meer, R.J.A. Goris. Inflammatory cytokines in an experimental model for the multiple organ dysfunction syndrome. *Crit. Care Med*. 1996, 24, 1196–1204.
[28] M.R. Mainous, P. Tso, R.D. Berg, E.A. Deitch. Studies of the route, magnitude, and time course of bacterial translocation in a model of systemic inflammation. *Arch. Surg*. 1991, 126, 33–37.
[29] F. D'Acquisto, F. Maione, M. Pederzoli-Ribeil. From IL-15 to IL-33: the never-ending list of new players in inflammation. Is it time to forget the humble aspirin and move ahead? *Biochem. Pharmacol*. 2010, 79, 525–534.
[30] S. Liu, J. Zhang, Q. Pang, S. Song, R. Miao, W. Chen, Y. Zhou, C. Liu. The protective role of curcumin in zymosan-induced multiple organ dysfunction syndrome in mice. *Shock*. 2016, 45, 209–219.
[31] J. Xie, L. Yang, L. Tian, W. Li, L. Yang, L. Li. Macrophage migration inhibitor factor upregulates MCP-1 expression in an autocrine manner in hepatocytes during acute mouse liver injury. *Sci. Rep*. 2016, 6, 27665.
[32] K.W. Moore, R. de Waal Malefyt, R.L. Coffman, A. O'Garra. Interleukin-10 and the interleukin-10 receptor. *Annu. Rev. Immunol*. 2001, 19, 683–765.
[33] F. Merlino, S. Tomassi, A.M. Yousif, A. Messere, L. Marinelli, P. Grieco, E. Novellino, S. Cosconati, S. Di Maro, Boosting fmoc solid-phase peptide synthesis by ultrasonication. *Org. Lett*. 2019, 21, 6378–6382.
[34] E. Buommino, F.P. Nocera, A. Parisi, A. Rizzo, G. Donnarumma, K. Mallardo, F. Fiorito, A. Baroni, L. De Martino. Correlation between genetic variability and virulence factors in clinical strains of *Malassezia pachydermatis* of animal origin. *New. Microbiol*. 2016, 39, 216–223.
[35] A. Schumacher, T. Vranken, A. Malhotra, J. J. C. Arts, P. Habibovic. *In vitro* antimicrobial susceptibility testing methods: agar dilution to 3D tissue-engineered models. *Eur. J. Clin. Microbiol. Infect. Dis*. 2018, 37, 187–208.
[36] C. Cafarchia, L.A. Figueredo, V. Favuzzi, M.R. Surico, V. Colao, R. Iatta, M.T. Montagna, D. Otranto. Assessment of the antifungal susceptibility of *Malassezia pachydermatis* in various media using a CLSI protocol. *Vet. Microbiol*. 2012, 159, 536–540.
[37] O.O. Olajuyigbe, A.J. Afolayan. *In vitro* antibacterial and time- kill evaluation of the Erythrina caffra thunb. extract against bacteria associated with diarrhea. *Sci. World. J*. 2012, 738314.

[38] S.K. Pillai, R.C. Moellering, G.M. Eliopoulo. Antimicrobial combinations. In Antibiotics in Laboratory Medicine, 5th ed; Lorian, V., Ed.; The Lippincott Williams & Wilkins Co.: Philadelphia, PA, USA, 2005; pp. 365–440.
[39] F. Barra, E. Roscetto, A.A. Soriano, A. Vollaro, I. Postiglione, G.M. Pierantoni, G. Palumbo, M.R. Catania. Photodynamic and antibiotic therapy in combination to fight biofilms and resistant surface bacterial infections. *Int. J. Mol. Sci.* 2015, 16, 20417–20430.
[40] S. Stepanović, D. Vuković, V. Hola, G. Di Bonaventura, I. Djukić, Ćirković, F. Ruzicka. Quantification of biofilm in microtiter plates: overview of testing conditions and practical recommendations for assessment of biofilm production by staphylococci. *Apmis*. 2007, 115, 891–899.
[41] A. Vollaro, M.R. Catania, M.R. Iesce, R. Sferruzza, B. D'Abrosca, B. Donnarumma G, De Filippis A, Cermola F, DellaGreca M, Buommino E. Antimicrobial and anti-biofilm properties of novel synthetic lignan-like compounds. *New Microbiol*. 2019, 42, 21–28.
[42] C. Irace, G. Misso, A. Capuozzo, M. Piccolo, C. Riccardi, A. Luchini, M. Caraglia, L. Paduano, D. Montesarchio, R. Santamaria. Antiproliferative effects of ruthenium based nucleolipidic nanoaggregates in human models of breast cancer in vitro: insights into their mode of action. *Sci. Rep*. 2017, 7, 45236.
[43] F. Raucci, A.J. Iqbal, A. Saviano, P. Minosi, M. Piccolo, C. Irace, F. Caso, R. Scarpa, S. Pieretti, N. Mascolo, F. Maione. IL-17A neutralizing antibody regulates monosodium urate crystal-induced gouty inflammation. *Pharmacol. Res*. 2019, 147, 104351.
[44] V. Baradaran Rahimi, H. Rakhshandeh, F. Raucci, B. Buono, R. Shirazinia, A. Samzadeh Kermani, F. Maione, N. Mascolo, V.R. Askari. Anti-inflammatory and anti-oxidant activity of portulaca oleracea extract on LPS-induced rat lung injury. *Molecules*. 2019, 24, 139.
[45] B.E. Chatterjee, S. Yona, G. Rosignoli, R.E. Young, S. Nourshargh, R.J. Flower, M. Perretti. Annexin 1-deficient neutrophils exhibit enhanced transmigration *in vivo* and increased responsiveness *in vitro*. *J. Leukoc. Biol*. 2005, 78, 639–646.
[46] S. Pace, A. Rossi, V. Krauth, F. Dehm, F. Troisi, R. Bilancia, C. Weinigel, S. Rummler, O. Werz, L. Sautebin, Sex differences in prostaglandin biosynthesis in neutrophils during acute inflammation. *Sci. Rep*. 2017, 7, 3759.
[47] F. Maione, N.N. Paschalidis, A.J. Iqbal, T. Crompton, M. Perretti, F. D'Acquisto. Analysis of the inflammatory response in HY-TCR transgenic mice highlights the pathogenic potential of CD4- CD8- T cells. *Autoimmunity*. 2010, 43, 672–681.
[47] M.J. Curtis, R.A. Bond, D. Spina, A. Ahluwalia, S.P.A. Alexander, M.A. Giembycz, A. Gilchrist, D. Hoyer, P.A. Insel, A.A. Izzo, A.J. Lawrence, D.J. MacEwan, L.D. Moon, S. Wonnacott, A.H. Weston, J.C. McGrath, Experimental

design and analysis and their reporting: new guidance for publication in BJP. *Br. J. Pharmacol*. 2015, 172, 3461–34.